Self-Assembled Liquid Crystal Polymer Gels

Thesis by

Rafael Verduzco

In Partial Fulfillment of the Requirements

for the Degree of

Doctor of Philosophy

California Institute of Technology

Pasadena, California

2007

(Defended February 5, 2007)

Abstract

The combination of liquid crystals (LCs) with polymer networks results in fascinating materials in which the elasticity of the polymer network is coupled to LC order, and they hold promise for a variety of applications which depend on an optical or a mechanical response to external stimuli. Unfortunately, the methods for preparing LC networks are limited. In this work, we present two types of LC gels with novel network architectures: a physical gel made by polymer self-assembly in an LC solvent and a chemical gel made by crosslinking telechelic side-group liquid crystalline polymers (SGLCPs). The physical gel thermoreversibly transitions to a liquid on heating, and it can be uniformly aligned using electric, magnetic, or flow fields. The gel exhibits a fast electro-optical response, making it potentially viable for display applications. The physical gel also reveals novel equilibrium and dynamic properties that arise due the coupling between LC order and the polymer network. When confined between cell substrates prohibiting macroscopic shape change, it exhibits a temperature-sensitive striped texture transition. We provide a theoretical model that captures the striped texture by accounting for the compromise between nematic rubber elasticity and LC elasticity. Dynamic light scattering studies reveal two distinct director relaxation modes, in contrast to covalent gels, which show a single relaxation mode. We argue that the slower dynamics arise from the coupling between the director and the physically associated network which restructures on long time scales. We also investigate the self-assembled micellar structure of the gel via neutron scattering and rheometry studies, and these studies reveal that the gels' structure changes dramatically across the nematic-to-isotropic phase transition. Finally, we investigate model LC networks made by crosslinking telechelic SGLCPs using "click" chemistry. These chemical networks can be swollen in a small-molecule LC, and they exhibit a low-threshold electro-optic response and a temperature dependent size. These novel physical and chemical LC gels provide insight into the role of network structure in determining the material properties of liquid crystalline elastomers and gels.

Acknowledgements

I would like to thank all the people who contributed in some way to the work described in this thesis. First and foremost, I thank my academic advisor, Professor Julia A. Kornfield, for accepting me into her group. During my tenure, she contributed to a rewarding graduate school experience by giving me intellectual freedom in my work, supporting my attendance at various conferences, engaging me in new ideas, and demanding a high quality of work in all my endeavors. Additionally, I would like to thank my committee members Professor David A. Tirrell, Professor John F. Brady, and Professor Zhen-Gang Wang for their interest in my work.

Every result described in this thesis was accomplished with the help and support of fellow labmates and collaborators. Neal Scruggs and I worked together on several different phases of the self-assembled gels project, and without his efforts my job would have undoubtedly been more difficult. I greatly benefited from his keen scientific insight, his knack for solving seemingly intractable practical difficulties, and his ability to put complex ideas into simple terms. Yan Xia joined the group when I was beginning my last year as a graduate student, and, with his knowledge of chemistry and relentless work ethic, he was able to successfully carry out the synthesis of the model covalent LC networks. I gained a lot from his vast chemistry knowledge and scientific curiosity. I was fortunate to have the chance to work with Dr. Michael Kempe, who patiently taught me his method for synthesizing LC triblocks, in addition to a number of other laboratory techniques, and who worked closely with me in the synthesis of the LC triblocks I present in this thesis. He was an extremely reliable source of practical scientific knowledge, and I am grateful for his achievements during his time at Caltech, from which the work described in this thesis followed. I worked (nonstop) in the laboratory of Professor Samuel Sprunt of Kent State University for one long week in July 2005, and two very

long weeks in July 2006. Sam graciously allowed us to utilize the dynamic light scattering setup that he built himself, and he fully supported our efforts with with his time, his interest, and his extensive knowledge of light scattering experiments. I am also indebted to Professor Peter Palffy-Muhoray who deserves the credit for initiating the light scattering project. Peter wholeheartedly supported us during our visit to Kent State, and his physical insight was instrumental for the completion of the project. I am very grateful to Professor Robert Meyer of Brandeis University and Dr. Guangnan Meng, who was Bob's graduate student at the time, for their work in understanding the buckling instability. We exchanged several emails and Mathematica files over the course of a year during which we made sense of the buckling instability. Dr. David Uhrig of the Macromolecular Systems Group at Oak Ridge National Laboratory provided a series of diblock copolymers, without which the structural studies into the LC block copolymers would not have been possible. Dr. Jyotsana Lal aided our efforts in designing and carrying out neutron scattering experiments during four separate trips to Argonne National Laboratory.

I would like to thank the various members of the Kornfield group with whom I had the opportunity to work and have not already mentioned: Dr. Eric Pape, Dr. Derek Thurman, Dr. Charles Nickerson, Dr. Rob Lammertink, Dr. María (Luján) Auad, Dr. Erica Thompson, Dr. Wei Shen, Professor Kyunghwan Yoon, Lucía Fernández-Ballester, Michael Mackel, Matthew Mattson, Ralph David, Dr. Suneel Kunamaneni, Dr. Shuichi Kimata, Zuleikha Kurji, Ryan Turner, and Diana Smirnova. They provided a friendly and cooperative atmosphere at work and also useful feedback and insightful comments on my work. I also had the opportunity to mentor a SURF student for one summer, Vivek Narsimhan, who tirelessly and with much enthusiasm tackled a difficult project over the course of several months. I would be remiss if I did not thank Anne Hormann, who deserves credit for providing much needed assistance with administrative tasks, reminding us of impending deadlines, and keeping our work running smoothly. Additionally, Suresha Guptha provided immediate support for any computer problems we encountered.

I am grateful for the funding sources that allowed me to pursue my graduate school studies: The National Defense Science and Engineering Fellowship, the James-Irvine Minority Fellowship, and

the AFOSR LC-MURI. The National Science Foundation and the Korean Science and Engineering Foundation, through the East Asia and Pacific Summer Institute Fellowship, provided me with the opportunity to work for a summer in South Korea in the laboratory of Professor Jin Kon Kim.

I would like to acknowledge the Department of Chemical Engineering at Caltech. My graduate experience benefitted greatly from the courses I took, the opportunities I had under Professor John F. Brady and Professor Zhen-Gang Wang to serve as a teaching assistant, and the high-quality seminars that the department organized.

Finally, I would like to acknowledge friends and family who supported me during my time here. First and foremost I would like to thank Mom, Dad, Ceci, Mickey, and Danny for their constant love and support. Justin Bois, Aditya Khair, Alex Brown, Mikhail Kislitsyn, and Matt Lucas made my time here at Caltech a lot more fun. I am lucky to have met Michelle Estuar here, and I thank her for her friendhip, love, and unyielding support. I owe a debt of gratitude to all the members of the Caltech Rugby Football Club of which I was a member for over five years. I would also like to thank the members of the Fuzzy Bunnies of Death, the Two Baggers, Ernie's A. F., and the Laugh Out Louds.

Contents

List of Figures

List of Tables

Chapter 1

Background

1.1 Introduction

Liquid crystals (LCs) have historically attracted scientific and technological interest due to their unique optical properties. Biologists were puzzled by a birefringent fluid well before 1888, the date commonly cited as the year liquid crystals were discovered. In that year, Austrian botanist Friedrich Reinitzer recorded the phase-transition temperatures of cholesteryl benzoate, which turns a milky white at 145.5 ^{o}C and transparent at 178.5 ^{o}C, and he considered the possibility that a phase intermediate between that of the isotropic liquid and crystalline solid could exist [1]. The subsequent 50 years of liquid crystal science saw slow but steady advances in understanding the molecular structure, surface interactions, and electric field response of liquid crystals, but it was not until the early 1970s that the successful commercialization of a pocket calculator with a display device that utilized liquid crystals sparked an intense interest in the field [2]. The discovery of the dynamic scattering mode and the twisted-nematic mode in displays was crucial to the commercial implementation of liquid crystals, which otherwise might have languished as a scientific curiosity with no practical utility. To this day, the term “liquid crystal” is widely associated with the acronym LCD (liquid crystal display), and the second most well known application of liquid crystals among the general public may be the mood ring, which takes advantage of the colorful textures that chiral nematic liquid crystals reflect.

In the last twenty years, however, as the interest in liquid crystals has blossomed, so has their incorporation in a wide variety of materials. The unique properties of liquid crystals affords them potential utility in a wide range of applications that extends beyond displays. Indeed, potential uses of liquid crystals recently cited in the scientific literature include artificial muscles [3, 4], acoustic polarizers [5, 6], tunable lasers [7], and optical data storage [8]. It is conceivable that in another twenty years, liquid crystals will come to dominate an entirely different market unrelated to displays.

The applications listed stem from a particular class of material known as a liquid crystal elastomer. Elastomers are more commonly known as rubbers, and their ability to sustain large deformations while retaining a memory of their initial configuration enables a wide range of functionality. When combined with liquid crystals, the result is a highly responsive material that can react to electric or magnetic fields, heat, or light by changing shape, color, and even size. Furthermore, they have a reliable memory of where they began, and will return to their initial state on removal of the external influence. These novel properties arise from the combination of LC order, polymer elasticity, and topological constraints or translational order of a crosslinked rubber.

The first liquid crystal elastomer was prepared in 1981 [9], and later the method was improved so that *aligned* liquid crystal elastomers could be produced [10]. The advantage of the method is its simplicity, and it gives liquid crystal scientists access to liquid crystal elastomers which can be made quickly and easily. Studies on these materials have led to a molecular model which can successfully explain most of the phenomena exhibited by these unique rubbers, in particular their ability to change shape and rotate the molecular orientational order in response to a variety of external stimuli [11]. The story of liquid crystal-polymer materials is by no means complete, however. The elastomers produced by Finkelmann and coworkers [9, 10] represent the first successful attempt at fabricating rubbery liquid crystal networks, and this initial success has inspired the search for new ways to combine liquid crystals and polymers [12]. Much remains to be done to improve the materials first produced over twenty years ago. In particular, the field lacks materials with a well-defined structure, which can give both improved material properties and also facilitate comparisons to theory, many predictions of which remain to be tested [11, 6, 13]. Additionally, novel ways of combining polymers and liquid crystals can enable new applications, and several examples from the past five years demonstrate this [14, 3, 15, 16, 17].

In this thesis, we present two novel materials that incorporate liquid crystal order and a polymer network. One is made by the self-assembly of block copolymers and the other by covalently crosslinking end-functionalized telechelic polymers. Both have unique structures, and we seek to understand how this affects their material properties. We begin this chapter with a brief review of scientific topics relevant to this work. We begin by defining the nematic liquid crystal phase and describing the elastic and viscous forces present. Next, we discuss different types of polymer-liquid crystal materials that have been studied, including liquid crystal elastomers. Finally, we discuss the theory of nematic rubber elasticity and its predictions for “soft” deformations in liquid crystal elastomers. After this overview of the field, we lay out the main objectives of this thesis.

1.2 Liquid crystals

1.2.1 The nematic mesophase

A useful definition of LCs is given by deGennes and Prost [18]: LCs have liquid-like order in at least one dimension, and they possess a degree of anisotropy in their mechanical, optical, and/or structural properties characteristic of some degree of order. Various types of molecules satisfy this definition. For example, amphiphilic molecules, such as surfactants in solution with a selective solvent, can form associated structures in which molecules are ordered in layers. Also, long, rigid molecules such as polypeptides, DNA, or viruses will display LC phases when highly concentrated in solution, due to steric interactions between highly anisotropic molecules. These types of LC phases that occur in solution, and whose phase behavior is strongly concentration dependent, are known as lyotropic LCs [18]. On the other hand, small organic molecules that exhibit LC ordering in the pure state are known as thermotropic LCs. This is because temperature, as opposed to concentration (as in lyotropic LCs), determines the phase of the thermotropic LC. Ordering in thermotropic LCs arises both from steric effects and from intermolecular Van der Waals forces [1]. LC molecules and phases are oftentimes referred to as mesogens and mesophases, respectively.

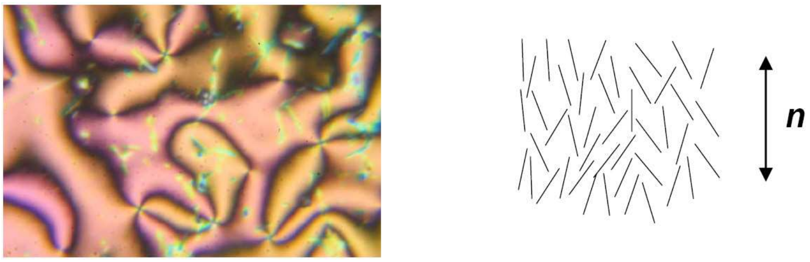

Figure 1.1: Nematic texture under polarized optical microscopy (left), and schematic of the nematic mesophase (right). The nematic phase has uniaxial symmetry, as indicated by the double-headed arrow.

The simplest LC phase is called the nematic phase. The term nematic comes from the Greek word for "threads" [18] and refers to the thread-like defects observed in nematics (Fig. 1.1). Molecules in the nematic mesophase have a preferred direction of orientational order, known as the director n, but they have no positional long-range order. The molecule 4-cyano-4′-n-pentylbiphenyl (5CB) is a thermotropic LC (Fig. 1.2). 5CB is crystalline below 20 ^{o}C, but displays the nematic mesophase from 20 ^{o}C up to 35 ^{o}C, above which temperature 5CB behaves like a conventional fluid. The transition temperature from the nematic to the isotropic phase is known as the T_{NI}. In this study, we are primarily concerned with thermotropic, nematic LCs.

The degree of order in a nematic LC is typically quantified by the order parameter S (Eq. 1.1), where θ is the angle between the director and the local molecular orientation. For a perfectly ordered nematic, S has a value of 1, while for an isotropic sample S has a value of 0. The order parameter is a useful way to quantify the degree of order in a liquid crystal, and it affects the anisotropy of material properties such as birefringence or dielectric anisotropy. Values of S typically vary between 0.3 and 0.8.

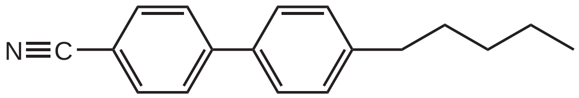

Figure 1.2: Chemical structure of 5CB. 5CB has a rod-like structure with a length of $\sim$ 20 $\mathring{A}$ and a width of $\sim$ 5 $\mathring{A}$.

$$S = \left\langle \frac{3}{2}\cos^2\theta - \frac{1}{2} \right\rangle \tag{1.1}$$

1.2.2 Liquid crystal elasticity

The lowest free energy state for a nematic is one in which all the mesogens are uniformly aligned with the director. In reality, thermal fluctuations prevent realization of this low energy state, and the molecules fluctuate around the preferred direction. Furthermore, uniform alignment may be incompatible with boundary conditions or external fields. Understanding the energy of these deviations from uniform alignment is important if we want to predict the equilibrium structure of nematics.

The situation is greatly simplified if we use a continuum approximation, which is justified by the much larger length scale ($\sim\ 1\,\mu m$) over which the director deviates, relative to the molecular size ($\sim\ 20\,\mathring{A}$). In this case, there are three basic types of deformation: splay, twist, and bend (Fig. 1.3), with associated elastic constants K_1, K_2, and K_3, respectively [18]. Each of these deformations has an associated elastic constant, which is in general temperature dependent. The LC elastic free energy density F_d is also known as the Frank elastic energy density (Eq. 1.2). The three elastic constants typically are of the same order of magnitude, typically 10^{-11} N – 10^{-12} N [19].

$$F_d = K_1(\nabla \cdot n)^2 + K_2(n \cdot \nabla \times n)^2 + K_3(n \times \nabla \times n) \tag{1.2}$$

1.2.3 Dynamic properties of the nematic director

In a uniform nematic monodomain, mesogens fluctuate about their equilibrium position due to thermal energy fluctuations. We can describe the amplitude and time scale for these thermal fluctuations by taking into account the Frank elastic and viscous forces for a fluctuation. Since orientational deformations over smaller length scales have a larger associated Frank penalty, the amplitude of the director fluctuations increases with increasing length scale. Similarly, the lifetime of an orientational fluctuation is larger for longer-wavelength distortions. These fluctuations are "overdamped" because

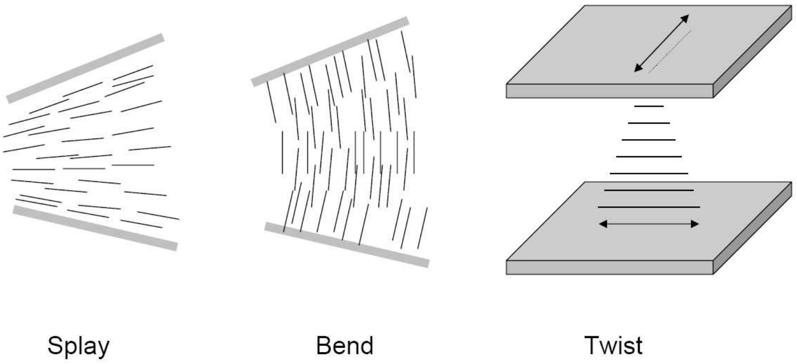

Figure 1.3: Splay, bend, and twist distortions of a nematic liquid crystal (Adapted from de Gennes and Prost, *The Physics of Liquid Crystals*, 1993, Oxford University Press, Inc., Oxford)

the rotational inertia of the molecules is small compared to the dissipation associated with rotational motion.

A quantitative treatment shows that there are two normal director modes for orientational fluctuations. These modes are a combination of splay-bend and twist-bend, and the relaxation rates associated with each will be different due to the different associated viscosities and elastic constants.

$$\begin{aligned}\langle|\delta n_1(\mathbf{q})|^2\rangle &= \frac{k_B T}{K_1 q_\perp^2 + K_3 q_{||}^2} \\ \langle|\delta n_2(\mathbf{q})|^2\rangle &= \frac{k_B T}{K_2 q_\perp^2 + K_3 q_{||}^2} \qquad (1.3)\end{aligned}$$

The amplitudes of the orientational fluctuations are determined by a ratio of thermal and elastic forces (Eq. 1.3), in which $\mathbf{q}$ is the wavevector for the distortion (inversely related to the length scale), k_B is the Boltzmann constant, and T is the temperature. The wavevector $\mathbf{q}$ has two components, $q_\perp$ and $q_{||}$, which are the components perpendicular to and parallel to the preferred direction, respectively. For pure LCs, orientational fluctuations decay exponentially with time, $\delta n_\alpha(\mathbf{q}, t) \sim \exp[-\Gamma_\alpha(\mathbf{q})t]$, where Γ is the relaxation rate. These relaxation rates are determined by a ratio of elastic and viscous forces (Eq. 1.4).

$$\begin{aligned}\Gamma_1(\mathbf{q}) &= \frac{K_1 q_\perp^2 + K_3 q_\parallel^2}{\eta_1(\mathbf{1})} \\ \Gamma_2(\mathbf{q}) &= \frac{K_2 q_\perp^2 + K_3 q_\parallel^2}{\eta_2(\mathbf{1})} \end{aligned} \tag{1.4}$$

The amplitude and lifetime of a fluctuation depends on its orientation relative to the nematic director, and different orientations will have different degrees of contribution from splay, twist, and bend, and different associated viscosities. Experimentally, these three contributions can be decoupled by measuring the time-correlation of the scattered-light intensity at a particular angle and sample orientation[20] (see Chapter 4 for experimental details). This is a useful way to measure the elastic constants and viscosity coefficients for LCs.

1.3 Liquid crystalline elastomers and gels

1.3.1 LC polymers: anisotropic chains

LC polymers (LCPs) consist of mesogenic groups incorporated in a polymer chain. They can be incorporated into the backbone of a polymer chain, in which case the polymer is called a main-chain LCP, or the mesogens can be linked to the backbone by a flexible spacer, resulting in a side-group liquid crystal polymer (SGLCP) (Fig. 1.4). As shown in Fig. 1.4, LCPs typically have an anisotropic backbone conformation. This anisotropy arises from the liquid coupling between the liquid crystal ordering of the mesogens and the polymer backbone conformation [21]. The degree of anisotropy is dependent on the LC order parameter, which in turn is temperature dependent [22] and can also be modulated by UV light [23]. This ability to control the polymer conformation with temperature changes and UV is the basis for a variety of potential applications [24].

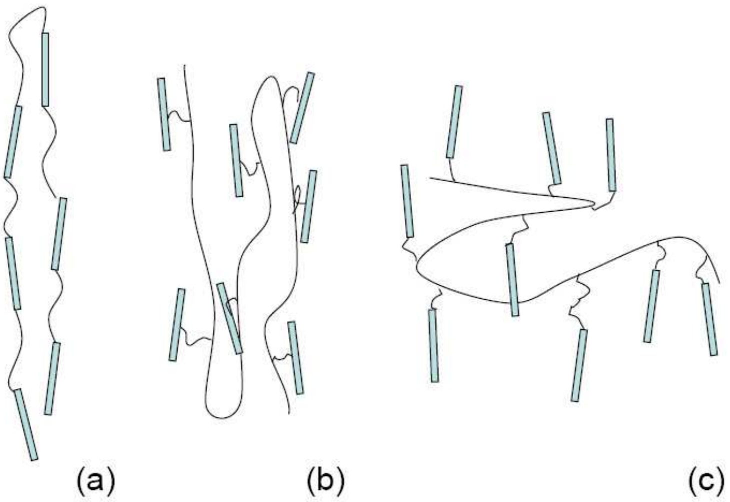

Figure 1.4: Schematic of (a) main-chain LCP, (b) side-on SGLCP, and (c) end-on SGLCP. (Adapted from Warner and Terentjev, *Liquid Crystal Elastomers*, 2003, Oxford University Press, Inc., Oxford.) As shown, main-chain LCPs and side-on SGLCPs typically have a prolate backbone conformation, while end-on SGLCPs typically have an oblate backbone conformation.

1.3.2 LC elastomers

Liquid crystal elastomers are composed of rubbery LCPs crosslinked into a network [11]. The anisotropic chain conformation of the network strands results in novel elastic properties not present in isotropic elastomers. In particular, nematic elastomers can exhibit a soft resistance to strains [25], and their macroscopic shape can change anisotropically in response to temperature [10].

The most popular method for preparing LC elastomers involves functionalization and crosslinking of a polysiloxane polymer (Fig. 1.5). This was first devised by Finkelmann et al. [9], and later work allowed the method to be used to form aligned LC elastomers [10].

1.3.3 LC gels

The term LC gels is loosely applied to materials that combine small molecule LCs with macromolecules [26, 27, 28, 12]. LC gels typically have faster dynamics and a lower threshold for response compared with LC elastomers. Therefore, LC gels are oftentimes studied for their potential use in displays. Also, LC gels can show shape changes in response to temperature and external fields, similar to LC elastomers.

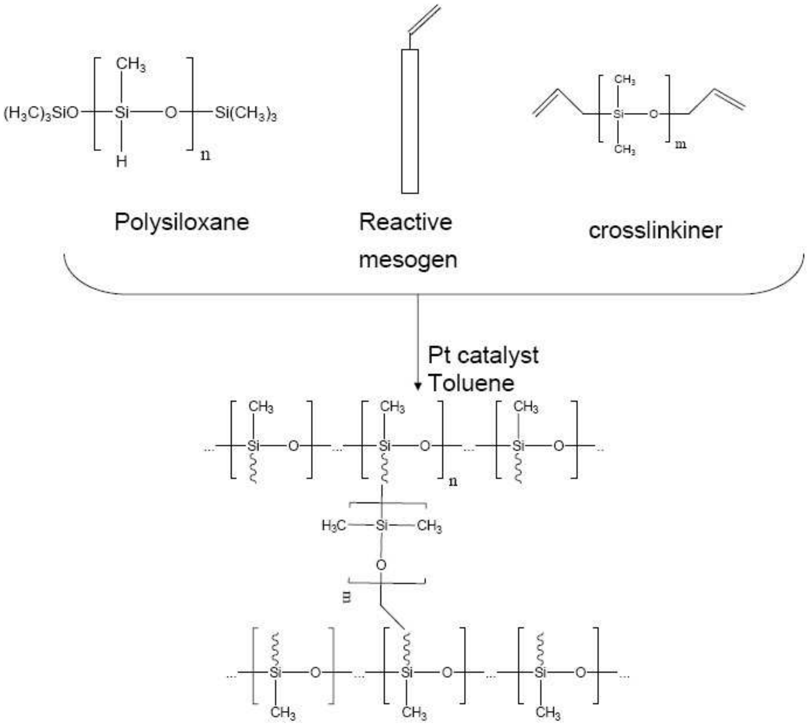

Figure 1.5: Schematic representation of a popular method [9] for preparing nematic LC elastomers

One type of LC gel is made by polymerizing mesogenic acrylates dissolved in an LC solvent [29]. In contrast to LC elastomers, the polymer backbone does not have to be rubbery, since the resulting network is swollen with solvent. The first LC gel of this type was produced in 1986 [26], but these types of LC gels drew little attention until more recently [30, 29]. Recent investigations have observed low-threshold electric field-induced shape changes [31], and temperature induced deswelling followed by reswelling when heating through the nematic-to-isotropic transition temperature [32].

Polymer-stabilized liquid crystals (PSLCs) are made by polymerizing exclusively mesogenic diacrylates (as opposed to monoacrylates) dissolved in an LC solvent [27, 33]. In contrast to LC gels made from monoacrylate monomers, PSLCs have a heterogenous structure that consists of a macroscopically phase separated polymer matrix encompassing the LC solvent [34]. The overall polymer concentration is dilute, typically 5 wt %, and therefore PSLCs retain the fast electro-optic response of small molecule LCs. The response can be faster, in fact, than small molecule LCs, since the polymer matrix provides a driving force throughout the volume of the material for the LC director to return to its original orientation upon removal of the field [27]. Different types of LC order have been incorporated into PSLCs, and they are of interest for electro-optic devices.

Another polymer-LC composite related to PSLCs, and also studied for its electro-optical properties, is known as a polymer-dispersed liquid crystal (PDLC). In contrast to PSLCs, PDLCs have a high polymer content, typically 90-95 wt % [35]. The structure of PDLCs consists of LC droplets dispersed in a continuous polymer matrix. Like PSLCs, PDLCs have a fast and reversible electro-optic response.

LC gels can also be made by mixing small-molecule gelators with a liquid crystal solvent [36, 28]. The gelators physically associate into a network of fibrous aggregates. The gels are thermoreversible, exhibit a fast electro-optic response, and gel at a low content ~ 1 wt % of added gelator.

1.3.4 Block copolymer self-assembly for LC elastomers and gels

Block copolymer self-assembly has recently been investigated for producing LC elastomers and gels. LC gels can be produced by the association of triblock polystyrene-SGLCP-polystyrene copolymers in a small molecule nematic LC [14], and this is the topic of Chapter 2. Nematic elastomers can also be made by block copolymer self assembly [3, 37, 15]. The advantages of these materials are that the macromolecular structure is produced in a controlled way, and therefore the resulting materials have a regular structure. Furthermore, self-assembly gives access to unique morphologies, such as a lamellar arrangement of blocks [3] and a thermally reversible structure [14, 3, 15].

1.4 The molecular theory of nematic rubber elasticity

The molecular theory of nematic rubber elasticity formulated by Warner and Terentjev [11] is an extension of classical rubber elasticity. In this “neo-classical” theory of nematic rubber elasticity, the chains in the network are assumed to be phantom, Gaussian, spontaneously anisotropic chains, and this neo-classical theory can successfully explain the spontaneous distortions, mechanical instabilities, and director-strain coupling [11]. Recent efforts have been made to include non-classical effects in nematic rubbers such as excluded volume interactions [13], entanglements [38], and deviations from the Guassian limit [39]. Here, we will focus exclusively on the neo-classical theory of nematic rubber elasticity, which we utilize in Chapter 3 to explain a spontaneous texture transition in LC gels. (The material reviewed here is covered extensively in Warner and Terentjev, *Liquid Crystal Elastomers*, 2003, Oxford University Press, Inc., Oxford.)

In contrast to classical elastomers, LC elastomers have an end-to-end distance that depends on the local orientation of the nematic director. This is because the chains in an LC network are anisotropic, as explained in Section 1.3.1. The anisotropy in the polymer chains can be expressed in terms of a step length tensor $l_{ij} = l_{\perp}\delta_{ij} + (l_{\parallel} - l_{\perp})n_i n_j$, in which $l_{\perp}$ and $l_{\parallel}$ are the effective lengths of steps parallel and perpendicular to the director $\mathbf{n}$ for a freely jointed chain. These step lengths are directly related to the mean square end-to-end distance, $\langle R_i R_j \rangle = \frac{1}{3} l_{ij} L$, where L is the arc length of the polymer chain. A more useful expression relates the ratio of the step lengths to the ratio of the radii of gyration of the chain, $\frac{l_{\parallel}}{l_{\perp}} = (\frac{R_{\parallel}}{R_{\perp}})^2$. The probability for an anisotropic strand having an end-to-end vector $\underline{\mathbf{R}}$, in terms of the step length tensor and the polymer arc length L, is given in Eq. 1.5.

$$p(\mathbf{R}) \sim \exp\left(-\frac{3}{2L}\mathbf{R} \cdot \underline{\underline{\mathbf{l}}}^{-1} \cdot \mathbf{R}\right) \tag{1.5}$$

Before computing the free energy expression for a crosslinked rubber, we need to distinguish between the conditions during crosslinking, described by step length tensor $\underline{\underline{\mathbf{l}}}_o$, and the conditions under which a strain is imposed which have an associated step length tensor $\underline{\underline{\mathbf{l}}}$. The resulting free energy expression is found by taking an average over all end-to-end vectors in the initial and final states (Eq. 1.6). Network deformations are accounted for by the deformation gradient tensor $\underline{\underline{\lambda}}$, which relates a separation vector on the undeformed body $\underline{\mathbf{R}}_o$ to that on the body under an imposed strain $\underline{\mathbf{R}}$, by the relationship $\underline{\mathbf{R}} = \underline{\underline{\lambda}} \cdot \underline{\mathbf{R}}_o$. The free energy expression (Eq. 1.6) is the basis for nematic rubber elasticity.

$$F = \frac{1}{2}\mu\left(Tr[\underline{\underline{l_o}} \cdot \underline{\underline{\lambda}}^T \cdot \underline{\underline{l}}^{-1} \cdot \underline{\underline{\lambda}}]\right) \tag{1.6}$$

1.4.1 Soft elasticity

Soft elasticity refers to a phenomenon in the framework of the neoclassical theory of rubber elasticity (Eq. 1.6) in which a nematic rubber can undergo a non-trivial deformation at no cost to the free energy. This is presented schematically in Fig. 1.6. Under some imposed strains, the network chains can rotate the distribution of chains at constant average shape of the network chains, and therefore the strain is perfectly "soft."

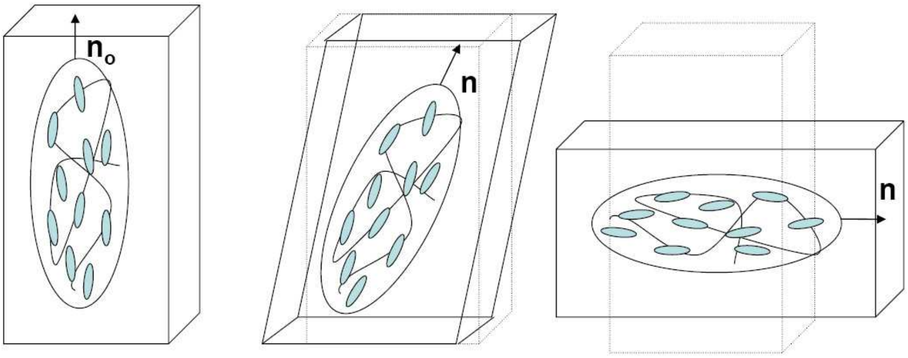

Figure 1.6: Schematic representation of a soft elastic distortion in a nematic elastomer. The box represents the macroscopic elastomer shape, and the LC chain depicts rotating nematic director which accomodates the shape change.

All soft deformations can be expressed in terms of the initial and final step length tensors, and an arbitrary rotation $\underline{\underline{\mathbf{W}}}_\alpha$ (Eq. 1.7) [40]. However, this does not give a practical method for computing optimal deformations. Most methods use Eq. 1.6 as a starting point [11], but it is also possible to begin by finding the displacements in the sample and computing the resulting deformation gradient tensor $\underline{\underline{\lambda}}$, as demonstrated in Chapter 3.

$$\underline{\underline{\lambda}} = \underline{\underline{l}}^{(1/2)} \cdot \underline{\underline{W}}_\alpha \cdot \underline{\underline{l}}_o^{(-1/2)} \tag{1.7}$$

1.4.2 Semi-softness

Several requirements must be met for softness to be possible in an elastomer. The network must be ideal, and all strands must be identical. Furthermore, the network must have an isotropic reference state. An elastomer that does not satisfy all these requirements cannot undergo strictly "soft" deformations, but it can nevertheless achieve nearly "soft" behavior, or "semi-softness." Experimentally, "semi-softness" has been observed as a small resistance to deformation before a "soft" plateau in the modulus [41]. Semi-softness that arises from polydispersity in the network or compositional fluctuations can be accounted for by including an additional term, weighted by the semi-softness parameter α, in the free energy expression (Eq. 1.8) [11].

$$\begin{aligned} F &= \frac{1}{2}\mu\left(Tr[\underline{\underline{l_o}} \cdot \underline{\underline{\lambda}}^T \cdot \underline{\underline{l}}^{-1} \cdot \underline{\underline{\lambda}}]\right) + \\ &\quad \frac{1}{2}\mu\alpha\left(Tr[(\underline{\underline{\delta}} - \underline{n_o}\ \underline{n_o}) \cdot \underline{\underline{\lambda}}^T \cdot \underline{n}\ \underline{n} \cdot \underline{\underline{\lambda}}]\right) \end{aligned} \tag{1.8}$$

1.5 Objectives

Experimental research is limited by the materials available. This work aims to further the understanding of LC-polymer materials by producing novel LC gels and investigating their equilibrium and dynamic properties. A major aim is to prepare LC networks which have a regular structure, and we achieve this using self-assembly and end-linking of telechelic polymers. In Chapter 2, we present our approach for preparing liquid crystal gels self-assembled from a triblock copolymer, and we demonstrate the gels' favorable electro-optical properties, as well as the various methods for alignment. In the subsequent three chapters, we seek to understand the structure of the gel and the manifestation of rubber elasticity in the gels' macroscopic properties. In Chapter 3, we detail investigations into a spontaneous texture transition that appears in a uniformly aligned gel subject to small changes in temperature. While stripes have been observed in previous LC elastomers, the response discussed in this chapter is unique for its sensitivity to small changes in temperature and appearance in a gel confined between substrates. We formulate a description based on the neo-classical molecular theory of nematic rubber elasticity that accounts for the observed texture transition. The dynamics of orientational fluctuations in liquid crystal gels are expected to be modified due to the presence of a polymer network, and our gels provide a unique opportunity to study the director dynamics in monodomains (Chapter 4). We find that the gels show long-time relaxation modes due to a coupling between the polymer network and the nematic director, and we present a qualitative picture that describes the observed anisotropy and time scale of the response. Chapter 5 presents the results of rheometry and neutron scattering experiments to investigate the structure of the physical gels. The studies show that the LC order of the host solvent imparts unique properties to the micellar gels. The micelles and intermicellar network inherit the anisotropy of the host solvent, and dramatic structural and rheological changes occur across the T_{NI} due to a changing solvent selectivity. In addition to our studies of physical LC gels, we pursued model covalent networks. Ring-opening metathesis polymerization (ROMP) allowed the preparation of end-functionalized LC polymers which could be crosslinked via "click" chemistry (Chapter 6). These networks hold promise for elucidating structure-property relationships in LC elastomers.

Bibliography

[1] P. J. Collings and M. Hird. *Introduction to Liquid Crystals.* Taylor & Francis, London, 1997.

[2] H. Kawamoto. The history of liquid-crystal displays. *Proc. IEEE*, 90(4):460–500, 2002.

[3] M.-H. Li, P. Keller, J. Yang, and P.-A. Albuoy. An artificial muscle with lamellar structure based on a nematic triblock copolymer. *Adv. Mater.*, 16(21):1922–1925, 2004.

[4] K. Urayama, H. Kondo, Y. O. Arai, and T. Takigawa. Electrically driven deformations of nematic gels. *Phys. Rev. E*, 71:051713, 2005.

[5] E. M. Terentjev and M. Warner. Linear hydrodynamics and viscoelasticity of nematic elastomers. *Eur. Phys. J. E*, 4:343–353, 2001.

[6] O. Stenull and T. C. Lubensky. Dynamics of nematic elastomers. *Phys. Rev. E*, 69:051801, 2004.

[7] H. Finkelmann, S. T. Kim, A. Munoz, P. Palffy-Muhoray, and B. Taheri. Tunable mirrorless lasing in cholesteric liquid crystalline elastomers. *Adv. Mater.*, 13(14):1069–+, 2001.

[8] T. Ikeda and O. Tsutsumi. Optical switching and image storage by means of azobenzene liquid-crystal films. *Science*, 268:1873–1875, 1995.

[9] H. Finkelmann, Hans-J. Kock, and Gunther Rehage. Investigations on liquid crystalline polysiloxanes 3. liquid crystalline elastomers – a new type of liquid crystalline material. *Makromol. Chem., Macromol Chem. Phys.*, 2:317–322, 1981.

[10] J. Küpfer and H. Finkelmann. Nematic liquid single-crystal elastomers. *Makromol. Chem., Macromol Chem. Phys.*, 12(12):717–726, 1991.

[11] M. Warner and E. M. Terentjev. *Liquid Crystal Elastomers.* Oxford University Press, Oxford, 2003.

[12] P. Xie and R. B. Zhang. Liquid crystal elastomers, networks and gels: advanced smart materials. *J. Mater. Chem.*, 15(26):2529–2550, 2005.

[13] F. T. Oyerokun and K. S. Schweizer. Thermodynamics, orientational order and elasticity of strained liquid crystalline melts and elastomers. *J. Phys. Chem. B*, 109(14):6595–6603, 2005.

[14] M. D. Kempe, N. R. Scruggs, R. Verduzco, J. Lal, and J. A. Kornfield. Self-assembled liquid-crystalline gels designed from the bottom up. *Nat. Mater.*, 3(3):177–182, 2004.

[15] S. V. Ahir, A. R. Tajbakhsh, and E. M. Terentjev. Self-assembled shape-memory fibers of triblock liquid-crystal polymers. *Adv. Funct. Mater.*, 16(4):556–560, 2006.

[16] M. Camacho-Lopez, H. Finkelmann, P. Palffy-Muhoray, and M. Shelley. Fast liquid-crystal elastomer swims into the dark. *Nat. Mater.*, 3:307–310, 2004.

[17] Y. L. Yu, M. Nakano, and T. Ikeda. Directed bending of polymer film by light – miniaturizing a simple photomechanical system could expand its range of applications. *Nature*, 425(6954):145, 2003.

[18] Pierre-Gilles de Gennes. *The Physics of Liquid Crystals.* Clarendon Press, Oxford, 2nd edition, 1993.

[19] K. Skarp, S. T. Lagerwall, and B. Stebler. Measurements of hydrodynamic parameters for nematic 5cb. *Mol. Cryst. Liq. Cryst.*, 60:215–236, 1980.

[20] John T. Ho. Light scattering and quasielastic spectroscopy. In Satyendra Kumar, editor, *Liquid Crystals.* Cambridge University Press, Cambridge, 2001.

[21] X. J. Wang and M. Warner. Theory of nematic comb-like polymers. *J. Phys. A: Math. Gen.*, 20:713–731, 1987.

[22] J. F. D'Allest, P. Maissa, A. ten Bosch, P. Sixou, A. Blumstein, R. B. Blumstein, J. Teixeira, and L. Noirez. Experimental evidence of chain extension at the transition temperature of a nematic polymer. *Phys. Rev. Lett.*, 61(22):2652–2565, 1988.

[23] H. Finkelmann, E. Nishikawa, G. G. Pereira, and M. Warner. A new opto-mechanical effect in solids. *Phys. Rev. Lett.*, 87(1):015501, 2001.

[24] M. Behl and A. Lendlein. Actively moving polymers. *Soft Matter*, 3(1):58–67, 2007.

[25] S. M. Clarke, E. M. Terentjev, I. Kundler, and H. Finkelmann. Texture evolution during the polydomain-monodomain transition in nematic elastomers. *Macromolecules*, 31(15):4862–4872, 1998.

[26] R. Zentel. Shape variation of cross-linked liquid-crystalline polymers by electric-fields. *Liq. Cryst.*, 1(6):589–592, 1986.

[27] R. A. M. Hikmet. Electrically induced light-scattering from anisotropic gels. *J. Appl. Phys.*, 68(9):4406–4412, 1990.

[28] N. Mizoshita, Y. Suzuki, K. Kishimoto, K. Hanabusa, and T. Kato. Electro-optical properties of liquid-crystalline physical gels: a new oligo(amino acid) gelator for light scattering display materials. *J. Mater. Chem.*, 12:2197–2201, 2002.

[29] K. Urayama, Y. Okuno, T. Kawamura, and S. Kohjiya. Volume phase transition of liquid crystalline gels in a nematic solvent. *Macromolecules*, 35:4567–4569, 2002.

[30] C. C. Chang, L. C. Chien, and R. B. Meyer. Electro-optical study of nematic elastomer gels. *Phys. Rev. E*, 56(1):595–599, 1997.

[31] Y. Yusuf, J. H. Huh, P. E. Cladis, H. R. Brand, H. Finkelmann, and S. Kai. Low-voltage-driven electromechanical effects of swollen liquid-crystal elastomers. *Phys. Rev. E*, 71(6), 2005.

[32] K. Urayama, Y. Okuno, T. Nakao, and S. Kohjiya. Volume transition of nematic gels in nematogenic solvents. *J. Chem. Phys.*, 118(6):2903–2910, 2003.

[33] I. Dierking. Polymer network-stabilized liquid crystals. *Adv. Mater.*, 12(3):167–181, 2000.

[34] P. Gautier, M. Brunet, J. Grupp, L. Noirez, and E. Anglaret. Structure and texture of anisotropic nematic gels. *Phys. Rev. E*, 68:011709, 2003.

[35] David Coates. Polymer-dispersed liquid crystals. *J. Mater. Chem.*, 5(12):2063–2072, 1995.

[36] T. Kato, T. Kutsuna, K. Hanabusa, and M. Ukon. Gelation of room-temperature liquid crystals by the association of a *trans*-1,2-bis(amino)cyclohexane derivative. *Adv. Mater.*, 10(8):606–608, 1998.

[37] A. J. Gabert, E. Verploegen, P. T. Hammond, and R. R. Schrock. Synthesis and characterization of aba triblock copolymers containing smectic c* liquid crystal side chains via ring-opening metathesis polymerization using a bimetallic molybdenum initiator. *Macromolecules*, 39(12):3993–4000, 2006.

[38] S. Kutter and E. M. Terentjev. Tube model for the elasticity of entangled nematic rubbers. *Eur. Phys. J. E*, 6(3):221–229, 2001.

[39] Y. Mao, M. Warner, E. M. Terentjev, and R. X. Ball. Finite extensibility effects in nematic elastomers. *J. Chem. Phys.*, 108(20):8743–8748, 1998.

[40] P. D. Olmsted. Rotational invariance and goldstone modes in nematic elastomers and gels. *J. Phys II France*, 4(12):2215–2230, 1994.

[41] I. Kundler and H. Finkelmann. Strain-induced director reorientation in nematic liquid single crystal elastomers. *Macromol. Rapid Commun.*, 16:679–686, 1995.

Chapter 2

Liquid Crystalline Gels by Self-Assembly of Triblock Copolymers

The work presented in this chapter represents a collaborative effort with Michael Kempe and Neal Scruggs.

Reproduced in part with permission from *Nature Materials*, (3):177-182, Copyright 2004 Nature Publishing Group, and from *Soft Matter*, (2):422-431, Copyright 2006 Royal Society of Chemistry.

2.1 Abstract

Liquid crystal (LC) gels are of interest for display applications and artificial muscles, but the methods for preparing LC networks are limited. Exploring novel approaches for synthesizing LC gels and elastomers can result in improved material properties and a better-defined network structure. Here, we explore the self-assembly of triblock copolymer to produce LC gels. The LC gels are produced by mixing a small molecule LC with an end-associating side-group liquid crystalline triblock copolymer. The resulting gels are thermoreversible, and they can be easily aligned to form uniform monodomains under shear or under external magnetic or electric fields. Electro-optic measurements demonstrate that the LC gels have potential use in an easily processible scattering-type display device. Additionally, the LC gels have a well-defined structure, making them useful for experimental comparison to theories of liquid crystal gels and networks.

2.2 Introduction

Liquid crystals (LCs) combine liquid-like fluidity with crystal-like properties such as birefringence, enabling LCs to be used in a variety of display devices [1]. The fluidity of liquid crystals is a key property that allows them to be quickly and easily reoriented in response to electric fields. On the other hand, the fluidity of liquid crystals poses problems and limitations for device applications. In the case of displays, the substrate surfaces must be coated with a polymer layer and rubbed to uniformly align the nematic director, and this alignment may be unstable to mechanical shock. Liquid crystals are therefore unsuitable for use in applications that require both birefringence and mechanical stability.

The combination of liquid crystals with polymers is an attractive method for fabricating materials with the optical properties and responsiveness of liquid crystals but with the mechanical properties and processing advantages of polymers. Liquid crystalline gels attempt to accomplish this. The potential applications of such materials include easily processible displays [2] but also other functional devices such as artificial muscles that respond to electric fields [3], heat [4], and light [5].

Several approaches have been used to make both chemical and physical LC gels [6, 7, 8]. Polymer stabilized liquid crystals (PSLCs) are made by the in situ uncontrolled radical polymerization of diacrylate LC monomers mixed with a non-reactive LC solvent [2, 8], resulting in a phase-separated polymer matrix encompassing small-molecule LC [9, 10]. In another method [11, 12], both acrylates and diacrylate LC monomers are in situ polymerized, resulting in a more soluble network. Both of these methods produce LC gels with favorable electro-optical properties, but they also have a poorly defined network structure. Another method for preparing LC gels is the addition of small molecule gelators to an LC solvent[13, 14, 15], resulting in a thermoreversible, physical LC gel.

In this study, we investigate a novel method for making LC gels. Our goal is to produce dilute LC gels with a uniform, well-defined structure. We make LC gels by the self-assembly of LC triblock copolymers in a small molecule LC. The copolymers have polystyrene (PS) endblocks and a side-group liquid crystalline (SGLCP) midblock. The midblocks are “nematophilic” and soluble in the LC solvent, but the endblocks are “nematophobic” and physically associate in the nematic phase, producing LC gels with a homogeneous nematic texture (Fig. 2.1). The LC gels have unique thermal, mechano-optic, and electro-optic properties, and they provide several advantages for display applications, such as thermoreversible gelation. In this chapter, we present the synthesis of the LC gels, and we investigate the phase behavior, alignment, and electro-optical properties of the LC gels. We find that the LC gels have a fast electro-optical response, and, because of their homogeneous structure, they are also useful for testing theoretical predictions [16, 17, 18] for liquid crysalline networks.

2.3 Experimental

2.3.1 Gel permeation chromatography (GPC)

GPC was carried out using three different systems. The first one used two 30 cm long PLgel 5 μm mixed-C columns from Polymer Laboratories (200 to 2,000,000 g/mol), connected in series with a DAWN 8 EOS multi-angle laser light scattering (MALLS) detector and an Optilab DSP differential refractometer, both from Wyatt Technology. Calculations were performed using the software package ASTRA from Wyatt Technology. The MALLS detector used a 30 mW, 690 nm, linearly polarized gallium-arsenide laser, and the differential refractometer used 690 nm light with a Wollaston prism. Tetrahydrofuran (THF) was used as the eluent at a flow rate of 1 mL/min and a temperature of 35 ^{o}C. No calibration standards were used and dn/dc values were obtained for each injection assuming 100% mass elution from the columns, and assuming dilute conditions where the second virial coefficient is negligible.

The second system used a Waters 410 differential refractometer with two Polymer Laboratories 30 cm long PLgel 10 μm analytical columns connected in series. These columns were calibrated with monodisperse polystyrene samples. The polydispersity index (PDI) (M_w/M_n) of the prepolymers, SGLCP homopolymers, and LC triblock copolymers was measured using THF flowing at a rate of 0.9 mL/min as the mobile phase.

The last column was only used to remove high molecular weight cross-linked polymer byproduct from the ABA LC polymers. The system consisted of a 30 cm long Polymer Laboratories PLgel 10 μm preparative column connected to the same Waters 410 differential refractometer.

2.3.2 Nuclear magnetic resonance

^{1}H NMR was performed on a Mercury-Vx 300 MHz NMR spectrometer with the software package VNMR Version 6.1B, using 32 scans with a 1 s delay time. Experiments were run at room temperature using $CDCl_3$ as a solvent and a polymer concentration of 10 to 20 mg/mL.

2.3.3 Liquid crystal phase identification

The transition temperatures and phases of the LC polymers were determined using both a Zeiss polarized optical microscope (POM) with a Mettler FP82 hot stage and a Perkin Elmer DSC7 differential scanning calorimeter (DSC) using the Pyris software. In the microscope the temperature was slowly raised at between 1 and 5 ^{o}C/min, and the phases were identified along with the temperature at which phase transitions began. In the DSC method the samples were heated well into the isotropic phase to remove any thermal history. Then the temperature was raised at a rate of 10 ^{o}C/min, and Perkin Elmers Pyris computer software (version 3.04) was used to determine the onset temperature of the various phase transitions. The DSC was calibrated using indium as a standard, at a heating rate of 10 ^{o}C/min.

2.3.4 Conoscopic imaging

Conoscopic imaging was performed using a Zeiss microscope equipped with an Olympus 1C20 high-numerical-aperture lens, a custom-made translation stage, and a computerized video capture system.

2.3.5 Rheometry

Rheometry was performed on a TA Instruments ARES-RFS rheometer equipped with a 25 mm diameter titanium shear cell in a cone-and-plate geometry having a 0.0202 radian cone angle. No surface treatment was applied, and the samples were heated into the isotropic state prior to measurement to erase any thermal history.

2.3.6 Electro-optic measurements

The optical properties and electro-optic responses of the gels were measured using a polarized HeNe laser, a beam splitter, two CCD cameras, and a function generator. A beam splitter between the laser and the sample sent half of the incident laser intensity to the sample and half to a CCD camera which was used to normalize the intensity of laser light incident on the sample. A CCD camera 10 cm behind the sample measured the intensity of transmitted light, and this intensity was normalized by the intensity transmitted for the sample in the isotropic state. The function generator was used to apply voltages from 0 V to 270 V at 1000 Hz.

2.3.7 Synthesis of SGLCPs: homopolymers and triblocks

All reagents were used as received from Aldrich unless otherwise stated. A "polymer analogous" approach to synthesis allowed high molecular weight polymers to be created. 1,2-polybutadiene (H) was used as the prepolymer for LC homopolymers, and polystyrene-*block*-1,2-polybutadiene-*block*-polystyrene triblock copolymer (ABA) was used as the prepolymer for LC triblock copolymers. H and ABA, synthesized by anionic polymerization, were used as received from Polymer Source (Montreal, Quebec). Hydrosilylation is used to attach LC mesogens to the pendant 1,2-polybuatiene vinyl groups [19, 20, 21, 22]. This method is chosen because it is compatible with a wide range of functionalities and limits the exposure of the polymers to only one reaction. Also, various mesogenic units can be attached to the pendant vinyl groups of 1,2-polybutadiene, so a homologous series of polymers of identical backbone length may be prepared, one of the advantages of a "polymer analogous approach." Here, we describe the attachment of a particular "side-on" type mesogen, 2,5-di(4-butoxybenzoate)-benzaldehyde (BB), to produce LC triblock ABASiBB and LC homopolymer HSiBB (Fig. 2.1).

The synthesis of this mesogenic unit was similar to that used by researchers making polyacrylates [23, 24]. In the first step of the reaction (Fig. 2.2) 4-butoxybenzoic acid (25 g, 0.127 mol) was

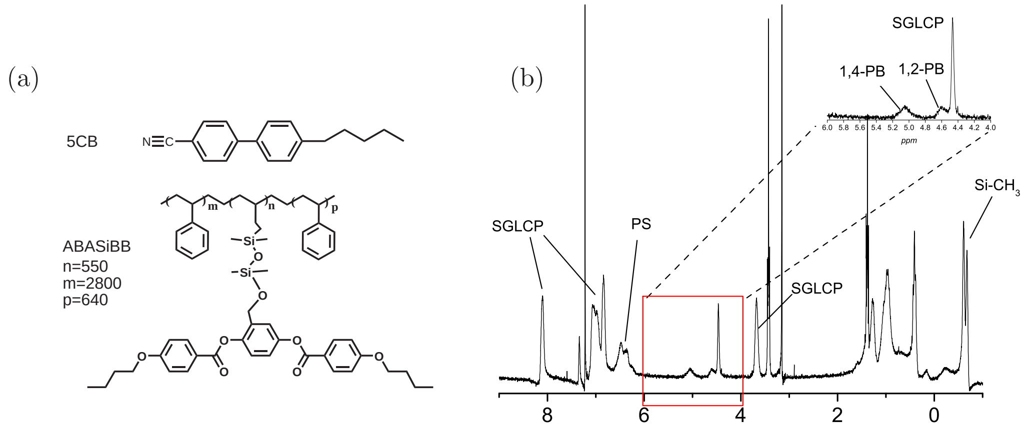

Figure 2.1: (a) Chemical structure of LC 5CB and the end-associating triblock copolymer ABASiBB used in this study and (b) an NMR of ABASiBB.

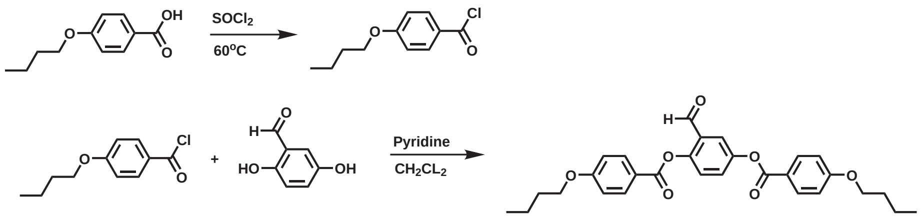

Figure 2.2: Synthesis of LC side-group mesogen

converted into 4-butoxybenzoyl chloride using a large excess of $SOCl_2$ (20 mL, 0.275 mol) as the solvent at 60 ^{o}C for one hour. Excess $SOCl_2$ was removed by evaporation under vacuum at 60 ^{o}C. 4-butoxy-benzoyl chloride was added at 20% excess to 2,5-dihydroxybenzaldehyde (7 g, 0.056 mol, Lancaster Chemical) in a dichloromethane (DCM) (50 mL) solution with anhydrous pyridine (20 mL), and the reaction was allowed to proceed at room temperature for several hours. The product 2,5-di(4-butoxybenzoate)-benzaldehyde was purified by liquid-liquid extraction using DCM and an aq. 1 N solution of HCl, followed by another extraction using DCM and a saturated aqueous solution of $NaHCO_3$. The product was further purified by recrystallization in ethanol for a yield of 60%.

The spacer was attached to the aldehyde via a hydrosilylation reaction using Wilkinson's catalyst, chlorotris(triphenylphosphine)-rhodium (I) [23] (Fig. 2.3). 3,5-di(4-butoxybenzoate)-benzaldehyde (3 g, 0.0057 mol) was mixed with Wilkinson's catalyst (20 mg) and ten molar equivalents of 1,1,3,3-tetramethyl disiloxane (TMDS) (15 mL, 0.085 mol) in anhydrous toluene (30 mL). The reaction was allowed to progress for 40 min at 60 ^{o}C, and then excess TMDS was removed in vacuo at 60 ^{o}C. The

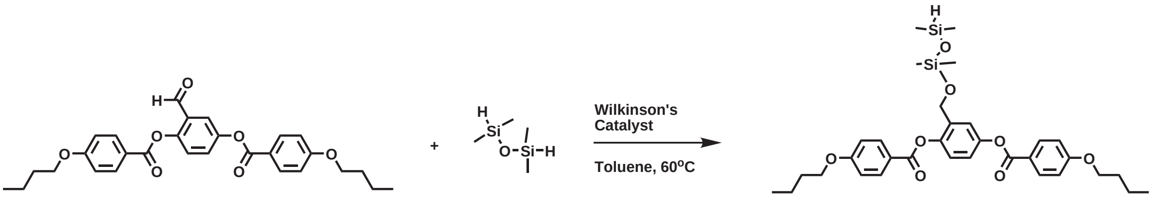

SiBB

Figure 2.3: Preparation of SiBB by attachment of siloxane spacer to LC side-group mesogen

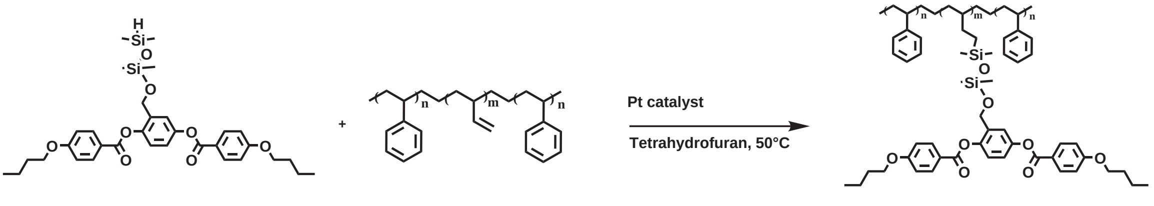

ABASiBB

Figure 2.4: Coupling reaction to attach LC side-group mesogen to ABA polymer

product 1,4-bis(4-butoxybenzoate)-2-methyl[(1,1,3,3-tetramethyl-disiloxane)oxy]-benzene (SiBB) was purified on an anhydrous silica gel column. The anhydrous column was prepared by first drying the silica under argon while heating it with a propane torch. Anhydrous hexane was then added to make a slurry and set up the column. The column was sealed with a septum and purged with argon while loading the product. The mesogen was added to the column in an anhydrous solution of toluene, and a solvent mixture of 10% anhydrous ethyl acetate in hexanes was used as the eluent. The yield of SiBB from the hydrosilylation step was 55%.

To attach the LC side group, ABA prepolymer (100 mg, 0.00088 mol vinyl groups) was dissolved in anhydrous THF (40 mL) and combined with three molar equivalents of SiBB (1.7 g, 0.0026 mol). A few drops of platinum catalyst PC085 was added and the mixture was stirred at 50 ^{o}C for a period of four days (Fig. 2.4).

To monitor the reaction progress, a small sample was taken periodically and proton NMR was performed to observe the disappearance of the vinyl peak near $\Delta = 4.9$ ppm. When the size of the vinyl peak did not change significantly over two consecutive readings, the reaction was quenched by adding 5 mL of styrene followed by stirring for one more day at 50 ^{o}C. The reaction solution was then concentrated under a stream of air, and the product was precipitated by the addition of a solution of 50 ppm 2,6-bis(1,1-dimethylethyl)-4-methylphenol (BHT) in methanol (5 mL). The product was purified by dissolving in THF and precipitating out in methanol five times. The polymer was then stored in the bulk at 0 ^{o}C.

The conversion was found by comparing the integrated area for the peaks corresponding to both the 1,2-polybutadiene and mesogen at 4.7-4.9, with the peak corresponding to the alkyl chain on the mesogen (Fig. 2.1b). Comparison of the areas of the peaks allowed determination of the degree of attachment of the side-group. The fraction of 1,4-polybutadiene groups in the prepolymer was determined from an NMR of the ABA prepolymer by comparing the peaks at 5.3 and 5.0 ppm.

2.3.8 Mixing of nematic gels

To create nematic gels, the copolymers were dissolved together with 4-pentyl-4′-cyanobiphenyl (5CB) (Fig. 2.1a) in dichloromethane, and the solvent was subsequently removed by blowing air over the mixture until it became milky white. It was then placed in a vacuum at room temperature for two days. To ensure that the gel was completely dry, the gel was periodically heated well into the isotropic phase (approximately 45 ^{o}C) and stirred periodically during the drying process.

2.4 Results

2.4.1 Polymer characteristics

The SGLCP copolymer ABASiBB and homopolymer HSiBB are rubbery, LC polymers at room temperature (Tab. 2.1). The low T_g of HSiBB can be attributed to the presence of tetramethyl-disiloxane in the mesogenic group. Similar polymers without siloxane typically have higher T_{NI}s [25, 26]. No T_g was observed for the ABASiBB midblock down to -30 ^{o}C, which may be due to the significant content of unconverted butadiene groups in the backbone. A T_g was also not observed for the polystyrene endblocks. The PDIs of the SGLCPs are higher than those of the prepolymers due to minute crosslinking of the polymers.

The type of LC order was inferred from the textures they exhibited when observed under POM.

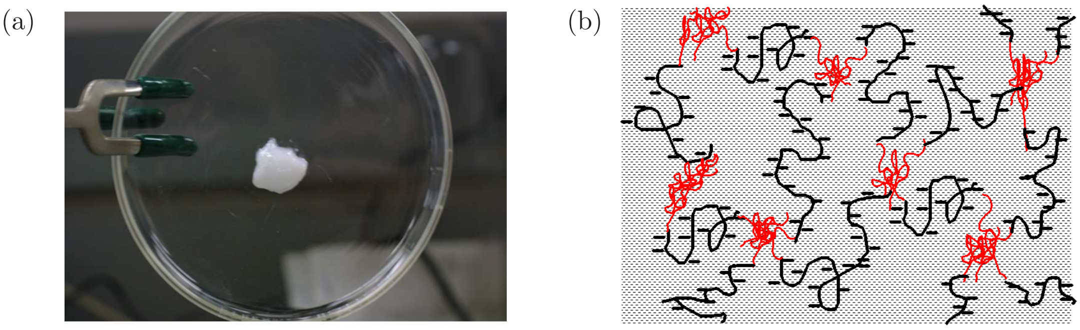

Figure 2.5: (a) A sample of LC physical gel, and (b) a schematic of the LC triblock gel. In the schematic, the speckled background represents the LC solvent 5CB, the dark black lines represent the SGLCP midblock, and the red chains represent the polystyrene endblocks.

Table 2.1: Polymer characteristics. “H” is the 1,2-polybutadiene prepolymer and “ABA” the polystyrene-*block*-1,2-polybutadiene-*block*-polystyrene triblock prepolymer. “HSiBB” and “ABASiBB” are the homopolymer and triblock SGLCPs, respectively. The number average molar mass (M_n) of the SGLCPs were determined by combining two measurements: GPC, to determine the size of the prepolymer, and ^{1}H NMR, to determine the fractional conversion to mesogenic side groups. The M_n of the different blocks of the ABA prepolymer were determined by Polymer Source using a MALLS system. DSC down to -30 ^{o}C did not detect a T_g for ABASiBB.

				LC BLock Composition				
Polymer	Total M_n $(\frac{\text{kg}}{\text{mol}})$	PDI	LC Block M_n $(\frac{\text{kg}}{\text{mol}})$	1,2 PB (mol %)	1,4 PB (mol %)	Mesogen (mol %)	T_{NI} (^{o}C)	T_g (^{o}C)
H	63	1.04	0	97	3	0	N/A	
HSiBB	713	1.08	713	8	3	89	120	7.7
ABA	270	1.26	N/A	86	14	N/A	N/A	-15.8,105.9
ABASiBB	1445	1.40	1321	16	14	70	74	<-30

Both ABASiBB and HSiBB had textures characteristic of nematic LCs. This is consistent with previous studies of side-on LC polymers [27]. The reduced isotropization temperature in the triblock as compared to the homopolymer is consistent for a variety of polymers with the same backbone and different side groups [22]. This is attributed both to the reduced number of LC side groups in the triblock relative to the homopolymer and to the presence of PS endblocks.

At temperatures below the T_{NI} of 5CB, 35 ^{o}C, HSiBB and ABASiBB were fully soluble in 5CB at all concentrations tested (0 - 20 wt %). From 35 ^{o}C up to 45 ^{o}C, solutions of HSiBB in 5CB exhibited a broad nematic-isotropic biphasic region at the concentrations tested. On the other hand, mixtures of ABASiBB in 5CB had a sharp nematic-isotropic transition, with a biphasic region narrower than 1 ^oC starting at 35 ^oC.

2.4.2 Monodomain alignment of LC gels

With only 5 wt % ABASiBB added to 5CB, the mixture forms a gel that does not flow (Fig. 2.5). When heated above its T_{NI} of 35 ^oC, however, the gel becomes clear and flows like a liquid. Furthermore, the gel has a homogeneous nematic texture under the optical microscope. Micron-sized thread-like aggregates have previously been observed for block copolymers in LC solvents [28], but these aggregates were only found for block copolymers with LC block weight fractions less than 90%. The present polymers have an LC block weight fraction of approximately 90%.

Unaligned LCs strongly scatter light, due to a spatially varying director orientation [29]. This is also true for the LC gels, as can be seen in the photograph of the bulk gel sample (Fig. 2.5). However, the LC gels can be uniformly aligned into a clear state by shear, electric fields, or magnetic fields. Such alignment is useful for characterizing the anisotropic properties of the LC gel and for utilizing the gel in a practical device.

Shear-induced alignment is demonstrated for a 5 wt % ABASiBB gel under conoscopic imaging (Fig. 2.6). In conoscopic imaging, convergent polarized light is passed through a sample viewed under an optical microscope. A resulting interference pattern indicates monodomain alignment and also provides information about the director orientation in uniform LC monodomains [30]. The gel was placed in a shear cell that allows for conoscopic imaging and heated above its T_{NI}. While cooling below the T_{NI}, a strain of 500% was applied at a rate of 1.2 s^{-1}. This resulted in uniform alignment of the gel as indicated by the appearance of an interference figure (Fig. 2.6). The interference figure indicates that the nematic director is oriented slightly off-axis in the plane of the sample.

The preferred direction of alignment under shear results from the coupling of the director field to the polymer conformation. The pendant mesogens of HSiBB tend to orient parallel to the backbone, and shear causes the backbone to preferentially orient at an angle between 45^o and 90^o relative to the velocity gradient direction. The direction of alignment induced by shear varies with molecular structure of the SGLCP. In contrast to the present sample, polymers with transverse attachment of

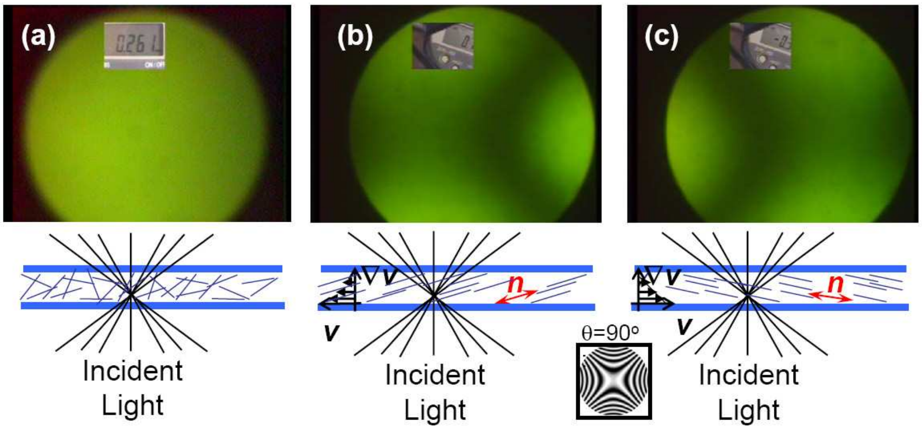

Figure 2.6: Conoscopic images of gel during shear. The sample under study is a 150 μm thick 5 wt % ABASiBB gel at 25 ^{o}C. (a) The gel before shear and (b),(c) during shear. The cross-section schematics under each image illustrate how light interacts with the corresponding polydomain (a) and single-crystal-like (b),(c) orientation of the director. The axes of (b) and (c) indicate the direction of shear v and define the angle θ of the director ($\boldsymbol{n}$). The interference figure (taken from Van Horn and Winter, *Appl. Opt.*, 40(13):2089-2094, 2001) below (b) and (c) is what is expected for the director aligned perfectly in the plane of the sample.

the LC side group exhibit homeotropic director alignment under shear, or alignment perpendicular to the cell substrates [31].

Gels can also be aligned by cooling from the isotropic to the nematic phase in a magnetic or electric field. In the case of magnetic field alignment, gels up to a concentration of 50 wt % polymer were amenable to alignment in approximately one hour under a field of 8.8 T. Similarly, gels can be aligned by cooling from the isotropic to the nematic phase while applying an electric field greater than 4 V/μm. The variety of methods available for alignment makes it possible to align LC gels with the director oriented either in the plane of the cell (using a magnetic field or shear) or perpendicular to the substrates (using an electric field).

2.4.3 Dynamic mechanical analysis

Rheometry was performed on single-phase solutions of the triblock copolymers in 5CB at various concentrations. As is often the case for block copolymer solutions, the viscoelastic relaxation spectrum changes shape with temperature rather than simply shifting to faster timescales with increasing temperature. This is particularly evident at temperatures near the isotropic-nematic transition temperature (Fig. 2.7). A dramatic change in G' and G'' is observed between T_{NI} and $T_{NI} + 2$ ^{o}C. This abrupt change cannot be attributed to a change in the overall mobility of the solvent; the dominant viscosity of 5CB in the nematic phase is only approximately 3 to 6 times higher than its isotropic viscosity [32].

The enhancement of the modulus in the nematic phase correlates with strong aggregation of the PS endblocks evident in small-angle neutron scattering (SANS) (see Chapter 5). Therefore, the increase in G' and G'' below T_{NI} can be attributed to microphase separation of the PS endblocks and the formation of a physical network in the nematic phase.

The gelation threshold in concentration is approximately 3 wt %. At 1 wt % (Fig. 2.7a) the gel is a viscoelastic liquid ($G'' > G'$), and the relaxation spectrum resembles power law behavior with an exponent of 2/3, i.e. ($G' = 3^{1/2} \cdot G'' \sim \omega^{2/3}$). With increasing polymer concentration, a plateau in G' emerges in the nematic phase: It is not present at 1 wt % but is clearly evident at 3 and 5 wt %, indicating gelation (Fig. 2.7). The gel displays solid-like ($G' >> G''$) rheological behavior in the nematic phase.

As the temperature increases toward the isotropization temperature (T_I), the plateau modulus decreases (Fig. 2.7 b,c), and in the isotropic phase, terminal behavior is observed. On cooling, the gel recovers its initial modulus, and therefore the gel thermoreversibly transitions between a liquid-like state above the T_{NI} and a solid-like state in the nematic phase below the T_{NI}.

At all concentrations there is a dense spectrum of relaxation times: There is no minimum in G'' for any of the concentrations examined, even when there is a broad plateau in G'. This is in contrast to the single relaxation time "Maxwell model" that describes some telechelic associative polymer gels [33].

2.4.4 Reversible electro-optic response

LC physical gels have a reversible electro-optic response and can be utilized as display layers. In typical twisted-nematic or super twisted-nematic displays, the director is uniformly aligned between substrates. Here, we are interested in a scattering-type device that can be reversibly switched

(a) 1 wt. %

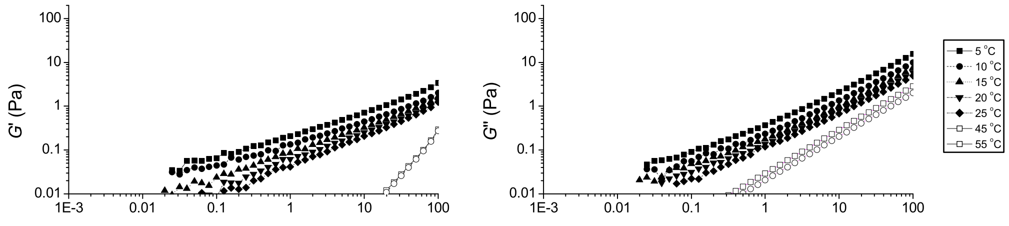

(b) 3 wt. %

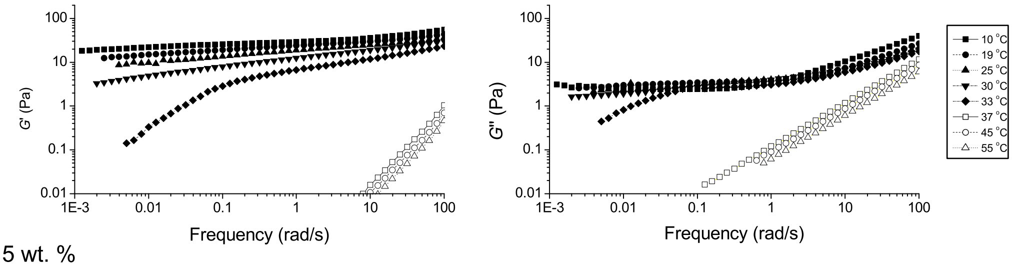

(c) 5 wt. %

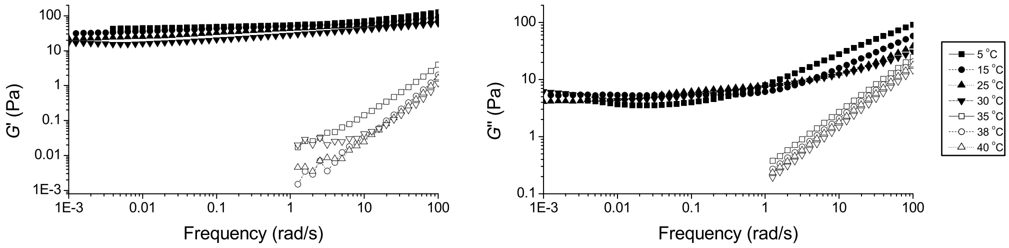

Figure 2.7: Dynamic storage modulus (G') and loss modulus (G'') of a mixture of (a) 1 wt %, (b) 3 wt %, and (c) 5 wt % of the side-on nematic triblock ABASiBB in 5CB. The mixture is isotropic for all $T \geq 35$ ^{o}C (open symbols) and nematic for $T \leq 35$ ^{o}C.

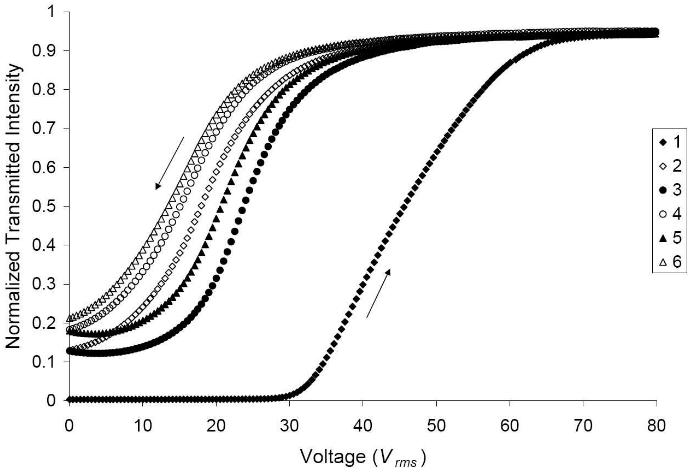

Figure 2.8: Transmitted intensity as a function of voltage V_{rms} for a 5 wt % gel in a 15 μm thick gap. The transmitted intensity when increasing the voltage (filled symbols) does not overlap with that when decreasing the voltage (empty symbols).

between a scattering polydomain state and a transmissive monodomain state [8, 14, 34]. These displays require a low (< 2.0 V/μm) threshold and a fast ($\sim$ 50 ms) response time.

In order to investigate the threshold for switching and for monodomain alignment, the transmitted intensity of a 15 μm thick gel layer was recorded as a function of applied voltage (Fig. 2.8). The transmitted intensity is normalized by the transmitted intensity of the gel in the isotropic state. The transmittance was initially linear, with voltage above a threshold field of 2.3 V/μm. With increasing voltage, the transmittance saturated to a maximum that was more than 90% that of the isotropic cell. Saturation was reached at approximately 4.5 V/μm for 5 wt % ABASiBB. Hysteresis is observed, meaning that the transmitted intensities while ramping voltage up are not superimposable on those recorded while ramping voltage down. After one full sweep, the threshold decreases, and the transmitted intensity at a voltage below the saturation voltage increases. If the gel is heated to the isotropic state and cooled, the gel recovers its initial electro-optic response.

The threshold field for switching was insensitive to gap thickness (Fig. 2.9). This is also true for PSLCs [11, 35] and for polymer-dispersed liquid crystals (PDLCs) [36] and originates from the elastic restoring force of the polymeric network throughout the volume of the gel rather than only at the surface alignment layers. In contrast, pure liquid crystals exhibit a threshold *voltage* for

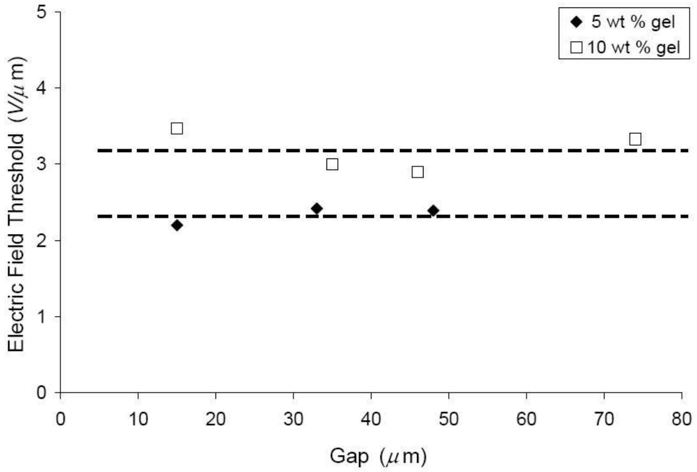

Figure 2.9: Electric field threshold for an electro-optic response in 5 and 10 wt % gels

switching, or a threshold field E_{th} that varies linearly with the gap thickness d, $E_{th} \sim d$ [36].

The transmittance of the LC gels were recorded transiently while an electric field was applied and removed. The time required for the transmitted intensity (I) to reach 90% of its maximum is defined as the orientation time, τ_{90}. On removal of the field, the time required for I/I_{max} to fall to 10% is defined as the relaxation time, τ_{10}. The response times were insensitive to gap thickness but highly dependent on the applied field (Fig. 2.10). For a 5 wt % gel, τ_{90} decreases strongly (from 10,000 ms to 100 ms) as the applied field increases from 2 V/μm to 6 V/μm. For the same gel, τ_{10} increases significantly (from 19 ms to 170 ms) with applied field (Fig. 2.10). The dynamic electro-optic response of the LC gels also depends on the polymer concentration and the sample history (Appendix A). For reference, the decay times are approximately 10 ms for PSLCs [35], 1 ms for small molecule gelators mixed with LC [37], 5 ms for PDLCs, and 5 ms for reverse-mode PDLCs [36].

2.5 Discussion

Physically associated triblock gels are LC systems with a fast electro-optic response and exceptional uniformity. The use of a triblock copolymer to form the self-assembled gels affords both flexibility in the molecular structure and control in the polydispersity. The resulting self-assembled gels are

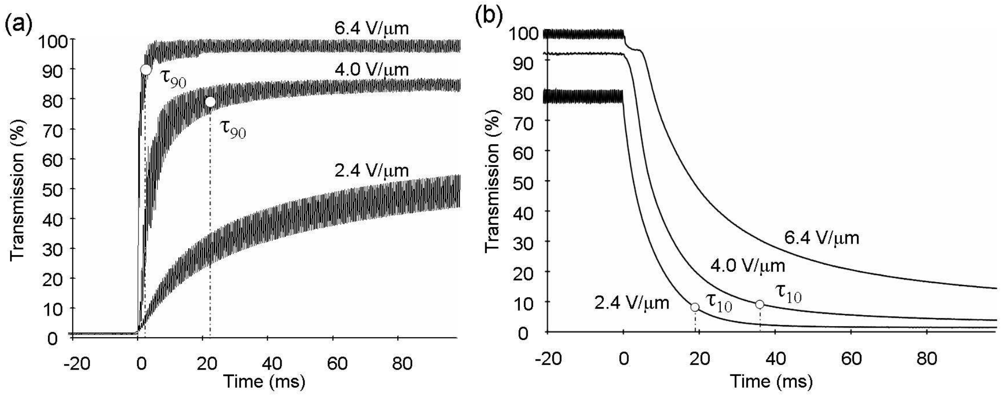

Figure 2.10: Transient electro-optic properties of a 5 wt % ABASiBB, 25 μm thick layer, under application of a.c. fields at 1000 Hz. (a) Switching the electric field on. The time required to reach 90% of the maximum transmittance is denoted τ_{90}. At the lowest field of 2.4 V/μm, the τ_{90} of 1000 ms is beyond the scale of the graph. (b) Switching the electric field off. The time required to return to 10% of the maximum transmittance is denoted τ_{10}. At the highest field of 6.4 V/μm, the τ_{10} of 170 ms is beyond the scale of the graph.

heterogenous at the scale of the microphase separated endblocks but homogenous at length scales much smaller optical wavelengths, making the gels potentially viable for display devices. Unlike the commonly studied PSLCs [38, 2, 8], the polymer strands are solvated by the host LC solvent 5CB, resulting in a higher degree of homogeneity and a potential for new effects in LC gels arising from the coupling of polymer conformation to LC order.

The electro-optic experiments suggest that an ABA nematic gel could be effectively used in a reflective electro-optic display by placing a layer of the LC gel in front of a uniform black background [39, 40]. Without an applied field, ambient light is scattered to produce a bright state analogous to the blank areas on a sheet of paper. Application of an electric field induces a transparent state that allows incident light to be transmitted and absorbed on the back surface, yielding a dark appearance, like ink on a printed page. At intermediate voltages, the ratio of absorbed to scattered light can be modulated to provide grayscale images. The most significant advantage of the present LC gels over PSLCs or PDLCs in a reflective display is the facile loading enabled by the self-assembled gels. However, several technical problems would have to be overcome before implementation of the gel in a commercially viable device, in particular the increased driving voltage and hysteresis. A potential solution to the latter problem would be to chemically crosslink the network after self-assembly.

Self-assembled LC gels also represent a significant step towards gaining a better understanding of LC networks. The unique properties of the self-assembled gel – namely its thermoreversible gel structure, optical clarity, and well-defined molecular architecture – make the gels useful tools for studying the coupling of LC order to a polymer network. Chapters 3 and 4 present experimental studies of novel equilibrium and dynamic properties that arise due to this coupling.

Bibliography

[1] H. Kawamoto. The history of liquid-crystal displays. *Proc. IEEE*, 90(4):460–500, 2002.

[2] R. A. M. Hikmet. Electrically induced light-scattering from anisotropic gels. *J. Appl. Phys.*, 68(9):4406–4412, 1990.

[3] K. Urayama, S. Honda, and T. Takigawa. Deformation coupled to director rotation in swollen nematic elastomers under electric fields. *Macromolecules*, 39(5):1943–1949, 2006.

[4] Y. Yusuf, Y. Ono, Y. Sumisaki, P. E. Cladis, H. R. Brand, H. Finkelmann, and S. Kai. Swelling dynamics of liquid crystal elastomers swollen with low molecular liquid crystals. *Phys. Rev. E*, 69(2):021710, 2004.

[5] Y. L. Yu, M. Nakano, and T. Ikeda. Directed bending of polymer film by light – miniaturizing a simple photomechanical system could expand its range of applications. *Nature*, 425(6954):145, 2003.

[6] SM Kelly. Anisotropic networks, elastomers and gels. *Liq. Cryst.*, 24(1):71–82, 1998.

[7] P. Xie and R. B. Zhang. Liquid crystal elastomers, networks and gels: advanced smart materials. *J. Mater. Chem.*, 15(26):2529–2550, 2005.

[8] I. Dierking. Polymer network-stabilized liquid crystals. *Adv. Mater.*, 12(3):167–181, 2000.

[9] A. Jakli, L. Bata, K. Fodor-Csorba, Rostas L., and Noirez L. Structure of polymer networks dispersed in liquid-crystals – small-angle neutron scattering study. *Liq. Cryst.*, 17(2):227–234, 1994.

[10] P. Gautier, M. Brunet, J. Grupp, L. Noirez, and E. Anglaret. Structure and texture of anisotropic nematic gels. *Phys. Rev. E*, 68:011709, 2003.

[11] C. C. Chang, L. C. Chien, and R. B. Meyer. Electro-optical study of nematic elastomer gels. *Phys. Rev. E*, 56(1):595–599, 1997.

[12] K. Urayama, Y. Okuno, T. Kawamura, and S. Kohjiya. Volume phase transition of liquid crystalline gels in a nematic solvent. *Macromolecules*, 35:4567–4569, 2002.

[13] T. Kato, T. Kutsuna, K. Hanabusa, and M. Ukon. Gelation of room-temperature liquid crystals by the association of a *trans*-1,2-bis(amino)cyclohexane derivative. *Adv. Mater.*, 10(8):606–608, 1998.

[14] N. Mizoshita, Y. Suzuki, K. Kishimoto, K. Hanabusa, and T. Kato. Electro-optical properties of liquid-crystalline physical gels: a new oligo(amino acid) gelator for light scattering display materials. *J. Mater. Chem.*, 12:2197–2201, 2002.

[15] K. Yabuuchi, A. E. Rowan, R. J. M. Nolte, and T. Kato. Liquid-crystalline physical gels: Self-aggregation of a gluconamide derivative in mesogenic molecules for the formation of anisotropic functional composites. *Chem. Mater.*, 12(2):440–443, 2000.

[16] M. Warner and E. M. Terentjev. *Liquid Crystal Elastomers.* Oxford University Press, Oxford, 2003.

[17] O. Stenull and T. C. Lubensky. Dynamics of nematic elastomers. *Phys. Rev. E*, 69:051801, 2004.

[18] E. M. Terentjev and M. Warner. Linear hydrodynamics and viscoelasticity of nematic elastomers. *Eur. Phys. J. E*, 4:343–353, 2001.

[19] A. Moment, R. Miranda, and P. T. Hammond. Synthesis of polystyrene-polysiloxane side-chain liquid crystalline block copolymers. *Macromol. Rapid Commun.*, 19(11):573–579, 1998.

[20] M. A. Hempenius, R. G. H. Lammertink, and G. J. Vancso. Well-defined side-chain liquid-crystalline polysiloxanes. *Macromol. Rapid Commun.*, 17(11):299–303, 1996.

[21] I. Ojima, M. Nihonyanagi, T. Kogure, M. Kumagai, S. Horiuchi, K. Nakatsugawa, and Y. Nagai. Reduction of carbonyl-compounds via hydrosilylation. 1. hydrosilylation of carbonyl-compounds catalyzed by tris(triphenylphosphine)chlororhodium. *J. Organomet. Chem.*, 94(3):449–461, 1975.

[22] M. D. Kempe, R Verduzco, N. R. Scruggs, and J. A. Kornfield. Rheological study of structural transitions in triblock copolymers in a liquid crystal solvent. *Soft Matter*, 2(5):422–431, 2006.

[23] M. A. Hempenius, R. G. H. Lammertink, and G. J. Cancso. Side-chain liquid-crystalline polysiloxanes via anionic polymerization: (n-undecyloxy)arenecarboxylic acid mesogens linked to poly(dimethylsiloxane-co-methylvinylsiloxane). *Macromolecules*, 30(2):266–272, 1997.

[24] M. C. Chang, H. W. Chiu, X. W. Wang, T. Kyu, N. Leroux, S. Campbell, and L. C. Chien. Phase transitions in mixtures of a side-on-side chain liquid crystalline polymer and low molar mass nematic liquid crystals. *Liq. Cryst.*, 25(6):733–744, 1998.

[25] S. Lecommandoux, M. F. Achard, F. Hardouin, A. Brulet, and J. P. Cotton. Are nematic side-on polymers totally extended? a sans study. *Liq. Cryst.*, 22(5):549–555, 1997.

[26] N. Leroux, P. Keller, M. F. Achard, L. Noirez, and F. Hardouin. Small angle neutron scattering experiments on "side-on fixed" liquid crystal polyacrylates. *J. Phys. II France*, 3:1289–1296, 1993.

[27] J. P. Cotton and F. Hardouin. Chain conformation of liquid-crystalline polymers studied by small-angle neutron scattering. *Prog. Polym. Sci.*, 22:795–828, 1997.

[28] M. Walther, H. Faulhammer, and H. Finkelmann. On the thread-like morphology of lc/i block copolymers in nematic solvents. *Macromol. Chem. Phys.*, 199:223–237, 1998.

[29] Pierre-Gilles de Gennes. *The Physics of Liquid Crystals.* Clarendon Press, Oxford, 2nd edition, 1993.

[30] Brett L. Van Horn and H. Henning Winter. Analysis of the conoscopic measurement for uniaxial liquid-crystal tilt angles. *Appl. Opt.*, 40(13):2089–2094, 2001.

[31] M. D. Kempe, N. R. Scruggs, R. Verduzco, J. Lal, and J. A. Kornfield. Self-assembled liquid-crystalline gels designed from the bottom up. *Nat. Mater.*, 3(3):177–182, 2004.

[32] H. Kneppe, F. Schneider, and N. K. Sharma. A comparitive study of the viscosity coefficients of some nematic liquid crystals. *Ber. Bunsenges. Phys. Chem.*, 85:784–789, 1981.

[33] Tom Annable, Richard Buscall, Rammille Ettelaie, and Diane Whittlestone. The rheology of solutions of associating polymer: Comparison of experimental behavior with transient network theory. *J. Rheol.*, 37(4):695–726, 1993.

[34] David Coates. Polymer-dispersed liquid crystals. *J. Mater. Chem.*, 5(12):2063–2072, 1995.

[35] R. A. M. Hikmet and H. M. J. Boots. Domain structure and switching behavior of anisotropic gels. *Phys. Rev. E*, 51(6):5824–5831, 1995.

[36] I.-C. Khoo and S.-T. Wu. *Optics and Nonlinear Optics of Liquid Crystals.* World Scientific, Singapore, 1993.

[37] N. Mizoshita, K. Hanabusa, and T. Kato. Fast and high-contrast electro-optical switching of liquid-crystalline physical gels: Formation of oriented microphase-separated structures. *Adv. Funct. Mater.*, 13(4):313–317, 2003.

[38] D.J. Broer, H. Finkelmann, and K. Kondo. In-situ photopolymerization of an oriented liquid crystalline acrylate. *Makromol. Chem., Macromol Chem. Phys.*, 190:185–194, 1988.

[39] H. E. A. Huitema, G. H. Gelinck, J. B. P. H. van der Putten, K. E. Kuijk, C. M. Hart, E. Cantatore, P. T. Herwig, A. J. J. M. van Breemen, and D. M. Leeuw. Plastic transistors in active-matrix displays. *Nature*, 414:599, 2001.

[40] D. K. Yang, L. C. Chien, and J. W. Doane. Cholesteric liquid-crystal polymer dispersion for haze-free light shutters. *Appl. Phys. Lett.*, 60(25):3102–3104, 1992.

Chapter 3

Buckling Instability in Physical LC Gels

The work described in this chapter was a collaborative effort with Professor Robert B. Meyer and his graduate student Guangnan Meng at Brandeis University. We also acknowledge helpful discussions with Professor Mark Warner (Cavendish Laboratory, Cambridge University).

Reproduced in part with permission from *Physical Review Letters*, (96):147802. Copyright 2006 The American Physical Society.

3.1 Abstract

We observe in a nematic gel a low-energy buckling deformation arising from soft and semi-soft elastic modes. The self-assembled gel is prepared by dissolving a triblock copolymer having a side-group liquid crystalline midblock and polystyrene endblocks in a nematic liquid crystal. Under polarized optical microscopy we observe a striped texture that forms when gels uniformly aligned at 35 ^{o}C are cooled to room temperature. We model the instability using the molecular theory of nematic rubber elasticity, and the theory correctly captures the change in pitch length with sample thickness and polymer concentration. This buckling instability adds to the library of fascinating texture transitions observed in liquid crystalline elastomers and gels.

3.2 Introduction

Rubbers, or elastomers, are unique in their ability to undergo large shape changes under external forces and then snap back to their initial shape when the forces are removed [1]. Elastomers are comprised of long, rubbery polymer strands connected together by covalent or physical bonds. These strands are initially randomly coiled, but they can stretch and change their configuration to accommodate large shape changes. In a liquid crystal (LC) elastomer, the network strands are LC polymers, and they have an anisotropic conformation that is temperature dependent and also affected by external electric and magnetic fields. Similarly, an LC gel is composed of an anisotropic polymer network swollen with solvent. Unlike conventional elastomers or gels, LC elastomers and gels are predicted to undergo "soft" and "semi-soft" deformations in which they can change shape at little cost to the free energy [2, 3, 4, 5]. These low-energy deformations are enabled by the anisotropy in the polymer network strands; when a strain is imposed on an LC elastomer, the network strands can accommodate the strain by rotating their sense of anisotropy instead of deforming the end-to-end distance of the chains, which is energetically more costly. Soft deformations oftentimes give rise to periodic textures [6], and they can also result in significant shape changes to temperature [2] or other external influences such as UV light [7, 8, 9].

Recently, we produced an LC gel by the physical association of a copolymer comprised of a side-group LC polymer (SGLCP) midblock and polystyrene (PS) endblocks [10, 11] (Fig. 3.1). When the LC gel is uniformly aligned and confined between rigid plates, it exhibits a reversible, striped texture change with small changes in temperature. Similar striped textures have been observed in LC elastomers[6, 4], but the instability observed here is unique for its geometry and sensitivity to small changes in temperature. We present the details of the striped texture in the physical gels, and we formulate a description of the instability based on the molecular theory of nematic rubber elasticity. The theory accounts for the changing network anisotropy, which in an unconfined sample would cause the gel to change shape macroscopically. Instead, due to the confining substrates which impose a no-slip condition, the gel undergoes a semi-soft deformation that involves a periodic modulation of the nematic director; in other words, the gel "buckles." The theory correctly accounts

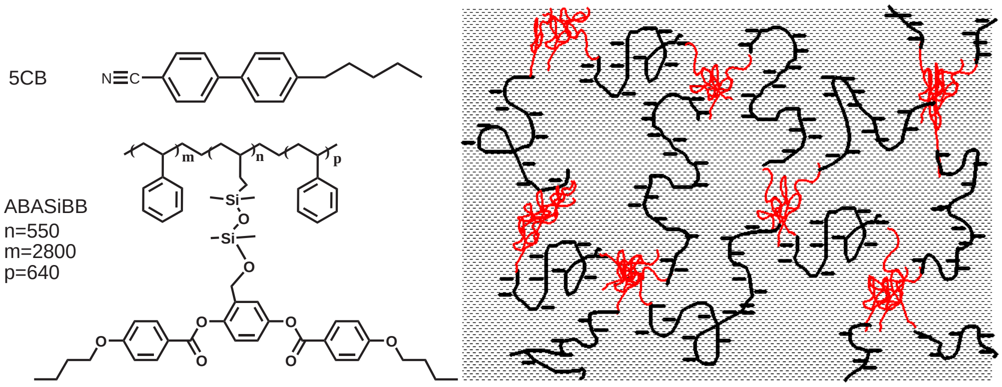

Figure 3.1: (a) Chemical structure of LC 5CB and the end-associating triblock copolymer used in this study, and (b) a schematic of the LC gel. The midblock is a random copolymer of LC side-group and butadiene monomer, with the LC side-group composing approximately 70 mol % of the midblock. The polydispersity ($\frac{M_w}{M_n}$) of the triblock is approximately 1.6, as measured by gel-permeation chromatography. In the schematic, the speckled background represents the LC solvent 5CB, the dark black lines represent the SGLCP midblock, and the red chains represent the polystyrene endblocks.

for the observed dependence of the stripe texture pitch and threshold temperature on the sample thickness and polymer concentration.

3.3 Experimental

The triblock copolymer was prepared by polymer-analogous synthesis starting with a polystyrene – *block* – 1,2-polybutadiene – *block* – polystyrene triblock copolymer, as described in Chapter 2. The self-assembled gels are prepared by dissolving the resulting high molecular weight ($\sim$ 1500 kg/mol) PS - SGLCP - PS triblock copolymer in the nematic LC 4-cyano-4′-n-pentylbiphenyl (5CB) (Fig. 3.1) [10]. The polystyrene block is considerably less soluble than the SGLCP block in 5CB, and in the nematic phase of 5CB the endblocks form aggregates which physically crosslink the triblock polymers. The resulting self-assembled network has a uniform molecular weight between crosslinks defined by the size of the SGLCP midblock.

In this work, we study gels with polymer concentrations of 10 wt % or less. Samples were loaded into cells with well-defined gap spacings and alignment layers. For gaps smaller than 10 μm, we used cells purchased from LC Vision. The cells consist of indium-tin-oxide coated glass plates with a layer of SiO_2 to induce planar alignment. For gaps larger than 10 μm, we used glass slides with teflon spacers and a rubbed polyimide layer for alignment. The cell thickness was determined with a UV/vis spectrophotometer by interferometry for gaps smaller than 10 μm [12] or by measuring the thickness with a micrometer for larger gaps. The nematic gels thermoreversibly transition to a viscous liquid when heated above the nematic-isotropic phase transition temperature (T_{NI}) of 5CB, 35.2 ^{o}C, and this allows for easy loading of the gel into the cell gap.

A magnetic field or shear was used to form uniform nematic monodomains. In the first case, the gel was placed in an 8.8 T magnetic field oriented parallel to the desired director orientation, heated above its T_{NI}, and allowed to cool to room temperature. After removing the cell from the magnetic field, the cell was heated to 34 ^{o}C and then cooled back down to room temperature at 1 ^{o}C/min to remove any residual irregularities. In some cases it was easier to use shear to align the sample. Shear proved effective in eliminating bubbles and defects at the solid-gel interface that were difficult to eliminate using magnetic field alignment. In order to shear align the sample, the sample was loaded into a Mettler FP 82 hot stage and the temperature set to 34.5 ^{o}C while the top slide was carefully moved back and forth across the sample.

3.4 Results

3.4.1 Details of the stripe texture

Gels that are uniform monodomains at 35 ^{o}C develop a striped texture visible under polarized optical microscopy when cooled to room temperature (Fig. 3.2). The periodic texture reversibly disappears and reappears when the gel is heated above and then cooled below a threshold temperature for stripe formation, and the pitch length of the striped texture is independent of temperature. The stripes run perpendicular to the initial director orientation $\underline{n}_o$. Rotating the crossed polarizer/analyzer pair by approximately $\pm 15^o$ relative to $\underline{n}_o$ maximizes the contrast between dark and bright bands, and the regions in the sample that appear dark at $+15^o$ appear bright at -15^o and vice-versa (Fig. 3.2). The stripes are less evident but still visible when the polarizers are aligned with $\underline{n}_o$. These observations indicate that the director rotates within the plane and in opposite directions in adjacent stripes but

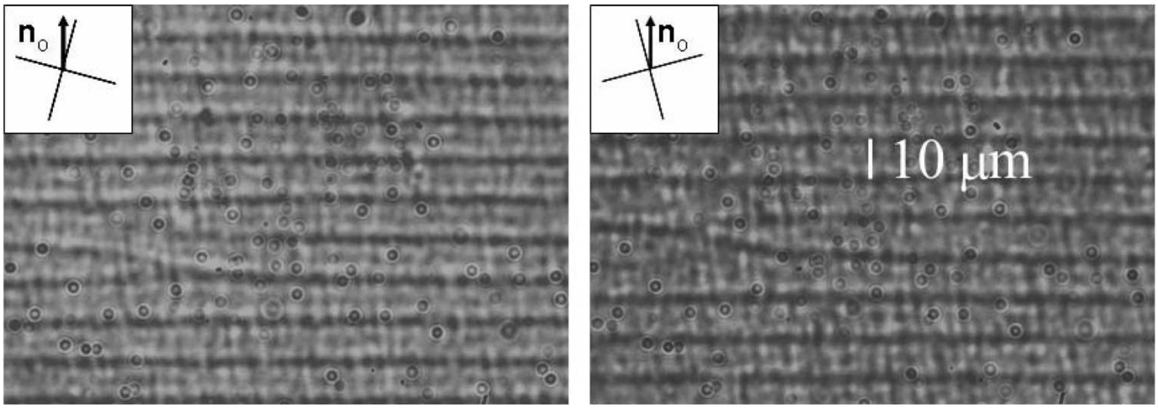

Figure 3.2: A 5 wt % gel in a 25 μm gap at 20.0 ^{o}C viewed with a polarizing optical microscope. The orientation of the director imprinted during crosslinking n_o and the orientation of the crossed polarizers is shown in the top left-hand corner of each image. Note that the dark lines, which represent regions in which the director is locally aligned with an axis of the crossed polarizers, shift positions in the left- and right-hand images, which were taken for the same sample in the same position and orientation but with a different orientation of the crossed polarizers. The positions of the extinction bands in the images are shifted relative to each other, and this indicates a spatially varying director orientation in the sample. The scale bar in the image shows the pitch length of approximately 10 μm for this particular sample.

does not preclude an out-of-plane rotation of the director coupled with this in-plane rotation.

The characteristics of the striped texture depend on the sample thickness and polymer concentration. The pitch length is larger in thicker samples and more dilute gels (Fig. 3.3). Stripes do not appear when the gap is too thin or the polymer concentration too dilute. In the case of a 5 wt % gel, stripes do not appear in 4- and 9-μm-thick cells but they do appear at larger gap thicknesses. For 10 wt % gels, stripes appear in the thinnest gaps tested, 4 μm.

3.4.2 Mathematical model

We propose that the buckling instability arises from a combination of rubber elasticity and LC elasticity, and that the instability represents a periodic network strain coupled to a periodic rotation of the director. We can formulate a molecular model of the instability by utilizing the theory for nematic rubber elasticity developed for LC elastomers [2, 13]. This theory assumes that the network is composed of anisotropic, gaussian chains and neglects excluded volume interactions. The anisotropic conformation of the polymer strands can be described by a step-length tensor $l_{ij} = l_\perp \delta_{ij} + (l_\parallel - l_\perp) n_i n_j$, where $l_\perp$ and $l_\parallel$ are the step lengths perependicular and parallel, respectively,

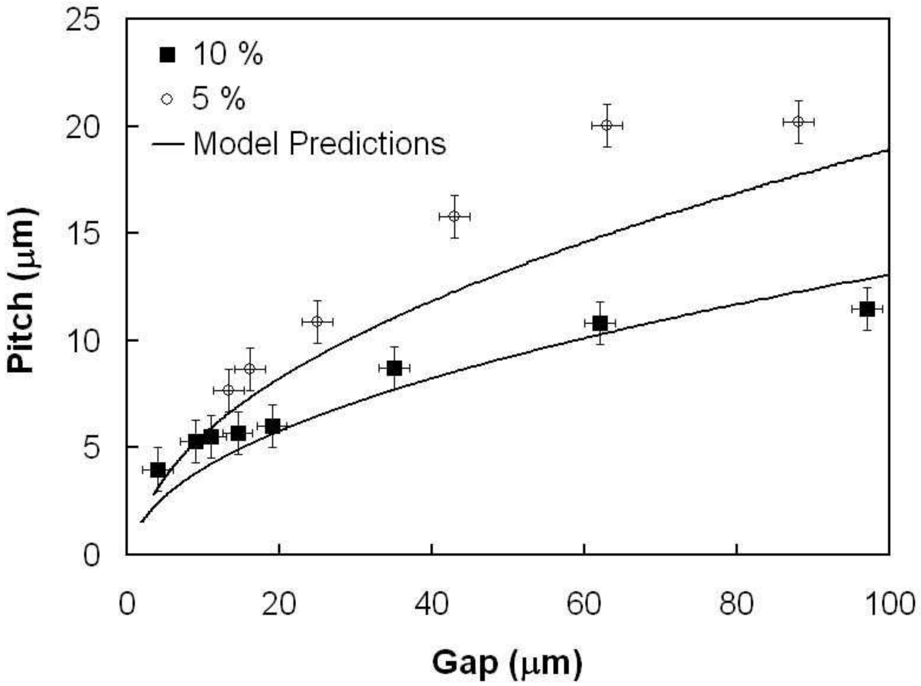

Figure 3.3: Dependence of pitch on gap in 10 and 5 wt % polymer gels.

to the nematic director for a freely jointed chain. These step lengths are directly related to the mean square end-to-end distance, $\langle R_i R_j \rangle = \frac{1}{3} l_{ij} L$, where L is the arc length of the polymer chain. A more useful expression relates the ratio of the step lengths to the ratio of the radii of gyration of the chain, $\frac{l_\parallel}{l_\perp} = (\frac{R_\parallel}{R_\perp})^2$. For the present polymer, which has a strongly prolate conformation (see Chapter 5, Fig 5.1), r is greater than 1 and decreases towards 1 as the temperature increases towards the T_{NI}. The ratio of the step lengths $\frac{l_\parallel}{l_\perp}$ is denoted as the network anisotropy r, and the anisotropy during crosslinking is denoted as r_o.

The free energy density of the gel consists of three terms: ideal nematic network elasticity, non-ideal nematic network elasticity, and Frank elasticity (Eq. 3.1). The free energy cost of deforming the gel includes the contribution of the network strands, expressed in terms of the deformation gradient tensor λ_{ij} (see Chapter 1). The ideal nematic elastic term is weighted by the rubber modulus μ. The non-ideal, or semi-soft, contribution is weighted by μ and the semi-softness parameter α. Semisoft elasticity arises from imperfections in the nematic network such as compositional fluctuations [4]. The last term is the Frank elastic term, which is a penalty for non-uniform director fields. We make the one-constant approximation [14] with Frank elastic constant K.

$$\begin{aligned} F \;=\;& \frac{1}{2}\mu\left(Tr[\underline{\underline{l_o}}\cdot\underline{\underline{\lambda}}^T\cdot\underline{\underline{l}}^{-1}\cdot\underline{\underline{\lambda}}]\right)+ \\ & \frac{1}{2}\mu\alpha\left(Tr[(\underline{\underline{\delta}}-\underline{n_o}\;\underline{n_o})\cdot\underline{\underline{\lambda}}^T\cdot\underline{n}\;\underline{n}\cdot\underline{\underline{\lambda}}]\right)+ \qquad (3.1)\\ & \frac{1}{2}K\left((\nabla\cdot\underline{n})^2+(\underline{n}\cdot\nabla\times\underline{n})^2+(\underline{n}\times\nabla\times\underline{n})^2\right) \end{aligned}$$

In order to model the phenomena, we start with a macroscopically uniform nematic gel in which the director $\underline{n}$ is aligned in a unique direction parallel to the substrates of the cell. Below a critical temperature, r becomes sufficiently large that the gel buckles. We assume that the director stays in the $x-y$ plane and that the director orientation depends on x and z but is independent of y. (Fig. 3.4). Coupled to the director rotation is a network strain field described by the deformation gradient tensor λ_{ij}. At the interface with the cell ($z=\pm\frac{d}{2}$), the substrates impose the boundary conditions of no-slip. We analyze the behavior near the transition to the striped state, where we assume small values for the amplitudes of the director rotation and the displacements. The displacement field $\underline{\Delta}$ satisfies the conditions of no-slip at the substrates ($\underline{\Delta}=0$ at $z=\pm\frac{d}{2}$) and incompressibility ($\nabla\cdot\underline{\Delta}=0$). Also, the displacement field and director rotation are independent of y.

We can develop simple sinusoidal functions (Eq. 3.2) that satisfy the boundary conditions, as follows. First, we assume a simple sinusoidal dependence for the director orientation, $\phi\sim\cos kx$,

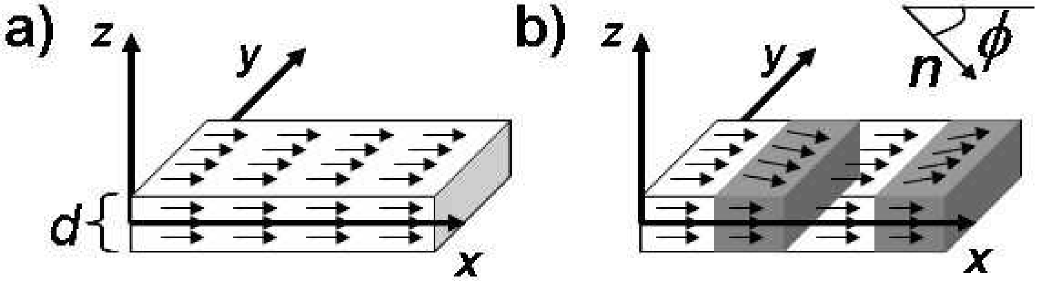

Figure 3.4: Nematic gel director orientation in **a)** the initial uniformly aligned state, and **b)** the striped state. The cell substrates are at $z=\pm\frac{d}{2}$.

where k is a constant that sets the wavevector for the distortion. Note that the pitch length in Fig. 3.2 corresponds to half the pitch of this periodic function, $\frac{\pi}{k}$. Since the director is confined to the $x-y$ plane, $\Delta_z = 0$ everywhere. It then follows, from the condition of incompressibility, that Δ_x is independent of x, and therefore Δ_x must also zero everywhere to be compatible with the symmetry of the nematic phase. Therefore, Δ_y is the only non-zero component of the displacement field $\underline{\Delta}$. The y displacement will be out of phase with the director rotation (the deformation gradient is in phase with the rotation), giving $\Delta_y \sim \sin kx$.

Since the director is coupled to the undeformed network at the substrates it retains the same orientation present during crosslinking. Director rotations independent of network deformations are in general costly, with $F \sim \frac{1}{2}\mu\phi^2$ for such rotations [2]. Therefore, $\phi = 0$ at $z = \pm\frac{d}{2}$. We also assume a simple sinusoidal dependence $\cos qz$, with $q = \frac{\pi}{d}$, for the director rotation and network strain fields along the z-axes. Note that this function decays to zero at the substrate interface. Finally, the terms ξ and γ set the amplitudes of the rotation and displacement fields, respectively (Eq. 3.2).

$$\begin{aligned} \phi(x,z) &= \xi\cos(qz)\cos(kx), \\ \Delta_y &= \gamma\cos(qz)\sin(kx), \\ \Delta_x &= \Delta_z = 0 \end{aligned} \tag{3.2}$$

We can calculate the deformation gradient tensor $\underline{\underline{\lambda}}$ from the displacement field ($\lambda_{ij} = \delta_{ij} + \frac{\partial \Delta_i}{\partial x_j}$), and substitution of $\underline{\underline{\lambda}}$ and $\underline{n}$ into Eq. 3.1 gives the free energy density of an incompressible nematic gel subject to the periodic deformation and director rotation described by Eq. 3.2. We Taylor expand this function in ξ around $\xi = 0$ and keep only terms of O(ξ^2) or greater. Next, we integrate the simplified free energy density over one wavelength of the deformation to obtain the average free energy density of the gel. Subtracting the energy of the uniformly aligned gel from this free energy gives the free energy relative to the monodomain state, so that a crossing from a positive to a negative value in the free energy indicates an onset of the buckling instability. (Eq. 3.3).

$$\begin{aligned} F = \quad & \frac{1}{8}K\xi^2(k^2+q^2) + \\ & \mu\{\frac{1}{8}\gamma^2(q^2+k^2r_o) + \frac{r_o}{4}\gamma\xi k(\frac{1}{r}-1) + \\ & \frac{1}{8}\xi^2(r_o - 1 + \alpha + \frac{1}{r} - \frac{r_o}{r})\} \end{aligned} \tag{3.3}$$

The first term in (Eq. 3.3) is the contribution from Frank elasticity and is always positive, as expected. The second, bracketed term (weighted by μ) is the contribution from nematic rubber elasticity, and it contains some terms that contribute negative values to the free energy. The various terms in the bracketed expression are grouped according to whether they arise from ideal or non-ideal nematic rubber elasticity. The first two terms in the bracketed expression, $\frac{1}{8}\gamma^2(q^2+k^2r_o)$ and $\frac{r_o}{4}\gamma\xi k(\frac{1}{r}-1)$, are the ideal or soft rubber elastic terms. The term $\frac{r_o}{4}\gamma\xi k(\frac{1}{r}-1)$ is always negative for $\gamma\xi > 0$ and is resposible for the buckling instability, while the term $\frac{1}{8}\gamma^2(q^2+k^2r_o)$ is always positive and increases the threshold to the buckled state.

The final term in the bracketed expression, $\frac{1}{8}\xi^2(r_o - 1 + \alpha + \frac{1}{r} - \frac{r_o}{r})$, is the contribution from non-ideal network elasticity. This term is always positive, and it arises from two sources of semi-softness, or non-ideality. The first source, weighted by α, accounts for compositional fluctuations or polydispersity in the molecular structure. α is always positive or zero, and a greater value of α indicates a greater degree of semi-softness. The second source of semi-softness arises from the anisotropy during crosslinking r_0. A perfectly soft network has $r_0 = 1$ and a perfect memory of the isotropic state [2]. Note that if $\alpha = 0$ and $r_0 = 1$, the semi-soft contribution vanishes.

In order to compute an anisotropy and wavevector for this general case, we look for the minimum value of r and critical wave vector k for which the right combination of infinitesimal displacement γ and rotation ξ costs zero energy (Eq. 3.4), signalling an instability as r passes through this value. For slightly larger r values, the amplitude of the instability grows rapidly, with the wavelength determined at the instability.

$$\gamma = \frac{k r_0 \xi (r-1)}{r(q^2 + k^2 r_0)} \tag{3.4}$$

The material parameters can be reasonably approximated from independent measurements or from known properties of the liquid crystal solvent 5CB. For example, the LC elastic constants K have been measured previously for 5CB at room temperature [12, 15] and have values of about 1×10^{-11} N. We measured the rubber modulus μ in a cone-and-plate rheometer and obtained a value of approximately 220 Pa for a 10 wt % gel and 50 Pa for a 5 wt % gel [10]. The endblocks associate at a temperature near the T_{NI} to form the gel, so we set the initial anisotropy r_o to the small value of 1.2. In addition to these parameters, we reasonably approximate the semi-softness parameter α to have a value of 0.05, based on previous studies of nematic elastomers [16].

3.5 Discussion

A periodic modulation of the nematic director is unexpected because it introduces a free energy contribution from Frank elasticity. The appearance of the stripes can be accounted for, however, by including the rubber elastic energy of the polymer network. (A periodic striped texture has also been observed in very thin (< 1 μm) films of small molecule nematic LC due to surface gradient terms in the elastic free energy expression [17, 18]. Our samples are thick enough that the surface gradient terms are not significant.) An SGLCP dissolved in a nematic solvent adopts an anisotropic chain conformation coupled to the nematic order of the solvent [10]. Based on prior literature on nematic elastomers [2], we expect that an unconstrained free standing gel will change shape: in the case of a strongly prolate alignment tendency, the gel will expand in the direction of director orientation with decreased temperature (our gel is too soft to carry out the same experiment). When constrained between glass plates, however, expansion of the gel in the direction of increasing anisotropy is prevented by the boundary conditions, and the network becomes increasingly frustrated as the temperature decreases. Increasing network elastic energy results in a buckling instability in which a periodic strain field reduces the rubber elastic free energy at the cost of a Frank elastic penalty.

Such a spontaneous deformation is possible only in nematic rubbers, where a coupling between the local nematic director orientation and macromolecular conformation significantly reduces the rubber elastic penalty associated with mechanical deformations, a phenomenon known as soft elasticty [2]. This coupling gives rise to macroscopic shape changes in nematic rubbers in response to heat and light and director rotations in response to strains.

It is instructive to look at the behavior predicted by Eq. 3.3 for various limiting cases. First, an infinitely small spatial frequency $k \approx 0$, or equivalently an infinitely large pitch, results in a positive free energy relative to the unbuckled state. This can be easily seen in Eq. 3.3 by noting that the only negative term in the expression, $\frac{r_o}{4}\gamma\xi k(\frac{1}{r}-1)$, disappears when $k = 0$. This indicates that there is always energetic penalty, from both LC elasticity and nematic rubber elasticity, for buckling in a sample of finite thickness. The penalty arises from the boundary condition which necessitates a bend distortion and shearing from the edges to the center of the sample.

In the case of an infinitely thick sample, $q \approx 0$, the penalties $\frac{1}{8}K\xi^2q^2$ and $\frac{1}{8}\gamma^2q^2$ for the bend distortion and shearing, respectively, vanish. If the gel is perfectly soft ($\alpha = 0$ and $r_0 = 1$), then the buckling instability carries no penalty from the rubber elastic term. This can be seen in the free energy expression (Eq. 3.3): In the limit $q \rightarrow 0$, the negative contribution $\sim r_o\gamma\xi k(\frac{1}{r}-1)$ can always compensate the positive contributions for any k by properly selecting γ and ξ. For $r > 1$, the buckling instability will always be favored over the monodomain state for a soft gel of infinite thickness. In the case of semi-soft ($\alpha > 0$ and/or $r_0 > 1$) gels in thick gaps, there is a finite threshold in r to the buckling instability.

The various contributions to the free energy are depicted graphically for a gel of finite thickness in Fig. 3.5a. The rubber elastic terms favor a large frequency. However, Frank elasticity goes inversely with the square of the wavelength, making very short wavelengths costly in energy. The final wavelength is a compromise of nematic rubber elasticity and Frank elasticity. The final wavelength is set by the rubber modulus μ, the Frank elastic constant K, the initial anisotropy r_0, and the semi-softness parameter α.

A comparison of the model prediction of the pitch and experimental results shows good qualitative

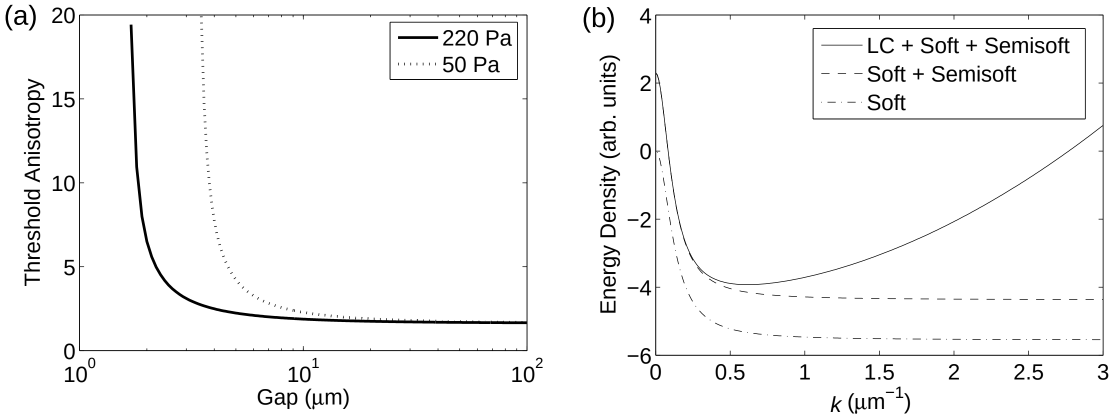

Figure 3.5: (a) Predicted value of the threshold anisotropy r_{th}, as a function of gap thickness d and rubber modulus μ. Bands form if the polymer has $r > r_{th}$. The values of μ correspond to those of the 5 wt % and 10 wt % gels. (b) The different components of the free energy expression (Eq. 3.3) for a gel with a modulus of 220 Pa, an initial anisotropy of 1.2, a present anisotropy of 3, a semi-softness parameter of 0.05, an LC elastic constant of 1×10^{-11} N, and a gap of 25 μm. The soft and semi-soft elastic parts refer to the ideal and non-ideal network elastic terms, respectively, and adding the LC part gives the full free energy density. The mimumum in the full free energy density corresponds to the predicted k for these sample conditions.

agreement (Fig. 3.3a). The model predicts the trends of increasing pitch with increasing gap and decreasing polymer concentration. The model also accounts for the disappearance of stripes at small gaps from a prediction of the threshold anisotropy (Fig. 3.5). Small-angle neutron scattering measurements show the anisotropy of the present midblock at 25^{o}C to be approximately 10 (see Fig. 5.2, Chapter 5. Based on this value, the model predicts that bands are suppressed for $d < 3.7$ μm for the 5 wt % gel and for $d < 1.9$ μm for the 10 wt % gel. As the gap decreases, q increases, increasing the cost of both Frank elasticity and nematic rubber elasticity (Eq. 3.3).

$$k = \sqrt{q\sqrt{\frac{\mu}{K}}\left(\frac{r-1}{r}\right) - \frac{q^2}{r_0}} \tag{3.5}$$

The functional dependence of the optimal wavevector on the gap has a square root dependence at large gaps (small q) (Eq. 3.5). At small enough gaps, however, for $q \sim \sqrt{\mu/K}$, the negative term in (Eq. 3.5) becomes comparable to the positive contribution. This would result in an increasing k with increasing q (longer pitch at smaller gap); however, this never occurs because the upper bound on q is $\sqrt{\mu/K}$.

To summarize, we have presented a stripe distortion that arises in uniformly aligned nematic gels in response to small temperature changes. A model based on the molecular theory of nematic rubber elasticity accounts for the observed experimental features: the onset of the instability with changes in the network anisotropy, the increase in the pitch with increasing sample thickness, the decrease in the pitch with increasing polymer concentration, and the disappearance of the instability at small sample thicknesses. The model indicates that the instability arises from a balance of Frank elasticity and polymer elasticity, resulting in a periodic structure on the length scale of micrometers.

The buckling instability in nematic gels is a remarkable transition that adds to the library of texture transitions observed in LC elastomers and gels. LC elastomers can show similarly striped states in response to mechanical strains [6, 19], and LC gels demonstrate non-uniform responses to external electric fields [20, 16]. These periodic textures in LC materials find analogy in an instability observed in deformable elastic crystals [21], which can develop an undulating texture at their surface in response to strains.

Bibliography

[1] P. J. Flory. *Principles of Polymer Chemistry.* Cornell University Press, Ithica, 1953.

[2] M. Warner and E. M. Terentjev. *Liquid Crystal Elastomers.* Oxford University Press, Oxford, 2003.

[3] M. Warner, P Bladon, and E. M. Terentjev. Soft elasticity – deformation without resistance in liquid-crystal elastomers. *J. Phys. II*, 4(1):93–102, 1994.

[4] H. Finkelmann, I. Kundler, E. M. Terentjev, and M. Warner. Critical stripe-domain instability of nematic elastomers. *J. Phys. II*, 7(8):1059–1069, 1997.

[5] E. M. Terentjev and M. Warner. Linear hydrodynamics and viscoelasticity of nematic elastomers. *Eur. Phys. J. E*, 4:343–353, 2001.

[6] I. Kundler and H. Finkelmann. Strain-induced director reorientation in nematic liquid single crystal elastomers. *Macromol. Rapid Commun.*, 16:679–686, 1995.

[7] H. Finkelmann, E. Nishikawa, G. G. Pereira, and M. Warner. A new opto-mechanical effect in solids. *Phys. Rev. Lett.*, 87(1):015501, 2001.

[8] M. Camacho-Lopez, H. Finkelmann, P. Palffy-Muhoray, and M. Shelley. Fast liquid-crystal elastomer swims into the dark. *Nat. Mater.*, 3:307–310, 2004.

[9] Y. L. Yu, M. Nakano, and T. Ikeda. Directed bending of polymer film by light – miniaturizing a simple photomechanical system could expand its range of applications. *Nature*, 425(6954):145, 2003.

[10] M. D. Kempe, N. R. Scruggs, R. Verduzco, J. Lal, and J. A. Kornfield. Self-assembled liquid-crystalline gels designed from the bottom up. *Nat. Mater.*, 3(3):177–182, 2004.

[11] M. D. Kempe, R Verduzco, N. R. Scruggs, and J. A. Kornfield. Rheological study of structural transitions in triblock copolymers in a liquid crystal solvent. *Soft Matter*, 2(5):422–431, 2006.

[12] I.-C. Khoo and S.-T. Wu. *Optics and Nonlinear Optics of Liquid Crystals.* World Scientific, Singapore, 1993.

[13] M. Warner and E.M. Terentjev. Nematic elastomers – a new state of matter? *Prog. Polym. Sci.*, 21:853–891, 1996.

[14] Pierre-Gilles de Gennes. *The Physics of Liquid Crystals.* Clarendon Press, Oxford, 2nd edition, 1993.

[15] K. Skarp, S. T. Lagerwall, and B. Stebler. Measurements of hydrodynamic parameters for nematic 5cb. *Mol. Cryst. Liq. Cryst.*, 60:215–236, 1980.

[16] E. M. Terentjev, M. Warner, R. B. Meyer, and J. Yamamoto. Electromechanical fredericks effects in nematic gels. *Phys. Rev. E*, 60(2):1872–1879, 1999.

[17] O. D. Lavrentovich and V. M. Pergamenshchik. Stripe domain phase of a thin nematic film and the k_{13} divergence term. *Phys. Rev. Lett.*, 74(7):979–982, 1994.

[18] V. M. Pergamenshchik. Spontaneous deformations of the uniform director ground state induced by the surfacelike elastic terms in a thin planar nematic layer. *Phys. Rev. E*, 61(4):3936–3941, 2000.

[19] G. C. Verwey, M. Warner, and E. M. Terentjev. Elastic instability and stripe domains in liquid crystalline elastomers. *J. Phys. II*, 6:1273–1290, 1996.

[20] C. C. Chang, L. C. Chien, and R. B. Meyer. Electro-optical study of nematic elastomer gels. *Phys. Rev. E*, 56(1):595–599, 1997.

[21] M. A. Grinfeld. The stress driven instability in elastic crystals: mathematic models and physical manifestations. *J. Nonlinear Sci.*, 3:35–83, 1993.

Chapter 4

Director Dynamics in Liquid Crystal Physical Gels

The work described in this chapter was done jointly with Neal Scruggs. We also collaborated with Professor Samuel Sprunt (Department of Physics, Kent State University) and Professor Peter Palffy-Muhoray (Liquid Crystal Institute, Kent State University). We thank Professor Sprunt's students, Sunil Sharma and Krishna Neupane, for their help with the light scattering experiments.

The contents of this chapter were submitted for consideration for publication in the journal *Soft Matter* on January 18th, 2007.

4.1 Abstract

Nematic liquid crystal (LC) elastomers and gels have a rubbery polymer network coupled to the nematic director. While LC gels and elastomers are expected to have a single, hydrodynamic relaxation mode, dynamic light scattering studies of self-assembled liquid gels reveal overdamped fluctuations that relax over a broad time scale. At short times, the relaxation dynamics exhibit the expected hydrodynamic behavior. In contrast, the relaxation dynamics at long times are non-hydrodynamic, highly anisotropic, and increase in amplitude at small scattering angles. We argue that the slower dynamics arise from coupling between the director and the physically associated network, which prevents director orientational fluctuations from decaying completely at short times. At long enough times the network restructures, allowing the orientational fluctuations to fully decay. Director dy-

namics in the self-assembled gels are thus quite distinct from those observed in LC elastomers, in both that they display soft orientational fluctuations at short times and that they exhibit at least two distinct relaxation modes

4.2 Introduction

Depolarized dynamic light scattering studies of nematic LCs give information about the dynamics of the nematic director. Small molecule nematic LCs have two independent hydrodynamic modes, corresponding to splay-bend and twist-bend elastic distortions of the axis of molecular orientational order (or director). These modes can be decoupled experimentally [1]. Addition of side-group liquid crystal polymer (SGLCP) to a nematic solvent significantly slows these relaxation processes [2], but qualitatively the relaxation dynamics are similar to those in small molecule LCs. In the case of an LC elastomer or gel, network elasticity enters into the director dynamics [3, 4, 5]. LC elastomers are weakly crosslinked LC polymers, and LC gels are made by swelling LC elastomers in an LC solvent. In LC elastomers and gels, the director fluctuations are coupled to deformations of the network.

Here, we study LC physical gels formed by end-associating triblock copolymers [6, 7]. Block copolymers are comprised of chemically distinct polymers covalently linked together. The present triblock copolymers consist of a side-group LC polymer (SGLCP) midblock flanked by polystyrene (PS) endblocks. When mixed with a small molecule nematic LC, the PS – SGLCP – PS triblock copolymer forms aggregated structures, known as micelles, due to the different solubilities of the PS and SGLCP blocks. The PS blocks are relatively insoluble in the small-molecule LC while the SGLCP block swells readily in the LC solvent, resulting in an interconnected micellar network when mixed with an LC solvent. A key feature of these LC gels is that the physical crosslinks can break and reform, and the network can therefore reconfigure over time. Also, we can efficiently produce highly uniform nematic samples because the LC physical gels self-assemble from field-aligned solutions on cooling through the isotropic-to-nematic phase transition. Such gels are therefore important and unique model systems for understanding the effect of a polymer network on director dynamics.

The focus of this paper is a dynamic light scattering study of orientational fluctuations in PS-

SGLCP-PS physical gels and, for comparison, in homopolymer solutions of the SGLCPs on which the gels are based. The gels reveal overdamped fluctuations that relax over a broad time scale – ranging from “short” times ($< 10^{-1}$ s and comparable to the director modes of the corresponding homopolymer solutions) out to much longer times ($>> 10^{-1}$ s). The faster relaxation exhibits the characteristic “q^2”-dependence on the scattering vector that is characteristic of hydrodynamic modes. We argue that the slow component of the fluctuations arises from the coupling of the nematic director to the physically associated polymers which restructure on much longer time scales. The expression of this slow “gel” mode is highly anisotropic – indeed, it is correlated with the scattering geometry in which the viscoelastic properties of homopolymer solutions are most significantly modified by the polymer component. The dynamics of physical LC gels, exhibiting a broadened spectrum combining *hydrodynamic* director modes and very slow relaxation associated with rearrangement of the gel structure, are thus quite distinct from previous studies of covalently bonded networks such as LC elastomers [5], where light scattering reveals only director modes that are *non-hydrodynamic*, due to a direct coupling of director rotation to network motion.

4.3 Experimental

Polymer-analogous synthesis was used to make SGLCP homopolymers and coil-SGLCP-coil triblock copolymers with mesogens attached either “end-on” or “side-on” (Fig. 4.1). The end-on and side-on polymers preferentially orient with the backbone perpendicular or parallel, respectively, to the nematic director, resulting in an oblate (end-on) or prolate (side-on) chain conformation [6]. Mesogenic side-groups were attached to the pendant vinyl groups of an anionically polymerized 1,2-polybutadiene (PB) homopolymer (65 kg/mol) or a polystyrene – *block* – (1,2-polybutadiene) – *block* – polystyrene (55 kg/mol PS, 120 kg/mol PB, 65 kg/mol PS) triblock copolymer according to published methods [7] (Fig. 4.1). The functionalized polymers contain a residual percentage of unmodified units in the form of unreacted 1,2-butadiene and non-reactive 1,4-butadiene present in the prepolymer (Table 4.1). All four polymers (Fig. 4.1) are nematic from room temperature up to a nematic-isotropic transition temperature (T_{NI}) (Table 4.1).

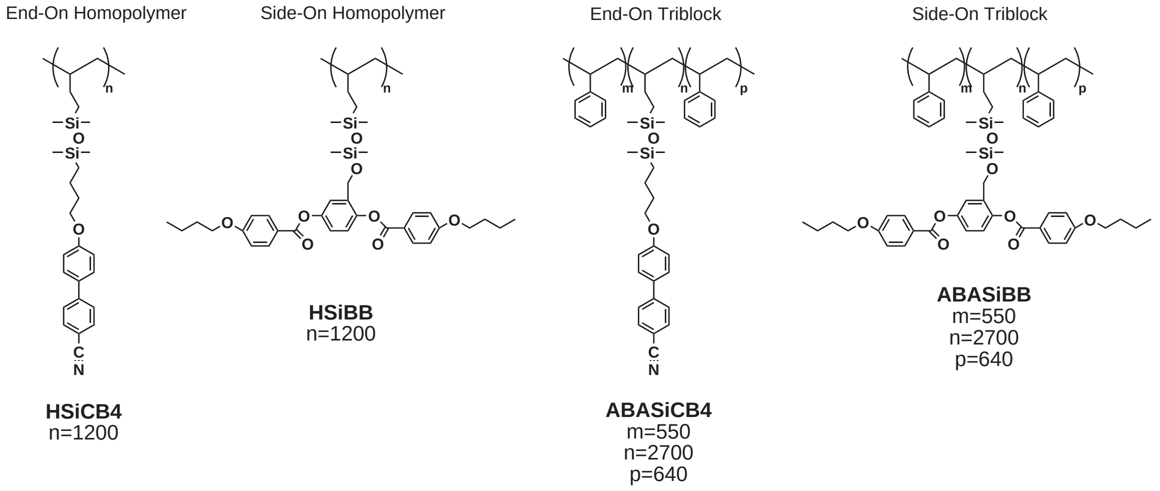

Figure 4.1: Chemical structure of the side-group LC homopolymers (HSiCB4 and HSiBB) and triblock copolymers (ABASiCB4 and ABASiBB).

Solutions of these polymers in the nematic LC 4-pentyl-4′-cyanobiphenyl (5CB) were prepared by dissolving the polymer and 5CB together in dichloromethane (DCM), then evaporating the DCM under vacuum for at least one day. In this study, we focus most of our attention on 5 wt % polymer solutions.

Mixtures of polymer in 5CB were loaded into cells consisting of glass plates separated by 4, 9, or 25 μm spacers. Cells having 4 or 9 μm gaps were purchased from LC Vision (Boulder, CO) and have SiO_2 alignment layers for homogeneous (planar) alignment. Cells having a 25 μm gap were purchased from EHC (Japan) and have rubbed polyimide alignment layers for homogeneous

Table 4.1: Polymer characteristics

				LC BLock Composition			
Polymer	Total M_n $\frac{\text{kg}}{\text{mol}}$	PDI	LC Block M_n $\frac{\text{kg}}{\text{mol}}$	1,2 Content (mol %)	1,4 Content (mol %)	Mesogen Content (mol %)	T_{NI} (°C)
H	63	1.04	N/A	97	3	N/A	N/A
HSiCB4	500	1.48	500	0	2	98	60
HSiBB	713	1.08	713	8	3	89	120
ABA	270	1.26	N/A	86	14	N/A	N/A
ABASiCB4	1200	1.16	1100	0	12	88	40
ABASiBB	1373	1.5	1249	21	14	65	70

alignment. All three cell types have 5 mm x 5 mm transparent indium-tin oxide (ITO) electrodes in their centers. Cells were filled with polymer/LC solutions by capillary action; homopolymer solutions readily flowed in at room temperature and triblock gels flowed readily when heated above the gel point (35 ^{o}C for ABASiCB4 and 33 ^{o}C for ABASiBB). Homopolymer solutions spontaneously aligned to form monodomains under the influence of the alignment layers. Gels were made to form homogeneous monodomains by heating them above the gel point then slowly cooling them inside the bore of an 8 T NMR magnet with the field parallel to the alignment direction. Gels were also aligned to form homeotropic monodomains by heating them above the gel point then cooling while applying a 15 $\mathrm{V_{rms}}$ potential difference across the ITO electrodes.

Aligned samples were mounted in a temperature controlled oven with optical access that was stabilized to better than $\pm$ 0.01 ^{o}C. The samples were illuminated with a focused, vertically polarized 20 mW HeNe laser beam (wavelength $\lambda_0 = 633$ nm) at normal incidence. Depolarized scattered light was collected at various scattering angles θ_s, with the optical scattering vector q lying in the horizontal plane. Monodomain LC samples were placed in the beam oriented so that the nematic director was either parallel to the incident polarization (vertical, V), perpendicular to both the incident polarization and the incident beam (horizontal, H), or parallel to the incident beam (parallel, P) (Fig. 4.2). The time autocorrelation of the scattered intensity ($< I(q,0)I(q,t) >$) collected at discrete angles was recorded in the homodyne regime. The resulting intensity autocorrelation functions were normalized by their maximum value, typically 1.95.

The H geometry corresponds to the twist-bend fluctuation mode of the LC director, with elastic energy density $K_2q_\perp^2 + K_3q_\parallel^2$ given approximately in terms of θ_s by $K_2k_o^2(n_\parallel - n_\perp)^2 + [K_3 + K_2(n_\parallel/n_\perp)]k_o^2 \sin^2\theta_s$. Here K_2, K_3 are twist, bend Frank elastic constants, $k_o = 2\pi/\lambda_o$, and $n_\perp$,$n_\parallel$ are the principal refractive indices of the uniaxial nematic medium. Since $n_\parallel/n_\perp - 1 << 1$, bend distortions dominate in the H geometry, except for small θ_s. In the P geometry, one again probes the twist-bend normal mode, with $K_2q_\perp^2 + K_3q_\parallel^2$ approximately equal to $[K_2 + K_3(n_\perp/n_\parallel)(1 - n_\perp/n_\parallel)]k_o^2 \sin^2\theta_s$. In this case, twist distortions are dominant. Finally, in the V geometry, we detect both twist and splay fluctuations as separate modes, with energy density $K_1q_\perp^2$ or $K_2q_\perp^2$, where $q_\perp^2$

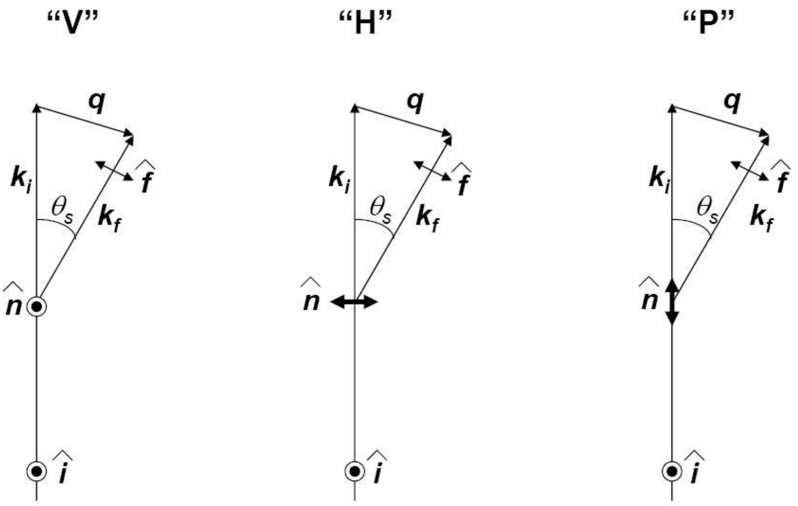

Figure 4.2: Top-view schematic of the three scattering geometries used. The scattering plane, which contains q, is in the plane of the page, perpendicular to i. Relative to the incident polarization, i, and wavevector, k_i, the LC director, n, is oriented parallel to i, ("V" for "vertical"), perpendicular to both i and k_i ("H" for "horizontal"), or parallel to k_i ("P" for "parallel"). The polarization direction of the analyzer, f, is horizontal, perpendicular to i. The intensity of the scattered, depolarized light is recorded at a discrete angle, θ_s, in the laboratory frame, corresponding to a particular final wavevector, k_f and scattering vector $q = k_f - k_i$.

is approximately proportional to $(n_{\|} - n_{\perp})^2 k_o^2 + 2(n_{\|}/n_{\perp}) k_o^2 \sin^2\theta_s$.

Thus, for all three geometries and assuming the main effect of the polymer on the director modes is simply to renormalize the elastic constants or relevant orientational viscosities, one expects the relaxation rate obtained from the measured decay of the scattered intensity time correlation function of these modes to scale basically as $\sin^2\theta_s$ (except at small θ_s, where the effects of the LC birefringence may be significant). The important distinction among the three scattering geometries is that in the H (P) cases, there is a substantial component of q along (perpendicular) to the extended axis of the polymer in the side-on (end-on) system, whereas the reverse applies in the V case.

As is common for liquid crystal polymer light scattering studies [8, 9], correlation functions from homopolymer solutions were fit to the empirical Williams-Watts function [10, 11] $\exp(-t\Gamma)^\beta$ where Γ is the relaxation rate and $0 < \beta < 1$ is a stretching exponent equal to one for purely exponential relaxation. If β is assumed to result from a spectrum of relaxation times, the average relaxation rate $<\Gamma>$ may be calculated [12] from $\beta\Gamma/[\Gamma_1(\beta^{-1})]$, where Γ_1 denotes the Gamma function.

Prior to initiating a time correlation experiment, the sample position was adjusted to a well aligned region of the sample that minimized the static intensity of the scattered light. Monodomains of homopolymer solutions were highly uniform and required little adjustment. On the other hand, it was more difficult to achieve high-quality monodomains with gels, and more sample adjustment was required prior to each experiment.

On small (< 100 nm) length scales, the gels have a heterogeneous structure that consists of an LC midblock solvated by the small molecule LC and phase-separated endblocks swollen with LC. Over the length scales probed by our scattering experiment, ranging between approximately 350 nm and 2900 nm, the system can be considered homogeneous.

In some samples, and particularly for lower values of θ_s, the intensity autocorrelation function did not decay completely, even after several hours. For a few representative cases, we separately recorded correlation functions over several weeks, fully confirming that the data decay to a stable baseline and that the observed fluctuations are ergodic (or characteristic of a system in thermodynamic equilibrium), though very slow, due to the cross-linked polymer structure within the gel.

4.4 Results

The comparison of intensity correlation functions for 5CB, homopolymer solutions, and triblock gels presented in Fig. 4.3 reveals qualitatively different director relaxation dynamics for each type of sample. At all orientations, 5CB shows single exponentially decaying relaxation modes, as has been previously established for small molecule LCs [1, 13, 14, 15]. Homopolymer solutions (with side-on and end-on SGLCPs, HSiBB and HSiCB4, respectively) exhibit stretched exponential time correlation functions with significantly slower relaxation rates than for the small molecule LC host, 5CB, in accord with prior literature on SGLCPs in nematic solvents [2, 8, 16, 17, 18, 19]. The relaxation rates have the q^2 dependence associated with diffusive hydrodynamic modes (Fig. 4.4), as expected [2], and the stretching exponent β falls in the range of 0.57 to 0.99.

Addition of homopolymer with mildly oblate chain anisotropy (HSiCB4) slows relaxation more strongly in the H geometry than in the V geometry (Fig. 4.4a). The asymmetry is reversed for the polymer with strongly prolate chain anisotropy (HSiBB), which instead shows more strongly

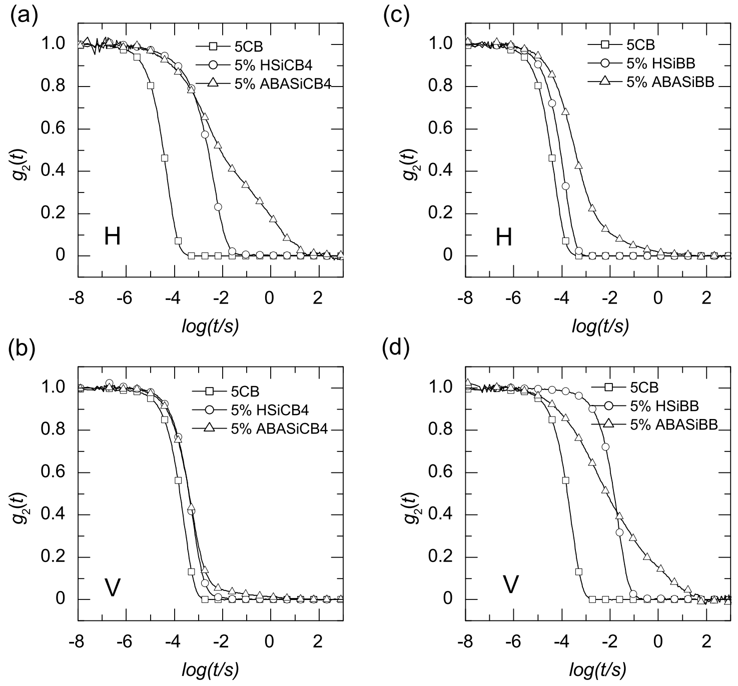

Figure 4.3: Normalized time correlation functions $g_2(t)$ at 25 ^{o}C and $\theta_s = 30$ ^{o}C for 5CB, 5 wt % homopolymer solutions, and 5 wt % triblock copolymer gels in the H and V orientations

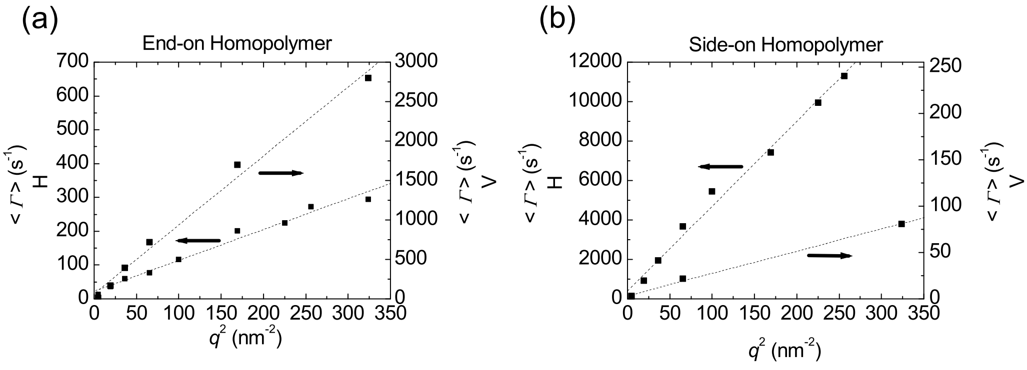

Figure 4.4: q-dependence of the average relaxation rates $< \Gamma >$ for (a) 5 wt % end-on homopolymer and (b) 5 wt % side-on homopolymer in both the H and V orientations. The dashed lines are linear fits to the data points

reduced relaxation rates in the V geometry (Fig. 4.4b). These results are in accord with extensive electrorheological and light scattering measurements by Jamieson and coworkers [2, 8, 16, 17, 18, 19] and with a theoretical model by Brochard [20], which predicts a strong reduction in director bend relaxation rate (probed in the H geometry) relative to splay (probed in the V geometry) for the oblate homopolymer (with end-on mesogen attachment) and the opposite for the prolate homopolymer (side-on attachment).

The triblock gels display highly broadened relaxation modes, with intensity correlations extending to much longer times than for the homopolymer solution; these data could not be fit by a conventional stretched exponential. The qualitatively different shape associated with the gel correlation functions is apparent in both scattering geometries, but it is most dramatic in the H geometry for ABASiCB4 (Fig. 4.3a) and the V geometry for ABASiBB (Fig. 4.3d), exactly the same pairing observed for the slowing down of director modes in the corresponding homopolymer solutions. On the other hand, in the P orientation, the slow dynamics are evident in both gels (Fig. 4.7).

Normalizing the delay time by $q^2 \sim (\sin\theta_s/\sin\theta_o)^2$ (where θ_o is a fixed reference angle) collapses the time autocorrelation functions of homopolymer solutions and 5CB onto one another, demonstrating that the relaxation rate has the q^2-dependence associated with diffusive hydrodynamic modes (Figs. 4.5a, 4.5b, 4.6a, 4.6b). On the other hand, the q^2-scaling superimposes the intensity autocorrelation functions of end-on (ABASiCB4) triblock gels only at short times (Figs. 4.5c and 4.5d). Significant deviations are observed at long times ($> 10^{-1}$ s) and lower angles ($\theta_s < 38^o$). Similarly, the autocorrelation functions for both gels in the P orientation have a $\sin^2\theta_s$ scaling only at short times and deviate from this behavior at long times (Fig. 4.7). By contrast, in the case of side-on gels (ABASiBB), the data at 25 ^{o}C superimpose well for almost all scattering angles (Figs. 4.6c and 4.6d).

In triblock copolymer solutions of different polymer concentration, a qualitative change in the shape of the intensity autocorrelation function coincides with the gel point: the slow dynamics in the end-on (ABASiCB4) gel abruptly appear at 5 wt % concentration but are not evident at a lower concentration [e.g., 1 wt % (Fig. 4.8)]. Prior rheological studies have shown that at 5 wt %

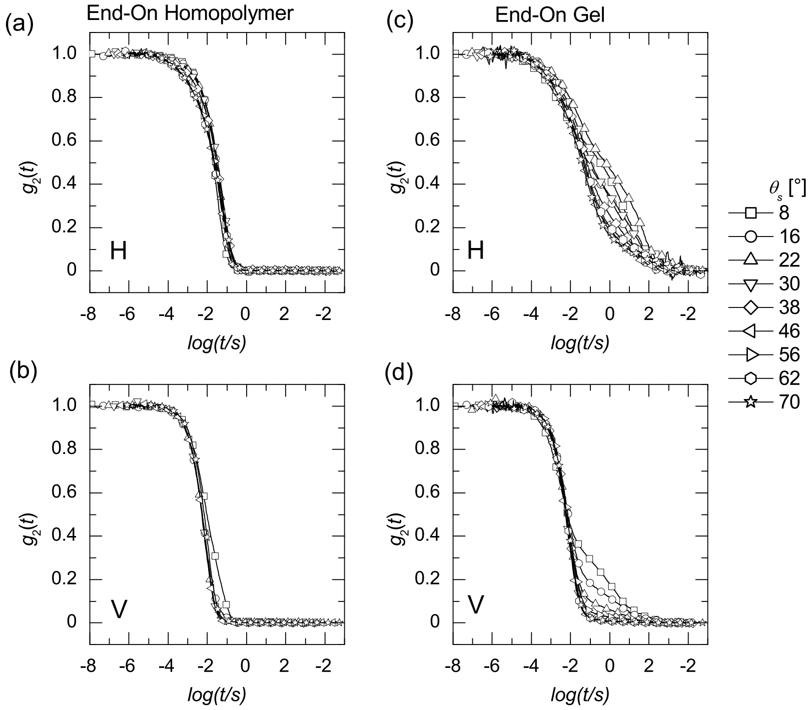

Figure 4.5: Normalized time correlation functions, $g_2(t)$, at 25 ^{o}C of end-on polymers at a variety of scattering angles as a function of rescaled delay time, $t(\sin(\theta_s)/\sin(\theta_o))^2$, where $\theta_o = 8^o$. 5 wt % end-on homopolymer (HSiCB4) in the (a) H orientation and (b) V orientation; and 5 wt % end-on triblock copolymer gel (ABASiCB4) in the (c) H orientation and (d) V orientation

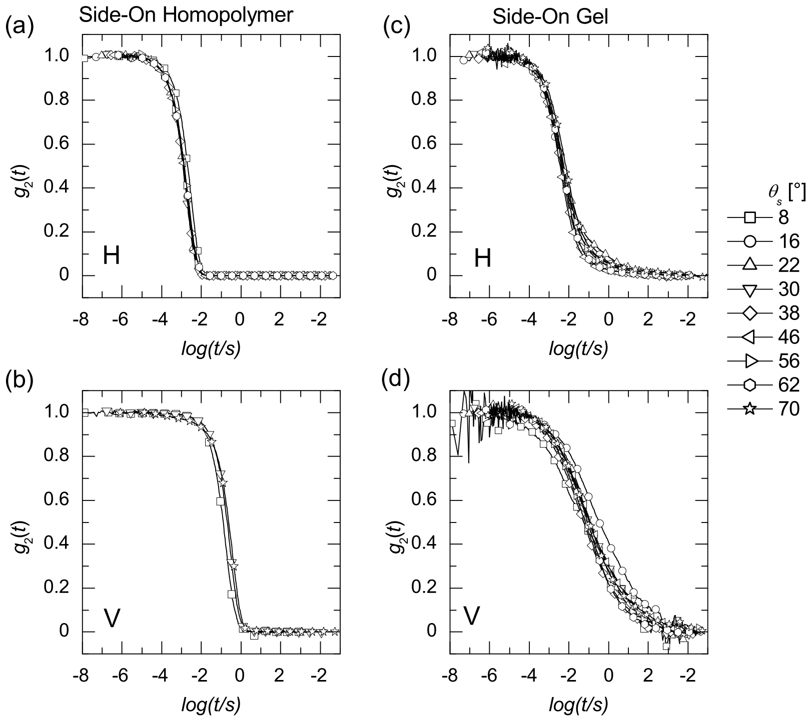

Figure 4.6: Normalized time correlation functions, $g_2(t)$, at 25 ^{o}C of side-on polymers at a variety of scattering angles as a function of rescaled delay time, $t(\sin(\theta_s)/\sin(\theta_o))^2$, where $\theta_o = 8^o$. 5 wt % side-on homopolymer (HSiBB) in the (a) H orientation and (b) V orientation; and 5 wt % side-on triblock copolymer gel (ABASiBB) in the (c) H orientation and (d) V orientation

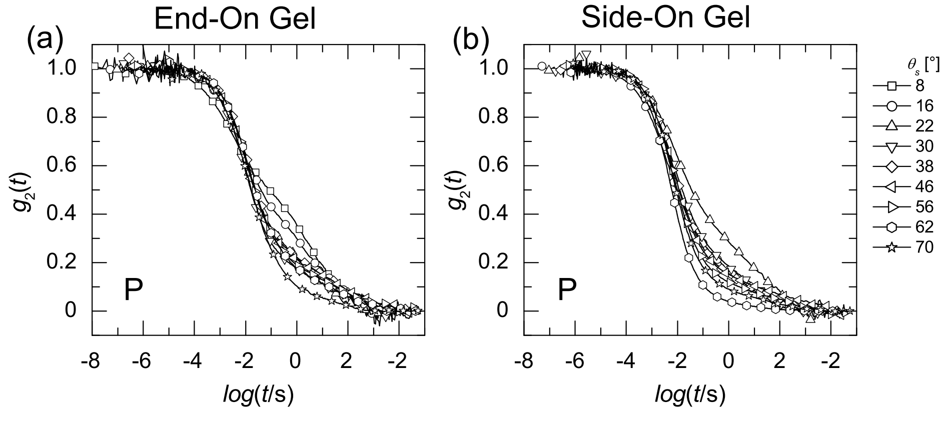

Figure 4.7: Normalized time correlation functions, $g_2(t)$, at 25 ^{o}C of triblock copolymer solutions in the P orientation at a variety of scattering angles as a function of rescaled delay time, $t(\sin(\theta_s)/\sin(\theta_o))^2$, where $\theta_o = 8^o$. (a) 5 wt % end-on triblock (ABASiCB4) and (b) 5 wt % side-on triblock (ABASiBB)

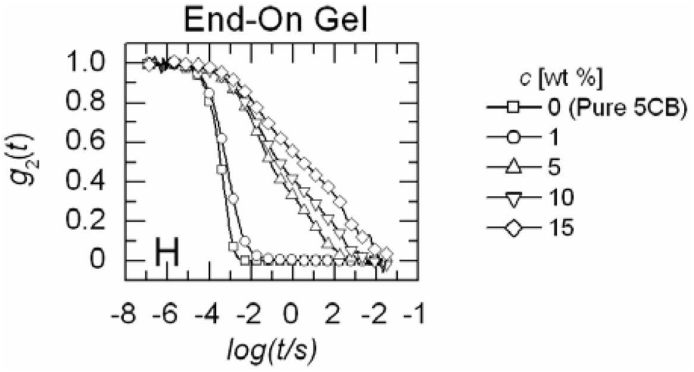

Figure 4.8: Concentration dependence of the intensity autocorrelation functions $g_2(t)$ at 25 ^{o}C and $\theta_s = 30^o$ of end-on triblock copolymer gels (ABASiCB4)

concentration end-on gels exhibit a wide plateau in their storage modulus that is characteristic of a gel [7]. Beyond the gel point, doubling and tripling the concentration has relatively mild effects (Fig. 4.8). The dynamics of relaxation become slower, but the shape of the correlation function is qualitatively the same.

End-on homopolymers and gels are relatively insensitive to temperature, as compared to their side-on counterparts. As temperature is increased from well below the nematic-isotropic transition (T_{NI}) to within 2 ^{o}C of T_{NI}, the intensity correlation functions of end-on (HSiCB4) homopolymer solution and end-on (ABASiCB4) gel hardly change (Fig. 4.9). In contrast, the relaxation time of side-on homopolymer in the V geometry speeds up by orders of magnitude (Fig. 4.10). Changing the temperature also significantly changes the observed dynamics in side-on (ABASiBB) gels (Figs. 4.10c and 4.10d). In the H orientation, the long-time tail in the intensity correlation function that can be seen at 25 ^{o}C almost disappears at 31.5 ^{o}C, and the initial drop-off in the decay shifts to shorter times with increasing temperature (Fig. 4.10c). In the V orientation, the long-time tail similarly diminishes as the temperature is increased, but the initial decay shifts to longer times (Fig. 4.10d). In contrast to their behavior at 25 ^{o}C (Figs. 4.6c and 4.6d), at 31.5 ^{o}C the side-on gels depart from pure q^2 hydrodynamic behavior at long times (Figs. 4.11c and 4.11d).

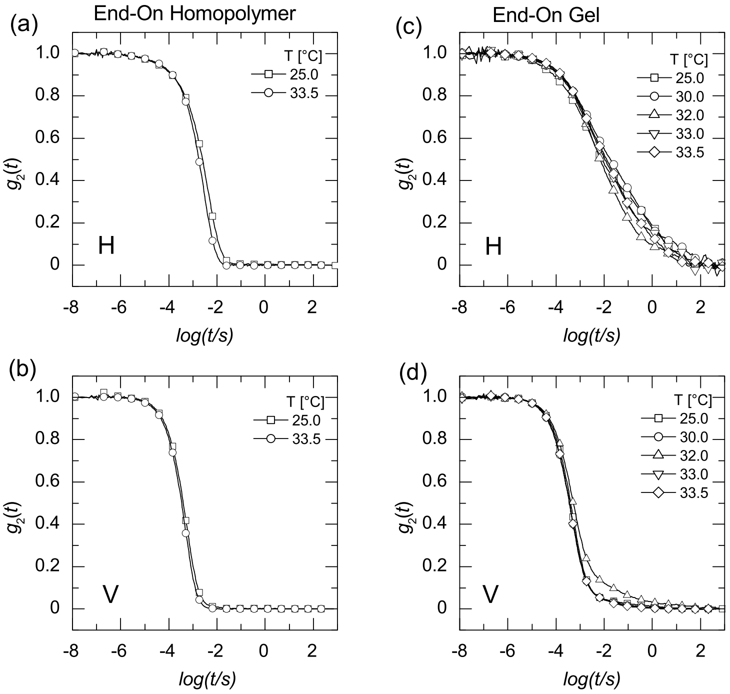

Figure 4.9: Temperature dependence of the normalized intensity autocorrelation functions $g_2(t)$ at $\theta_s = 30^o$ of 5 wt % end-on homopolymer HSiCB4 in the (a) H orientation and (b) V orientation and 5 wt % end-on triblock copolymer gel ABASiCB4 in the (c) H orientation and the (d) V orientation

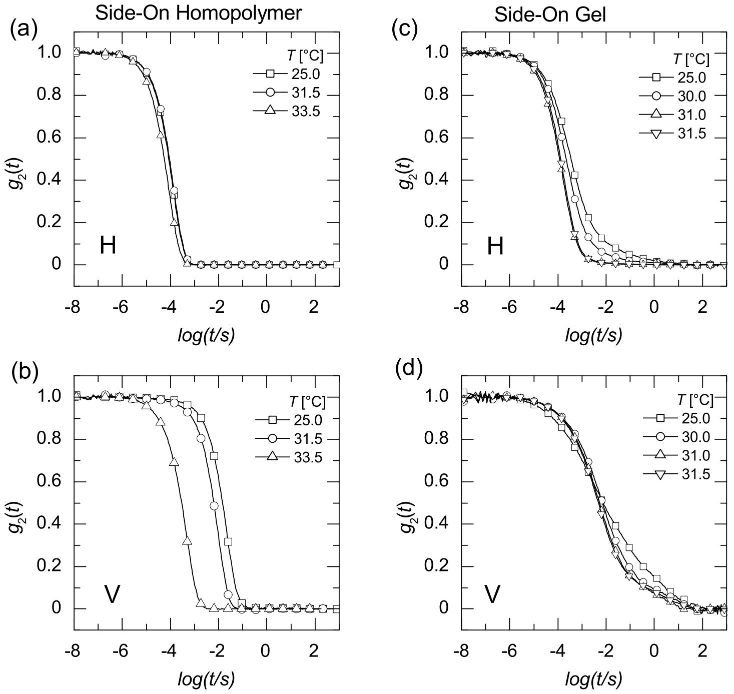

Figure 4.10: Temperature dependence of the normalized intensity autocorrelation functions $g_2(t)$ at $\theta_s = 30^o$ of 5 wt % side-on homopolymer HSiBB in the (a) H orientation and (b) V orientation and 5 wt % side-on triblock copolymer gel ABASiBB in the (c) H orientation and (d) V orientation

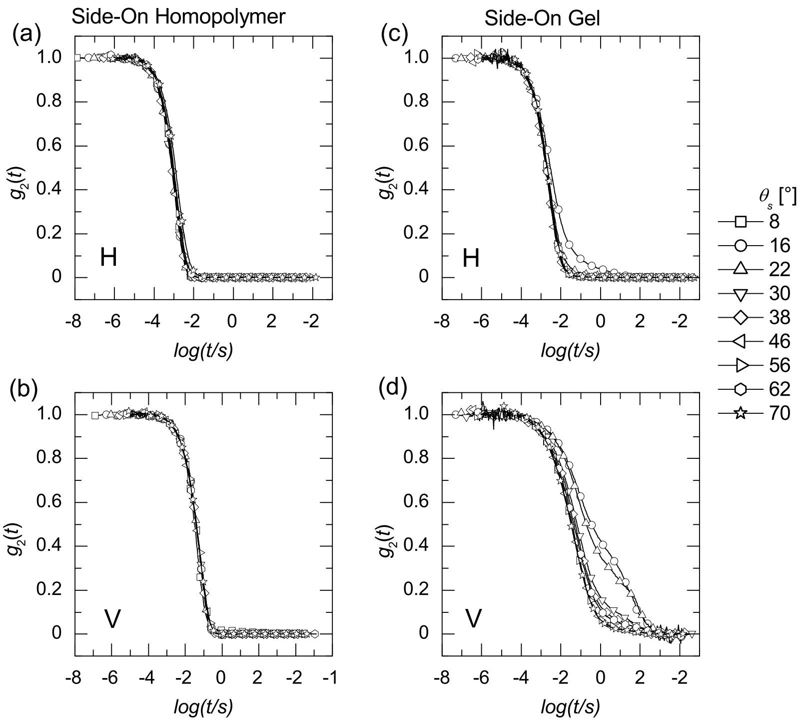

Figure 4.11: Normalized intensity autocorrelation functions $g_2(t)$ at 31.5 ^{o}C of side-on polymers at a variety of scattering angles as a function of rescaled delay time, $t(\sin(\theta_s)/\sin(\theta_o))^2$, where $\theta_o = 8^o$. 5 wt % side-on homopolymer (HSiBB) in the (a) H orientation and the (b) V orientation; and 5 wt % side-on triblock copolymer gel (ABASiBB) in the (c) H orientation and the (d) V orientation

4.5 Discussion

The data for the LC gels qualitatively resemble those observed from previous light scattering studies of associating polymers [21, 22, 23, 24, 25, 26, 27, 28], with the appearance of slow relaxation modes above a critical concentration and highly stretched intensity autocorrelation functions with a strong q-dependence. However, in the present study, the scattered light arises primarily from fluctuations in the orientation of the nematic director, not density fluctuations as in the previous light scattering studies of gelled systems. Therefore, structural changes such as micellar diffusion or concentration fluctuations in the polymer network are revealed indirectly by their effect on the nematic director dynamics.

Our data indicate that in the LC physical gels at least two distinct relaxation processes couple to the director and scatter light. The faster relaxation process shows a q^2 scaling characteristic of hydrodynamic modes, as in homopolymer solutions and pure low molecular weight nematics. The relaxation rate for this process is reduced with the addition of triblock copolymer and is dependent on the polymer/gel architecture, but it remains hydrodynamic. This behavior contrasts sharply with light scattering results on LC elastomers [5], where the LC director modes are strictly non-hydrodynamic (relaxation rate independent of q), due to the full incorporation of the LC into the cross-linked polymer network and the consequent nature of the director-network coupling required by rotational invariance [29]. The theoretical description of relaxation modes in LC gels does not contain such a strong coupling [3, 4], and our experimental results confirm this, at least for physical gels: orientational fluctuations are soft in all directions at long wavelengths.

The slow gel dynamics expressed in the correlation data at long times are associated with long length scales: the smaller the scattering angle, the more strongly the intensity autocorrelation persists at long time (Figs. 4.5c, 4.5d, 4.6c, 4.6d, 4.7a, and 4.7b). Indeed, the q-dependence of the slow relaxation appears to be stronger than q^2 (or $\sin^2\theta_s$) for small wavevectors (or low θ_s), and is reminiscent of hindered relaxational dynamics in colloidal glasses and associative polymers [21, 22, 23, 24, 26, 28]. We propose that the nematic director is coupled to the associated gel structure, yielding long-lived orientational fluctuations. The nematic director can relax via the fast

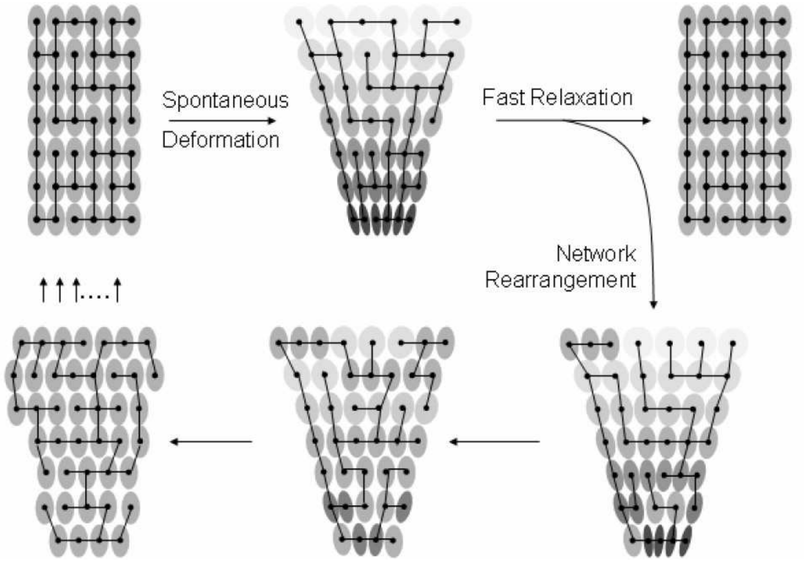

Figure 4.12: Schematic for network relaxation via a fast mode that retains the network structure and a slow mode that requires the reorganization of the physical network. The ellipsoids represent polymer micelles with an SGLCP corona (gray shading), a polystyrene core (dark circle), and intermicellar bridges (dark lines). The shading represents the local density of micelle coronal chains, with darker shading corresponding to a higher density. The schematic shows that a network deformation stretches the intermicellar bridges as well as deforming micelles. A slow network rearrangement process re-establishes the equilibrium configuration through a combination of micelle-hopping and the nucleation or evaporation of micelles.

relaxation mode only to a certain extent, due to a coupling to the polymer gel structure. At long enough times, however, the physical junctions in the network reorganize and allow the nematic director to fully lose correlation with its initial orientation.

This idea is demonstrated schematically in Fig. 4.12. Under a deformation, the network can undergo a “fast” viscoelastic relaxation mode in which none of the physical junctions are broken. On the other hand, the physical junctions in the network are constantly broken and reformed, and on long time scales the network can significantly reorganize its structure. This network reorganization process can appear as a second, much slower director relaxation mode. The picture presented in Fig. 4.12 is only a schematic, and in the actual gel the polymer micelles are not ordered on a lattice [30]. However, the model appropriately represents the association of polymers into micelles and the interaction of micelles by repulsive forces as well as bridging between micelles, and it qualitatively accounts for two separate relaxation modes.

While both prolate (side-on) and oblate (end-on) polymer gels strongly modify predominantly

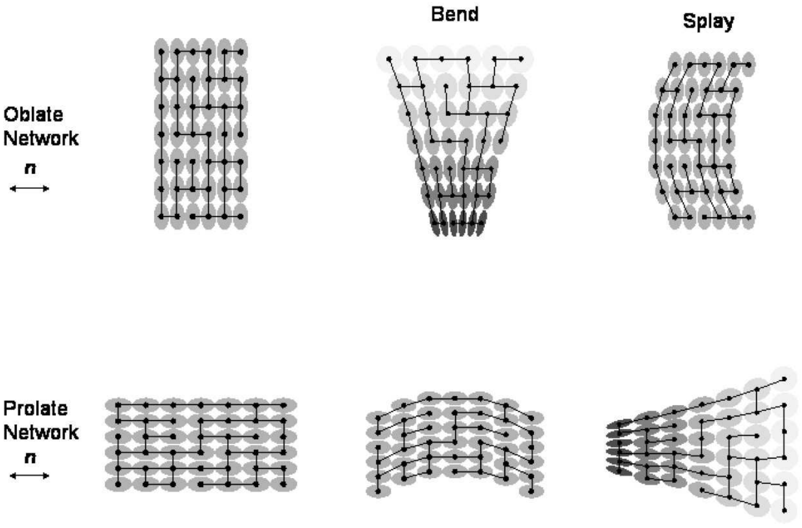

Figure 4.13: Schematic for network deformations associated with splay and bend LC deformations.

twist relaxation of the director (Fig. 4.7 and Figs. 4.5d and 4.6d for small θ_s), the impact of the gel is clearly selective in slowing and stretching predominantly bend fluctuations (Fig. 4.5c) relative to splay fluctuations (Fig. 4.5d for larger θ_s) in the end-on gel and just the opposite in the side-on gel (Figs. 4.6c and 4.6d). The viscoelastic anisotropy of the homopolymer solutions is thus reflected in the corresponding gels, pointing to an anisotropic gel structure – specifically, an anisotropy in the intermicellar distance and in the size of the micellar bridges, which have a longer dimension along the aligned director (side-on gel) or perpendicular to the director (end-on gel), as depicted in Fig. 4.13. In this case, "undulation" (or an elastic bending) of the gel network along the long axis does not require a severe distortion of the micellar positions or stretching of the bridges, while a twisting or splaying of the long axis causes either a substantial reorientation of the micelles or stretching of the shorter bridges. This results in a strong coupling of slow gel dynamics to twist director distortions in both gel types and a selective coupling to bend and splay director distortions, respectively, in the end-on and side-on gels (see Fig. 4.13).

Another aspect of anisotropic gel structure is observed in the initial decay of the correlation data – specifically, the faster initial relaxation observed in the side-on gels relative to the corresponding homopolymer solution (Fig. 4.6d). Interestingly, this case corresponds to the gel with the largest polymer shape anisotropy or aspect ratio – 5:1 in the side-on, compared to 1.6:1 in the end-on gel at

25 ^{o}C [6]. At higher temperatures, the initial decay in the side-on gels becomes slower (Figs. 4.11c and 4.11d), and this coincides with a decreasing network anisotropy, as confirmed by the changing relaxation rates in the side-on homopolymer solutions (Figs. 4.11a and 4.11b). Therefore, a faster initial decay is associated with more anisotropic networks. Recently, Lubensky and coworkers have predicted [3] a modification to the elastic free energy in LC elastomers that provides for an additional torque on the director that strongly depends on network anisotropy. Our evidence of faster director relaxation in the more anisotropic side-on gel at lower temperatures is thus consistent with the theory developed for elastomers. The weaker coupling between the nematic director and network deformations in less anisotropic networks also apparently results in more widely separated relaxation dynamics and modified hydrodynamic behavior at long times (compare Figs. 4.5c, 4.5d, 4.11c, and 4.11d to Figs. 4.6c and 4.6d).

4.6 Conclusions

We studied the director relaxation dynamics in LC physical gels via dynamic light scattering. We found that the gels exhibited overdamped dynamics over a broad range of time scales. The faster component is hydrodynamic and corresponds to director relaxation modes predicted by dynamic theories of homopolymer solutions, where prolate chains strongly decreased the splay relaxation rate and oblate chains strongly decreased the bend relaxation rate. We also observed a slow component to the relaxation that increases in amplitude at low scattering angles, exhibits a stronger q dependence than the faster component of the dynamics, and is expressed with a strong anisotropy that depends on the chain architecture. The slow component arises from coupling of the nematic director to the rearrangement of crosslinks in the self-assembled polymer structure and is a consequence of the physical nature of the gel structure. At long enough times the gel structure reorganizes, allowing the nematic director to fully relax, resulting in the long-time decay in the observed correlation function. The network anisotropy is also manifested in the initial decay of the correlation function: The most anisotropic networks show a faster initial decay than the corresponding homopolymer solution, indicating that the network can provide an additional restoring torque on the director.

Bibliography

[1] John T. Ho. Light scattering and quasielastic spectroscopy. In Satyendra Kumar, editor, *Liquid Crystals*. Cambridge University Press, Cambridge, 2001.

[2] A. M. Jamieson, D. F. Gu, F. L. Chen, and S. Smith. Viscoelastic behavior of nematic monodomains containing liquid crystal polymers. *Prog. Polym. Sci.*, 21(5):981–1033, 1996.

[3] O. Stenull and T. C. Lubensky. Dynamics of nematic elastomers. *Phys. Rev. E*, 69:051801, 2004.

[4] E. M. Terentjev and M. Warner. Linear hydrodynamics and viscoelasticity of nematic elastomers. *Eur. Phys. J. E*, 4:343–353, 2001.

[5] M. Schnstein, W. Stille, and G. Strobl. Effect of the network on the director fluctuations in a nematic side-group elastomer analysed by static and dynamic light scattering. *Eur. Phys. J. E*, 5:511–517, 2001.

[6] M. D. Kempe, N. R. Scruggs, R. Verduzco, J. Lal, and J. A. Kornfield. Self-assembled liquid-crystalline gels designed from the bottom up. *Nat. Mater.*, 3(3):177–182, 2004.

[7] M. D. Kempe, R Verduzco, N. R. Scruggs, and J. A. Kornfield. Rheological study of structural transitions in triblock copolymers in a liquid crystal solvent. *Soft Matter*, 2(5):422–431, 2006.

[8] D. F. Gu, A. M. Jamieson, C. Rosenblatt, D. Tomazos, M. Lee, and V. Percec. Dynamic light scattering from a nematic monodomain containing a side-chain liquid crystal polymer in a nematic solvent. *Macromolecules*, 24(2385-2390), 1991.

[9] J. Schmidtke, S. Werner, and G. Strobl. Static and dynamic light scattering of a nematic side-group polysiloxane. *Macromolecules*, 33:2922–2928, 2000.

[10] Graham Williams and David C. Watts. Non-symmetrical dielectric relaxation behaviour arising from a simple empirical decay function. *Trans. Faraday Soc.*, 66:80–85, 1970.

[11] Graham Williams, David C. Watts, S. B. Dev, and A. M. North. Further considerations of non-symmetrical dielectric relaxation behaviour arising from a simple empirical decay function. *Trans. Faraday Soc.*, 67:1323–1335, 1977.

[12] C. P. Lindsey and G. D Patterson. Detailed comparison of the williams-watts and cole-davidson functions. *J. Chem. Phys.*, 73(7):3348–3357, 1980.

[13] Pierre-Gilles de Gennes. *The Physics of Liquid Crystals*. Clarendon Press, Oxford, 2nd edition, 1993.

[14] Orsay Liquid Crystal Group. Quasielastic rayleigh scattering in nematic liquid crystals. *Phys. Rev. Lett.*, 22:1361–1363, 1969.

[15] Orsay Liquid Crystal Group. Dynamics of fluctuations in nematic liquid crystals. *J. Chem. Phys.*, 51(2):816–822, 1969.

[16] Y.-C. Chiang, A. M. Jamieson, S. Campbell, Y. Lin, N. O'Sidocky, L. C. Chien, M. Kawasumi, and V. Percec. Effect of molecular architecture on the electrorheological behavior of liquid crystal polymers in nematic solvents. *Rheol. Acta*, 36:505–512, 1997.

[17] Y.-C. Chiang, A. M. Jamieson, S. Campbell, T. H. Tong, N. D. Sidocky, L. C. Chien, M. Kawasumi, and V. Percec. Electro-rheological behavior of liquid crystal polymers dissolved in a nematic solvent: dependence on temperatrue and lcp structure. *Polymer*, 41:4127–4135, 2000.

[18] F.-L. Chen, A. M. Jamieson, M. Kawasumi, and V. Percec. Viscoelastic properties of dilute nematic mixtures containing cyclic and hyperbranched liquid crystal polymers dissolved in a nematic solvent. *J. Polym. Sci., Part B: Polym. Phys.*, 33:1213–1223, 1995.

[19] D. F. Gu, A. M. Jamieson, M. Kawasumi, M. Lee, and V. Percec. Dynamic light scattering from nematic monodomains containing mesogenic polymers of differing architectures. *Macromolecules*, 25(2151-2155), 1992.

[20] F. Brochard. Viscosities of dilute polymer-solutions in nematic liquids. *J. Polym. Sci., Part B: Polym. Phys.*, 17(8):1367–1374, 1979.

[21] M. Adam, M. Delsanti, and J. P. Munch. Dynamical studies of polymeric cluster solutions obtained near the gelation threshold: glasslike behavior. *Phys. Rev. Lett.*, 61:706–709, 1988.

[22] V. Castelletto, I. W. Hamley, and T. A. Waigh. Dynamic light scattering study of the dynamics of a gelled polymeric micellar system. *J. Chem. Phys.*, 121:11474–11480, 2004.

[23] C. Konák, G. Fleischer, Z. Tuzar, and R. Bansil. Dynamics of solutions of triblock copolymer in a selective solvent: Effect of varying copolymer concentration. *J. Polym. Sci., Part B: Polym. Phys.*, 38:1312–1322, 2000.

[24] Cestmr Konk, Martin Helmstedt, and Rama Bansil. Dynamics in solutions of associating statistical copolymers. *Macromolecules*, 30:4342–4346, 1997.

[25] J. Martin and J. Wilcoxon. Critical dynamics of the sol-gel transition. *Phys. Rev. Lett.*, 61:373–376, 1988.

[26] E. Raspad, Didier Lairez, Mireille Adam, and Jean-Pierre Carton. Triblock copolymers in a selective solvent. 2. semidilute solutions. *Macromolecules*, 29:1269–1277, 1996.

[27] B. Nystrm and B. Lindman. Dynamic and viscoelastic properties during the thermal gelation process of a nonionic cellulose ether dissolved in water in the presence of ionic surfactants. *Macromolecules*, 28:967–974, 1995.

[28] J. E. Martin, J. Wilcoxon, and J. Odinek. Decay of density fluctuations in gels. *Phys. Rev. A*, 43(2):858–872, 1991.

[29] P. D. Olmsted. Rotational invariance and goldstone modes in nematic elastomers and gels. *J. Phys II France*, 4(12):2215–2230, 1994.

[30] N. R. Scruggs, J. A. Kornfield, and J. Lal. Using the “switchable” quality of liquid crystal solvents to mediate segregation between coil and liquid crystalline polymers. *Macromolecules*, 39(11):3921–3926, 2006.

Chapter 5

Micellar Structure of Block Copolymers in an LC Solvent

Much of the work in this chapter represents the combined efforts both of myself and of Neal Scruggs. We acknowledge the support of Dr. Jyotsana Lal and Ed Lang in designing and conducting the neutron scattering experiments. In addition, Dr. Michael Kempe and Zuleikha Kurji provided assistance in carrying out the neutron scattering experiments during separate trips to Argonne National Laboratory. Finally, the work in this chapter could not have been done without materials obtained from Dr. David Uhrig of the Macromolecular Complex Systems group at Oak Ridge National Laboratory. They provided most of the polystyrene-polybutadiene diblock copolymers used for this study.

5.1 Abstract

Block copolymers comprised of polystyrene (PS) segments and side-group liquid crystal polymer (SGLCP) segments self-assemble when mixed in a nematic liquid crystal (LC) solvent to form LC gels. We investigate a series of diblock PS-SGLCP and triblock PS-SGLCP-PS copolymer gels by small-angle neutron scattering (SANS) and rheometry. These studies show that the LC order of the host solvent imparts unique properties to the micellar gels. The micelles and intermicellar network inherit the anisotropy of the host solvent, and dramatic structural and rheological changes occur across the T_{NI}, due to a changing solvent selectivity. SANS shows that the micelles are disordered, and the micelles decrease in size with temperature. The microphase separation temperature T_{MST}

can be coincident with or higher than the T_{NI} depending on the copolymer block lengths. Rheometry reveals that both diblock and triblock copolymer mixtures can exhibit solid-like properties, depending on the PS and SGLCP block lengths. Both SANS and rheometry show that the driving force for self-assembly is increased with the PS block size: a larger PS block size results in a higher T_{MST} and a higher sol-gel transition temperature. The block copolymer micelles have a "hairy" structure with extended SGLCP coronas, small PS cores swollen with 5CB, and a soft intermicellar potential.

5.2 Introduction

Block copolymers are comprised of chemically distinct polymers covalently linked together. When a block copolymer is dissolved in a solvent that preferentially solvates one block, the block copolymers oftentimes assemble into aggregates known as micelles, and this dramatically alters the rheological properties of the solution. Unlike liquids, a micellar suspension can have a finite yield stress, but it can also coat a surface or fill a container. This type of behavior that is neither purely liquid-like or purely solid-like is termed viscoelastic, and these types of materials have wide-ranging practical interest. Block copolymer additives are used regularly in the cosmetics industry, and potential uses include their addition to jet fuels to prevent droplet formation [1] and as hydrogels to form scaffolds for tissue regeneration [2].

Block copolymers can also be combined with LC order for use in functional materials. We have demonstrated that triblock copolymers composed of a side-group LC polymer (SGLCP) midblock and non-mesomorphic polystyrene (PS) endblocks can form LC gels when mixed with a small molecule liquid crystal (Chapter 2). In this study, we investigate the structure of the LC copolymers in the small molecule LC 4-pentyl-4′-cyanobiphenyl (5CB). PS is insoluble in nematic 5CB due to the entropic penalty of dissolving an isotropic polymer in a liquid crystal phase [3], resulting in self-assembly of the triblock copolymers to form an LC gel. We study a series of SGLCP-PS diblock and PS-SGLCP-PS triblock copolymers with different block lengths by SANS and rheometry. An interesting property of the gels is that they undergo a nematic-to-isotropic transition near 35

^{o}C. Therefore, the nematic-to-isotropic transition of the solvent is expected to result in significant changes to the self-assembled micellar structure. Both SANS and rheometry reveal significant structural changes with temperature across the T_{NI}. Also, the PS block length is a significant parameter for the phase behavior of the gels, and samples with large ($>$ 100 kg/mol) PS blocks form gels even above the T_{NI}.

5.3 Experimental

5.3.1 Preparation of nematic gels

The synthesis and characterization of the LC homopolymers and copolymers and the preparation of the LC gels was carried out as described in Chapter 2. The diblock and triblock PS-SGLCP copolymers are named by the size of the SGLCP block, the size of the PS block, and the polymer architecture ("AB" for diblock, "ABA" for triblock, and "LCP" for SGLCP homopolymer), as shown in Table 5.1. The homopolymers, triblock prepolymers, and diblock prepolymer for 890(70)AB and 840(190) AB were purchased and used as received from Polymer Source. All the other diblock prepolymers were obtained from the Macromolecular Complex Systems group from Oak Ridge National Labs and used as received.

5.3.2 LC phase identification

The transition temperatures of the LC gels were determined using a Zeiss polarized optical microscope (POM) with a Mettler FP82 hot stage. The temperature was slowly raised at 1 ^{o}C/min, and the phases were identified along with the temperature at which phase transitions began. Some samples exhibited a biphasic region in between single-phase isotropic and single-phase nematic mixtures. The T_{NI} was taken to be the onset temperature of the biphasic region.

5.3.3 Rheometry

Rheometry was performed on a TA Instruments ARES-RFS rheometer equipped with a 25 mm diameter titanium shear cell. Except where otherwise noted, rheometry was performed in a cone-and-plate geometry having a 0.0202 radian cone angle. All experiments were performed in the linear regime as verified by dynamic strain sweeps.

5.3.4 SANS

SANS experiments were performed on the small-angle scattering instrument (SASI) at the Intense Pulsed Neutron Source at Argonne National Laboratory. Diblock and triblock copolymer samples were mixed with perdeuterated 5CB (D5CB) [4] at concentrations of 5 and 10 wt %. The samples were loaded into 1 mm-thick quartz cells, except where otherwise noted, and the cells were placed in a temperature-controlled sample holder. The scattering experiments were performed on polydomain samples at temperatures ranging between 25 ^{o}C and 60 ^{o}C. Polydomain samples can be azimuthally averaged and therefore have a much better signal to noise ratio compared to monodomain samples. Only selected samples were aligned to form monodomains for investigation under SANS. The scattering trace for pure 5CB was used as a background.

5.4 Results

5.4.1 Polymer characteristics and phase behavior

A series of LC diblock copolymer samples were prepared in addition to an LC triblock copolymer (Table 5.1). The diblock copolymers were designed to investigate a series of block copolymers with varying PS block size, LC block size, and overall molecular weight. The diblock copolymers 590(40)AB, 530(60)AB, and 620(80)AB have similar LC block M_n but different PS block M_n. The diblocks 620(80)AB and 890(70)AB have similar PS block sizes with different LC block sizes. Finally, 450(120)AB and 840(190)AB have similar ratios of PS block M_n to LC block M_n with different overall M_n. These diblock copolymers can be compared to triblock copolymers 1320(60)ABA and

800(20)ABA which can form “bridges” where one polymer strand associates with two different micelles.

Table 5.1: Polymer characteristics

Polymer	PDI	LC Block M_n $(\frac{\text{kg}}{\text{mol}})$	PS Block M_n $(\frac{\text{kg}}{\text{mol}})$	LC BLock Composition 1,2 Content (mol %)	 1,4 Content (mol %)	 Mesogen Content (mol %)
710LCP	1.08	713	0	8	3	89
500LCP	1.15	497	0	7	11	82
590(40)AB	1.37	592	40	21	1	78
530(60)AB	1.09	534	60	24	3	73
890(70)AB	1.11	886	70	18	12	70
620(80)AB	1.13	620	80	9	5	86
450(120)AB	1.65	445	120	31	1	68
840(190)AB	2.06	839	190	11	23	66
1320(60)ABA	1.40	1321	67,57	16	14	70
800(20)ABA	1.20	799	14,24	8	10	82

The phase behavior of PS [3] in 5CB and the present SGLCP [5] in 5CB has previously been studied. PS is insoluble in nematic 5CB, and the SGLCP was found to be soluble at all concentrations tested, up to concentrations of 20 wt %. Therefore, micelles formed by PS-SGLCP block copolymers in 5CB will consist of a PS core and an SGLCP corona.

All polymers were soluble in 5CB in both the nematic and isotropic phases at concentrations up to 10 wt %. Mixtures of 710LCP, 590(40)AB, 620(80)AB, 840(190)AB, and 800(20)ABA with 5CB had a biphasic region between the nematic and isotropic phases. The T_{NI} was taken to be the onset of this biphasic transition, observed under polarized optical microscopy. Pure 5CB has a T_{NI} of approximately 35.2 ^{o}C, and D5CB has a slightly lower T_{NI} of 33.5 ^{o}C.

Single phase mixtures of block copolymer in 5CB showed a homogenous nematic texture under the microscope. This agrees with previous studies [6], which found that LC diblock copolymers with large LC block fractions (greater than 90%) formed uniform nematic solutions, as observed under optical microscopy. In contrast, Finkelmann and coworkers observed that block copolymers with smaller LC block fractions can form micrometer-thick, phase-separated threads when mixed with a small molecule nematic LC [6].

5.4.2 Neutron scattering

SANS experiments give information about structure present on various length scales. Information at larger length scales is reflected at smaller scattering angles, and the characteristic length scale is inversely related to the scattering vector $q = (4\pi/\lambda)\sin(\theta/2)$. We performed SANS experiments with q ranging between 0.0067 Å^{-1} and 1.0 Å^{-1}. Scattering at low q ($<$ 0.03 Å^{-1}) reveals information about micellar ordering and structure. The mid-q region of the scattering pattern (0.03 Å^{-1} $<$ q $<$ 0.10 Å^{-1}) reflects intrachain correlations, and the high q region gives information about the concentration of scattering centers in the sample and reflects incoherent background scattering.

Scattering experiments were performed on monodomain SGLCP homopolymer 710LCP in D5CB to investigate the conformation of the SGLCP in solution. The scattering pattern for SGLCP homopolymer 710LCP shows much stronger scattering in the direction perpendicular rather than parallel to the director (Fig. 5.1), indicating that the polymer backbone conformation is anisotropic and preferentially extended along the nematic director. The bow-tie shape observed in the scattering pattern has previously been observed in highly extended side-on side-group LC polymers [7, 8] and main-chain LC polymers [9] and suggests a highly extended polymer conformation. A Debye model fit gives an approximate anisotropy $R_{\|}/R_{\perp}$ of 5 [5]. Neutron scattering patterns for shear-aligned triblock gels show that the anisotropy observed for SGLCP homopolymer in solution is also present in the physically associated polymer network (Fig. 5.2). The scattering patterns for the gels exhibit a smaller anisotropy compared to the SGLCP homopolymer. For both 710LCP and 1320(60)ABA, the scattering patterns are isotropic for temperatures higher than the T_{NI}.

SANS experiments on polydomain diblock and triblock polymers in D5CB reveal the micellar structure present (all SANS data is given at the end of the chapter in Section 5.6). For samples at a given concentration, the data converge onto a single curve in the mid-q region of the spectrum, overlapping with the SANS data for an SGLCP homopolymer of a similar concentration (Fig. 5.3). Therefore, the mid-q region is dominated by single chain contributions. Micellar structure is reflected at lower q, and, relative to homopolymers, diblock and triblock copolymers have significant low-q scattering in the nematic phase (Fig. 5.3). While block copolymer micelles in selective isotropic

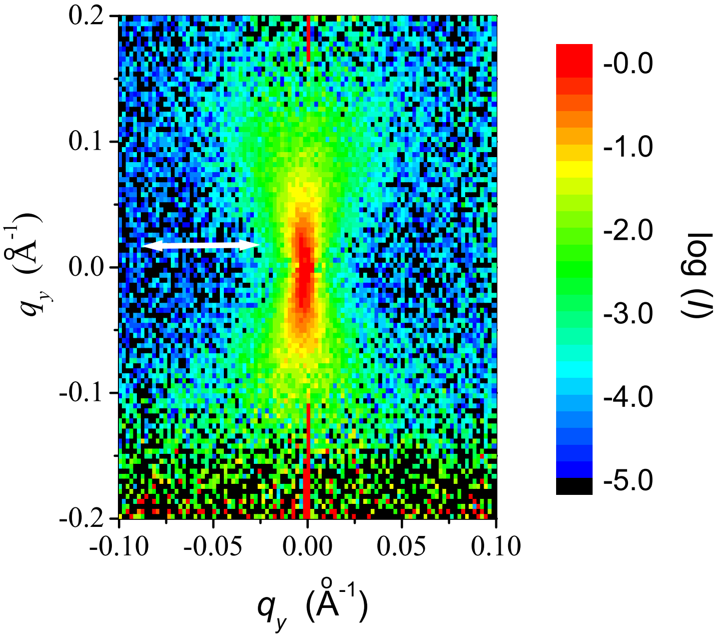

Figure 5.1: Neutron scattering pattern for a monodomain solution of 710LCP in perdeuterated 5CB. Uniform alignment was achieved by coating the cell surface with a rubbed polyimide layer. The double-headed arrow denotes the director, and q_x and q_y denote components of the scattering vector.

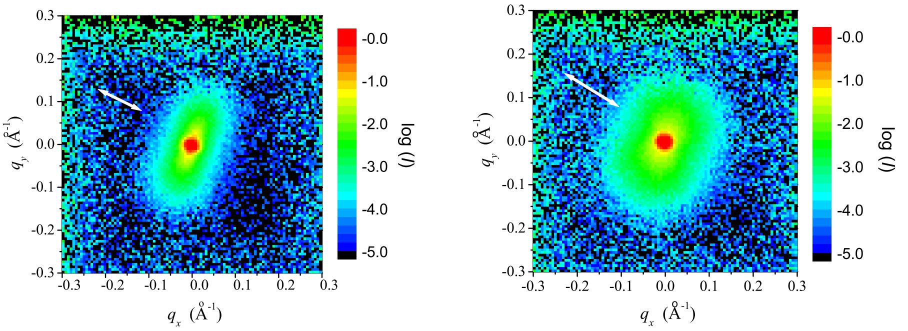

Figure 5.2: Neutron scattering pattern for shear-aligned 1320(60)ABA in D5CB at 5 wt % (left), and 10 wt % (right). The double-headed arrow denotes the director, and q_x and q_y denote components of the scattering vector. The samples were shear aligned by hand.

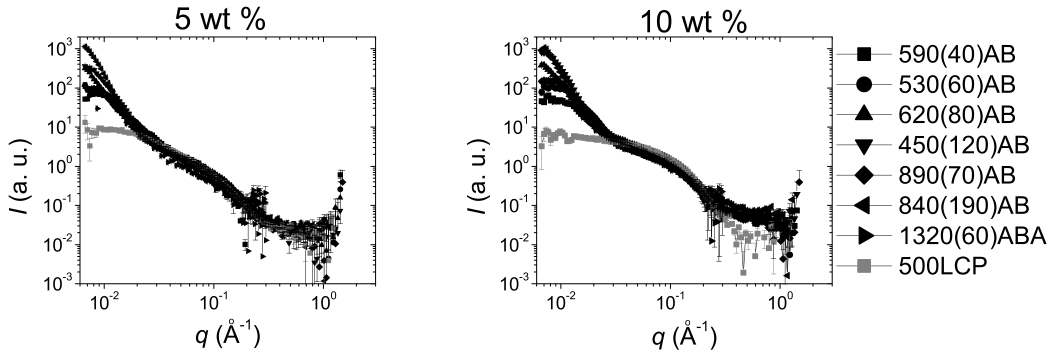

Figure 5.3: Neutron scattering pattern for LC polymers in D5CB. All data are for polydomain samples at 25 °C, with the exception of 890(70)AB and 1320(60)ABA. The scattering pattern for 890(70)AB was collected at 29 °C. 1320(60)ABA was aligned by shear, and the data shown were averaged over a 15° wedge region oriented along the direction parallel to the director.

solvents oftentimes assemble into hexagonally ordered phases [10, 11, 12, 13], the block copolymer micelles in the present system are disordered, as evidenced by the absence of Bragg lattice peaks.

In principle, we would like to fit the scattering patterns with an appropriate model that includes the form factor of the micelle along with a structure factor that accounts for micelle-micelle correlations [14, 15]. A proper fit could provide quantitative data about the size of the micelle core, the micelle corona, and the intermicellar distance [12, 16]. However, several difficulties impeded useful fitting of the data. The solvent is not matched to either block of the copolymer samples, and therefore the form factor must account for scattering from both the micellar cores and the corona. The cores may be highly swollen with solvent, and the aggregation number of the micelles is unknown. Therefore, fitting requires a large number of parameters that have not been independently measured. We therefore chose to rely on the qualitative features of the neutron scattering patterns to gain insight into the block copolymer structure and, in particular, its temperature dependence.

Diblock and triblock gels show one or more peaks in the scattering pattern at low q (Section 5.6). Most samples have a peak near $q = 0.008$ Å^{-1}, and data for 530(60)AB and 620(80)AB show a second peak near $q = 0.02$ Å^{-1} (Figs. 5.5 and 5.7). The position of the first peak changes with temperature and concentration, and it depends on the polystyrene block length (Table 5.2). The position of

Table 5.2: Peak positions in 10^{-3} Å^{-1} for block copolymer-D5CB mixtures at 25 ^{o}C, T_{NI} - 2 ^{o}C, and T_{NI} + 2 ^{o}C. The lowest q probed is 6.7 10^{-3} Å. "NP" means "no peak".

	25 ^{o}C		T_{NI} - 2 ^{o}C		T_{NI} + 2 ^{o}C	
Polymer	5 wt %	10 wt %	5 wt %	10 wt %	5 wt %	10 wt %
560(40)AB	9.8	9.8	10.8	10.8	NP	NP
540(60)AB	8.1	8.1	8.1	7.7	NP	NP
850(70)AB	8.1	8.9	N/A	N/A	N/A	N/A
600(80)AB	≤ 6.7	≤ 6.7	≤ 6.7	≤ 6.7	NP	NP
410(120)AB	≤ 6.7	≤ 6.7	7.0	7.4	7.0	7.4
910(190)AB	7.0	7.0	7.0	7.0	7.0	7.0
1340(60)ABA	≤ 8.7	≤ 8.7	N/A	N/A	NP	NP

the peak is qualitatively correlated with the size of the micelles. In most mixtures, the peak shifts to higher q with increasing polymer composition and temperature. For example, at 25 ^{o}C, three diblock samples have peaks below 0.067 Å^{-1}, but above the T_{NI} two of these peaks shift to higher q and only the 600(80) gels retain peaks below 0.067 Å^{-1}. The PS block length also affects the peak position, as can be seen by comparing the diblock series 564(40)AB, 540(60)AB, 600(80)AB, and 410(120)AB (see the data for $T_{NI} + 2$). The peak shifts to lower q with increasing PS block length. These results show that smaller micelles are formed at higher polymer concentrations, higher temperatures, and with copolymers with smaller PS block lengths.

Increasing the temperature across the T_{NI} significantly diminishes the low-q scattering for most but not all mixtures (Section 5.6). The loss of low-q scattering is associated with the loss of microphase separated structure, and the temperature above which the copolymers exist as free chains in solution is known as the microphase separation temperature T_{MST}. We use the expression microphase separation temperature to distinguish the present samples from block copolymer micelles which are ordered on a periodic lattice and show order-disorder transitions [17], although the terms are oftentimes used interchangeably [18]. Diblock and triblock copolymers with PS block smaller than 80 kg/mol show a T_{MST} coincident with the T_{NI} of the gel (Figs. 5.4, 5.5, 5.6, and 5.10). This is clearly shown by a dramatic drop in low-q intensity and loss of features in the data at low q. The diffuse excess scattering observed for 530(60)AB (Fig. 5.5) is likely due to compositional fluctuations in the vicinity of the T_{MST} [17]. By contrast, diblock copolymers with larger PS blocks show low-q scattering above the T_{NI} for some concentrations. In the case of 530(60)AB, a 5 wt % mixture has a T_{MST} coincident with the T_{NI}, but a 10 wt % mixture shows significant low-q scattering with discernable features up to 40 ^{o}C (Fig. 5.7). 450(120)AB mixtures with 5CB show micellar structure above the T_{NI} for both 5 wt % and 10 wt % mixtures. The T_{MST} is approximately 50 ^{o}C for 10 wt % 450(120)AB (Fig. 5.8). In the case of 840(190)AB, 5 and 10 wt% gels show significant low-q scattering at all temperatures tested, up to 60 ^{o}C (Fig. 5.9).

Increasing the temperature within the nematic phase also results in decreased scattering at low q. A decreased volume fraction of micelles due to an increasing number of free chains is unlikely given the low solubility of PS in nematic 5CB [3]. If the concentration of associated chains is independent of temperature in the nematic phase and micelles are assumed to be non-overlapping particles, then decreased scattering at low q is correlated with a smaller aggregation number [19].

5.4.3 Rheometry

Dynamic mechanical rheological measurements at low strains give information about the equilibrium mechanical properties of the diblock and triblock copolymer mixtures with 5CB. The data from dynamic rheological measurements for all the diblock and triblock copolymer mixtures in 5CB is given in Section 5.7. The various samples with different PS and SGLCP block lengths and polymer architecture (diblock vs. triblock) share many characteristics in their rheological behavior. All the systems show solid-like behavior at sufficiently high polymer concentrations, with $G' >> G''$ and a plateau modulus over a wide range of frequencies. These properties are characteristic of crosslinked rubbers [20]. For the purposes of this study, the term “gel” will refer to a mixture that exhibits solid-like behavior over a wide range of frequencies [21]. The mixtures that do not show solid-like behavior in the nematic phase (e.g., 5 wt % 530(60)AB at 25 ^{o}C, Fig. 5.13), do show viscoelastic behavior in the nematic phase – their rheological behavior is not like that of an elastic solid ($G' >> G''$, and G' frequency independent) nor a like that of a liquid ($G'' >> G'$, $G' \sim \omega^2$, $G'' \sim \omega$).

Both diblock and triblock LC copolymers can form gels in 5CB, as evidenced by the rheological behavior of 5 wt % 850(70)AB (Fig. 5.15) and 5 wt % 1340(6)ABA (Fig. 5.23). Bridging between micelles, where one polymer strand has its end associated in two different micelle cores, is only possible in triblock copolymer mixtures. The fact that diblock LC copolymers can form gels indicates that micellar repulsion plays an important role in gelation. These diblock and triblock gels share characteristics with the "soft" gel phases [11, 13, 22], which are disordered and have a modulus significantly lower than that for ordered micellar phases, typically 10^4 Pa [13].

In all mixtures studied, significant changes to the rheological behavior were observed with temperature, in particular near the T_{NI} (e.g., Figs. 5.24 and 5.22). Many mixtures transition from viscoelastic behavior below the T_{NI} to terminal behavior ($G' << G''$, $G'' \sim \omega$) above the T_{NI} (e.g., Fig. 5.15). All the mixtures exhibited liquid-like behavior at sufficiently high temperatures, but recovered their viscoelastic behavior on cooling (e.g., Figs. 5.24 and 5.22). In addition, increasing the temperature within the nematic phase results in a decreased storage modulus for all diblock and triblock mixtures.

The rheological behavior of the SGLCP block copolymer – 5CB mixtures depends on the PS and SGLCP block lengths. Diblock copolymers with larger PS blocks have higher storage moduli at a particular concentration, as shown in the series 590(40)AB, 530(60)AB, and 620(80)AB at a concentration of 10 wt % (Table 5.3). Furthermore, diblock copolymers with larger PS block lengths more readily show gel-like behavior. For example, the dynamic rheometry measurements show that 5 wt % 620(80)AB is a gel (Fig. 5.17), while 5 wt % 590(40)AB and 530(60)AB are viscoelastic liquids (Figs. 5.11 and 5.13). Diblock copolymers with longer SGLCP blocks also have a higher storage modulus, as can be seen by comparing 890(70)AB to 530(60)AB (Table 5.3).

The sol-gel transition temperature, which marks the transition from solid-like behavior to liquid-like behavior, also depends on the PS block length of the copolymer in the mixture. The sol-gel transition is taken to be the temperature above which the loss modulus exceeds the storage modulus ($G'' > G'$) at a frequency of 1 rad/s. Almost all the samples studied have a sol-gel transition coincident with the T_{NI} (Table 5.4). Two notable exceptions are gels formed by the copolymers with the largest PS blocks, 840(190)AB and 450(120)AB. In the case of 5 wt % 840(190)AB, the

Table 5.3: Gel storage modulus (Pa) at 20 ^{o}C and 1 rad/s

Polymer	5 wt %	10 wt %
590(40)AB	4.52	53.3
530(60)AB	2.93	99.4
890(70)AB	28.8	202
620(80)AB	29.1	201
450(120)AB	14.9	142
840(190)AB	48.5	100
1320(60)ABA	68.6	192
800(20)ABA	70.3	196

sol-gel transition occurs well above the T_{NI} of the gel, at approximately 42 ^{o}C (Fig. 5.22). Also, 10 wt % 450(120)AB exhibits a significant range of temperatures above the T_{NI}, up to 40 ^{o}C, where it exhibits viscoelastic behavior with $G' \sim G''$ (Figs. 5.35 and 5.36).

This temperature-dependent and frequency-dependent behavior suggest that the PS aggregates are not glassy (even though T_g for PS is $\sim$ 105 ^{o}C). Polymers linked together with glassy crosslinks exhibit solid-like behavior at all frequencies [23]. For the present samples, we observe liquid like behavior at low frequencies, especially near the T_{NI}. For example, 5 wt % 1320(60)ABA shows liquid-like behavior at 34 ^{o}C for frequencies lower than 0.1 rad/s (Fig. 5.23). We conclude that the PS endblocks are swollen with LC solvent and that PS endblocks can disengage from the physical crosslinks on finite time scales. This is consistent with the “slow” dynamic relaxation processes observed in dynamic light scattering studies (Chapter 4).

A comparison between the rheological behavior of triblock and diblock samples shows that bridging does take place in triblock gels and increases the modulus relative to diblock gels. Diblock 530(60)AB has a matching PS endblock and the same mass ratio of PS to SGLCP as that of triblock 1320(60)ABA. Triblock 1320(60)ABA forms a gel at 5 wt % (Fig. 5.23), but a 5 wt % mixture of 530(60)AB does not (Fig. 5.13). A comparison of 590(40)AB and 800(20)ABA, which has a shorter PS block, provides further evidence of bridging. While 5 wt % 800(20)ABA exhibits a plateau modulus at low temperatures (Fig. 5.25), 5 wt % 590(40)AB does not (Fig. 5.11).

We can gain insight into the relationship between micelle formation and the gels’ rheological

Table 5.4: The reduced temperature $T - T_{NI}$ for the sol-gel transition measured by rheology and the T_{MST} measured by SANS. The rheological measurement is the temperature (while heating) at which the storage modulus drops below the loss modulus, and the SANS measurement is the lowest temperature at which the low-q scattered intensity is significantly diminished (overlapping or nearly overlapping with the SANS data for 710LCP) and lacks features characteristic of micellar structure.

	Rheology (^{o}C)		SANS (^{o}C)	
Polymer	5 wt %	10 wt %	5 wt %	10 wt %
590(40)AB	no gel	-1.0	3.0	2.0
530(60)AB	no gel	-0.5	7.5	6.5
890(70)AB	0.0	0.0	4.5	4.5
620(80)AB	1.5	1.5	7.5	3.5
450(120)AB	-1.0	2.5	>17.0	16.5
840(190)AB	6.0	17	>27.5	>27.5
1320(60)ABA	0.0	0.0	6.5	6.5

properties by comparing the temperatures at which micellar structure vanishes in the SANS experiments to the sol-gel transition measured by rheology (Table 5.4). The neutron scattering experiments are performed at much larger temperature intervals, and therefore they necessarily have a greater uncertainty in temperature. Nevertheless, the comparison shows an interesting correlation between micelle formation and rheology. First, the data suggest that micelles can persist well above the sol-gel transition measured by rheology. In the most extreme case, 910(190)AB gels display a sol-gel transition at 45 ^{o}C, but micelles persist up to at least 60 ^{o}C. The data also show that the location of the sol-gel transition is correlated with micelle formation. Diblocks that gel in 5CB above the T_{NI} (600(80)AB, 410(120)AB, and 910(190)AB) also show low-q scattering far into the isotropic phase (Table 5.4).

5.5 Discussion

LC gels formed by diblock and triblock LC copolymers represent a novel example of block copolymer self-assembly for two distinct reasons. First, the gel structure inherits the anisotropy of the host solvent. Micelles are anisotropic, as is the interconnected micellar network present in triblock gels. This anisotropy in the gel structure has significance for texture transitions and dynamic properties of the gels, as discussed in Chapters 3 and 4. A second reason arises from the existence of a nematic-to-isotropic phase transition of the solvent. The solvent quality for the isotropic PS blocks changes drastically across the T_{NI}, resulting in significant structural changes in a small temperature window. This can result in useful properties, such as a thermoreversible gelation, and is also interesting for the potentially novel phase transitions that may arise [24].

The SANS and rheometry results establish several trends for the diblock and triblock copolymer micelle structure with temperature, concentration, and block sizes. SANS revels smaller micelles at higher polymer concentrations and higher temperatures, and the aggregation number decreases with temperature in the nematic phase. SANS also reveals that a larger PS block length is correlated with an increase in the T_{MST}. Rheometry reveals a decreased storage modulus with temperature in the nematic phase and an increased sol-gel transition temperature for copolymers with larger PS blocks.

The neutron scattering and rheometry studies establish a relationship between micelle formation and the mechanical properties of the gel. Micelle formation drives gel formation through intermicellar interactions, namely micelle-micelle repulsion and bridging between micelles. These interactions are temperature dependent. Increasing the temperature within the nematic phase decreases the size of the micelles, which corresponds with a decreasing storage modulus. Heating the sample above the T_{NI} oftentimes results in loss of physical associations, resulting in a drop in the modulus and a transition to a sol state. In some cases, the T_{MST} is significantly higher than the sol-gel transition temperature (see 10 wt % 620(80)AB, Figs. 5.7 and 5.33). In this case, micelles may exist in a “gas-like” state of non-interacting micelles above the sol-gel transition temperature [11]. The positional correlations of the micelles has a finite lifetime even in triblock gels, demonstrating that the PS endblocks are not glassy but plasticized by LS solvent. Furthermore, the strength of self-assembly that drives gel formation can be controlled by increasing the size of the PS blocks, which increases the driving force for self assembly and results in stiffer gels, higher sol-gel transition temperatures, and a higher T_{MST}.

Based on the relative sizes of the PS and SGLCP blocks of the copolymers, we expect the micelles to have a “hairy” structure, with an extended corona and a much smaller core [25]. Scaling arguments by Halperin et al. for “hairy” micelles predict that the aggregation number is strongly dependent on the PS-core block size [25]. The SANS data show an increasing micelle size with increasing PS block size (Table 5.2), consistent with this prediction. The physical picture of “hairy” micelles suggests that coronal repulsions may play an equal or dominant role to bridging in determining intermicellar interaction, which can explain the comparable dynamic rheological behavior observed for 1320(60)ABA (Fig. 5.23) and 870(70)AB (Fig. 5.15). Also, this may explain the lack of ordering observed for the diblock mixtures, which in a separate study were investigated to concentrations as high as 20 wt % [24]. “Hairy” micelles are expected to have a softer intermicellar potential, reducing the tendency for long-range lattice ordering, although few experimental studies exist to corroborate this [13, 22].

In summary, SANS experiments and rheometry found that the micellar structure of LC block copolymer gels changes significantly across the T_{NI}. The loss of orientational order of the LC solvent is associated with a decreased selectivity for the isotropic PS block and an associated loss of micellar structure in many cases. The size of the PS block is an important variable determining the driving force for self-assembly, with larger PS blocks associated with gelation even above the T_{NI}. No long-range lattice order was exhibited by the copolymer micellar gels, and this may be related to the “hairy” structure of the block copolymer micelles.

5.6 SANS of diblock and triblock gels

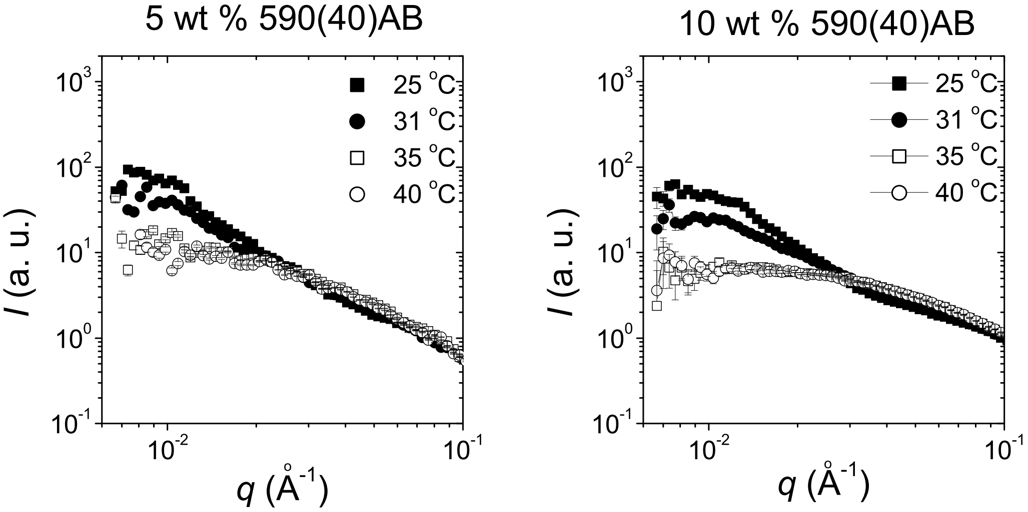

Figure 5.4: Azimuthally averaged SANS pattern for 5 and 10 wt % 590(40)AB in perdeuterated 5CB. The 5 wt % mixture is single-phase nematic for all $T \leq 32.1$ ^{o}C and single-phase isotropic for $T \geq 34.0$ ^{o}C. The 10 wt % mixture is single-phase nematic for all $T \leq 33.0$ ^{o}C and single-phase isotropic for $T \geq 36.0$ ^{o}C.

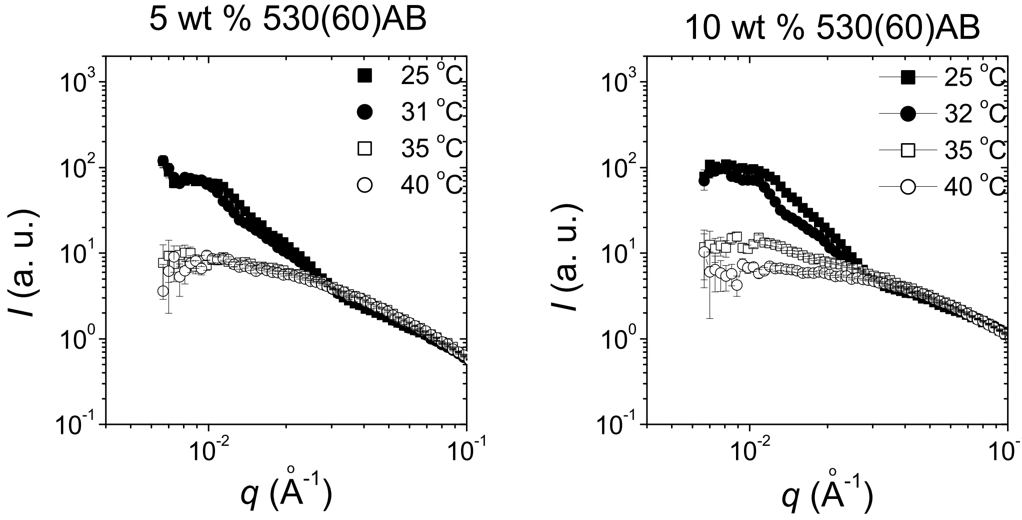

Figure 5.5: Azimuthally averaged SANS pattern for 5 and 10 wt % 530(60)AB in perdeuterated 5CB. The 5 wt % mixture is single-phase nematic for all $T \leq 32.5$ ^{o}C and single-phase isotropic for $T \geq 34.0$ ^{o}C. The 10 wt % mixture is single-phase nematic for all $T \leq 33.5$ ^{o}C and single-phase isotropic for $T \geq 34.5$ ^{o}C.

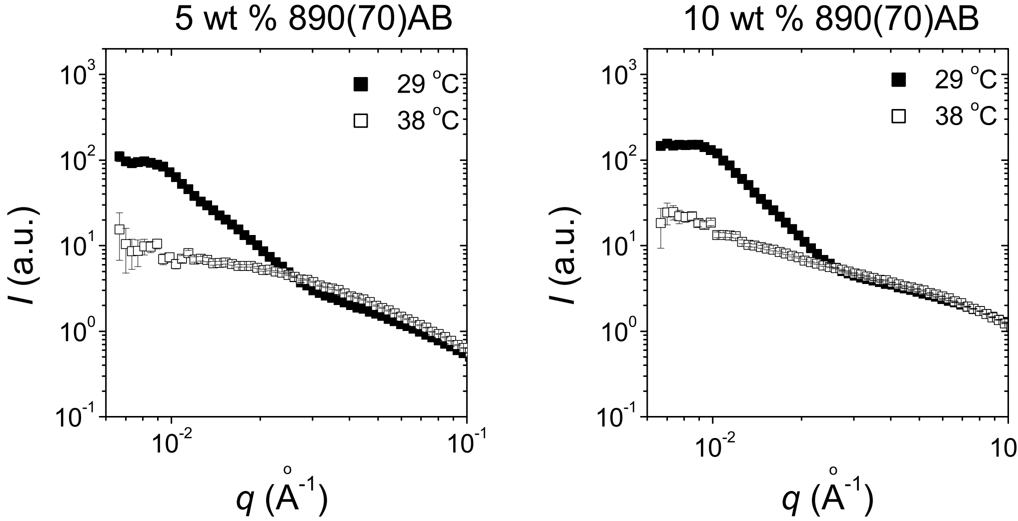

Figure 5.6: Azimuthally averaged SANS pattern for 5 and 10 wt % 890(70)AB in perdeuterated 5CB. The mixtures are single-phase nematic for all $T \leq 33.5$ ^{o}C and single-phase isotropic for $T > 33.5$ ^{o}C.

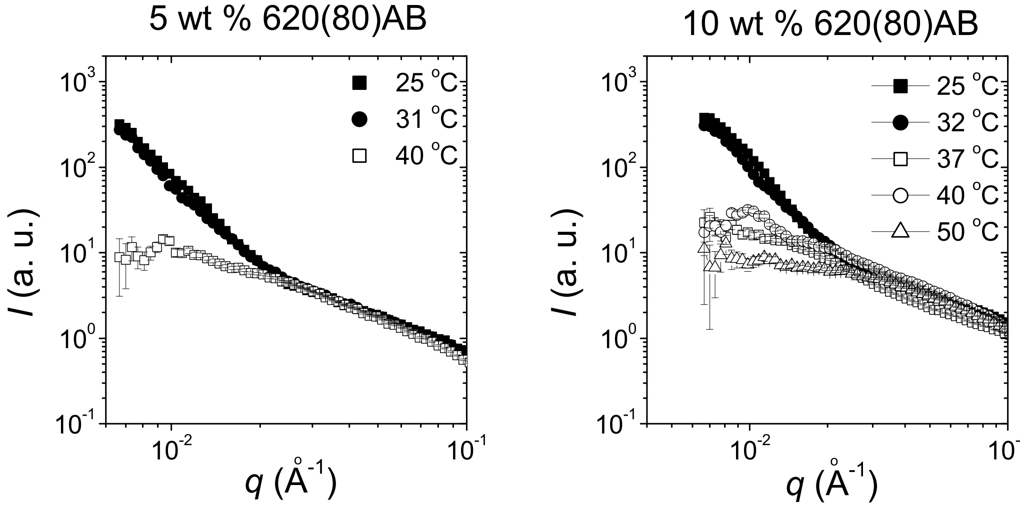

Figure 5.7: Azimuthally averaged SANS pattern for 5 and 10 wt % 620(80)AB in perdeuterated 5CB. The 5 wt % mixture is single-phase nematic for all $T \leq 32.5$ ^{o}C and single-phase isotropic for $T \geq 39.0$ ^{o}C. The 10 wt % mixture is single-phase nematic for all $T \leq 33.5$ ^{o}C and single-phase isotropic for $T \geq 38.5$ ^{o}C.

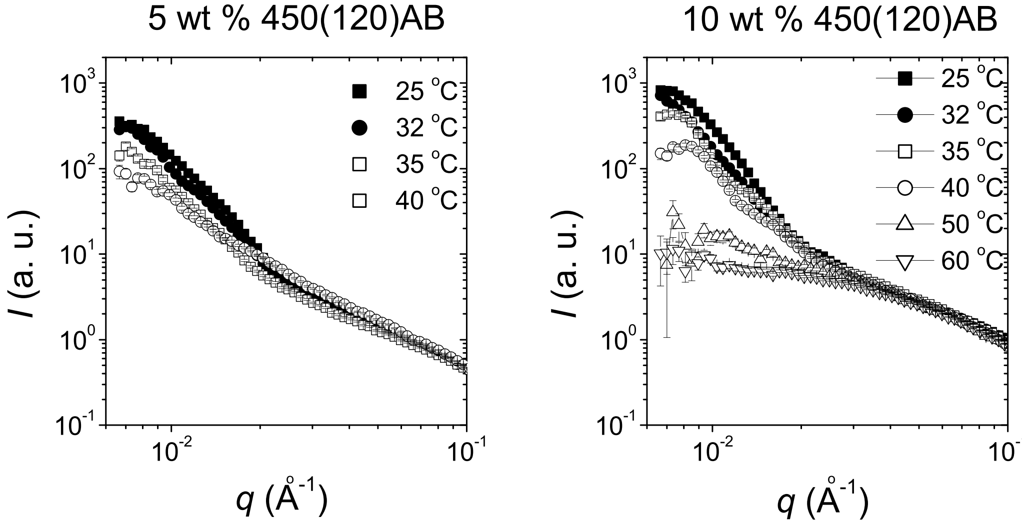

Figure 5.8: Azimuthally averaged SANS pattern for 5 and 10 wt % 450(120)AB in perdeuterated 5CB. The 5 wt % mixture is single-phase nematic for all $T \leq 33.0$ ^{o}C and single-phase isotropic for $T \geq 34.0$ ^{o}C. The 10 wt % mixture is single-phase nematic for all $T \leq 33.5$ ^{o}C and single-phase isotropic for $T \geq 34.0$ ^{o}C.

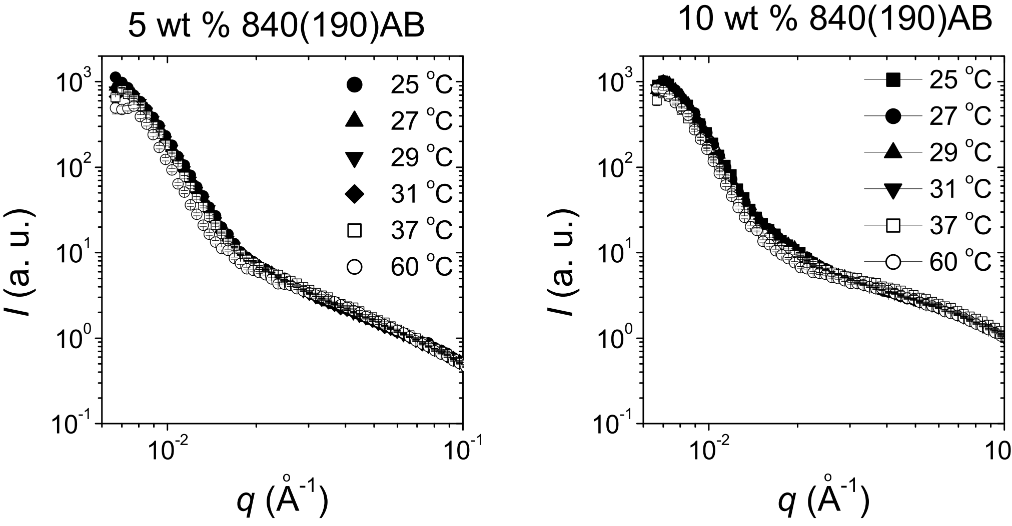

Figure 5.9: Azimuthally averaged SANS pattern for 5 and 10 wt % 840(190)AB in perdeuterated 5CB. The 5 wt % mixture is single-phase nematic for all $T \leq 32.9$ ^{o}C and single-phase isotropic for $T > 32.9$ ^{o}C. The 10 wt % mixture is single-phase nematic for all $T \leq 31.5$ ^{o}Cand single-phase isotropic for $T \geq 34.7$ ^{o}C.

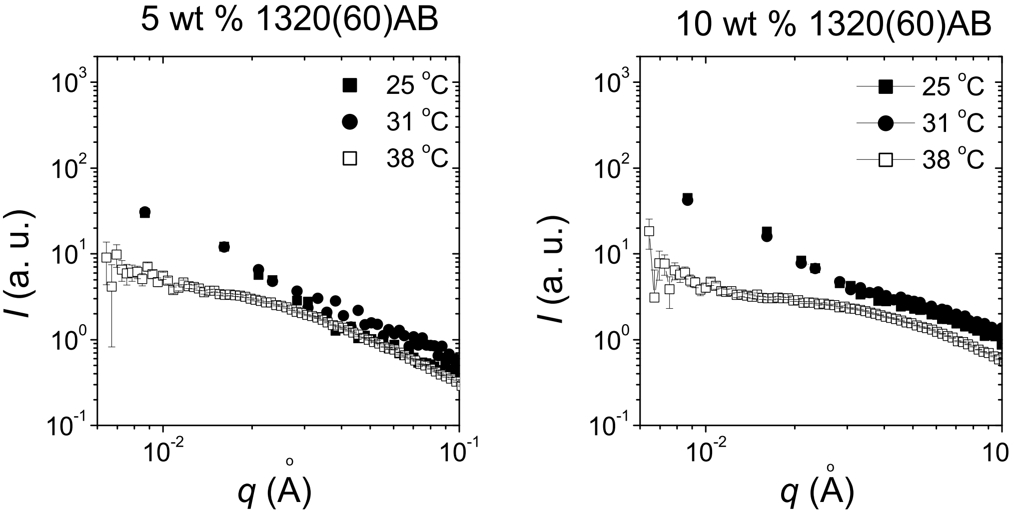

Figure 5.10: SANS pattern for 5 and 10 wt % 1320(60)ABA in D5CB. The data shown is averaged over a 15^o wedge oriented along the nematic director. Both the 5 and 10 wt % mixtures are single-phase nematic for all $T \leq 33.5$ ^{o}C and single-phase isotropic for $T > 33.5$ ^{o}C.

5.7 Rheometry of diblock and triblock mixtures

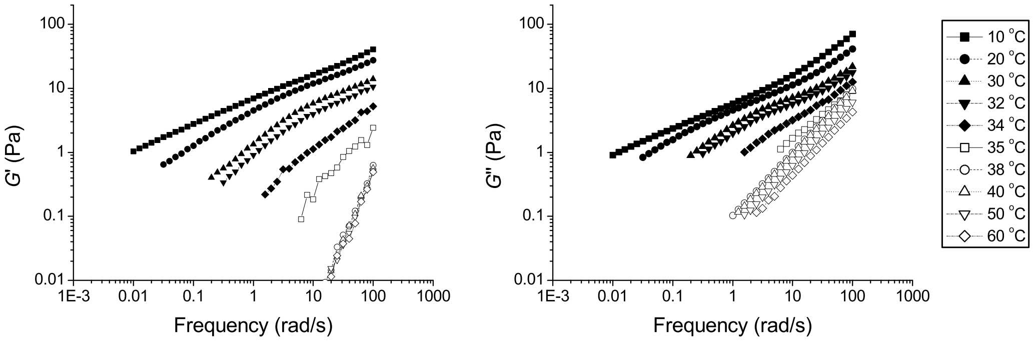

Figure 5.11: Dynamic storage modulus (G') and loss modulus (G'') of 5 wt % 590(40) AB diblock in 5CB. The mixture is single-phase nematic for all $T \leq 35.5$ ^{o}C (closed symbols) and single-phase isotropic for $T \geq 37.5$ ^{o}C (open symbols).

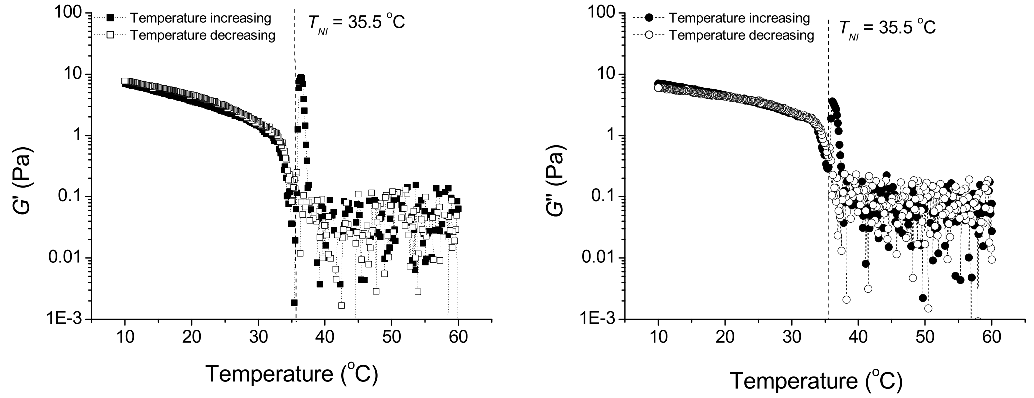

Figure 5.12: Dynamic storage modulus (G') and loss modulus (G'') of 5 wt % 590(40) AB diblock in 5CB while heating (closed symbols) and cooling (open symbols) at 0.5 ^{o}C/min

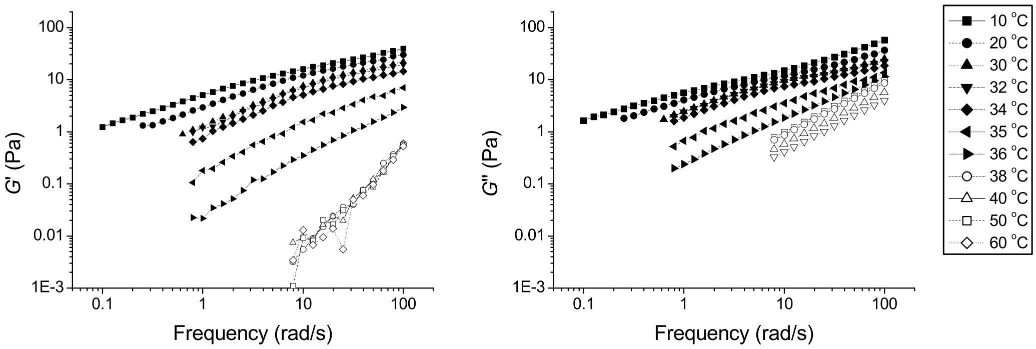

Figure 5.13: Dynamic storage modulus(G') and loss modulus (G'') of 5 wt % 530(60) AB diblock in 5CB. The mixture is single-phase nematic for all $T \leq 36.0$ ^{o}C (closed symbols) and single-phase isotropic for $T > 36.0$ ^{o}C (open symbols).

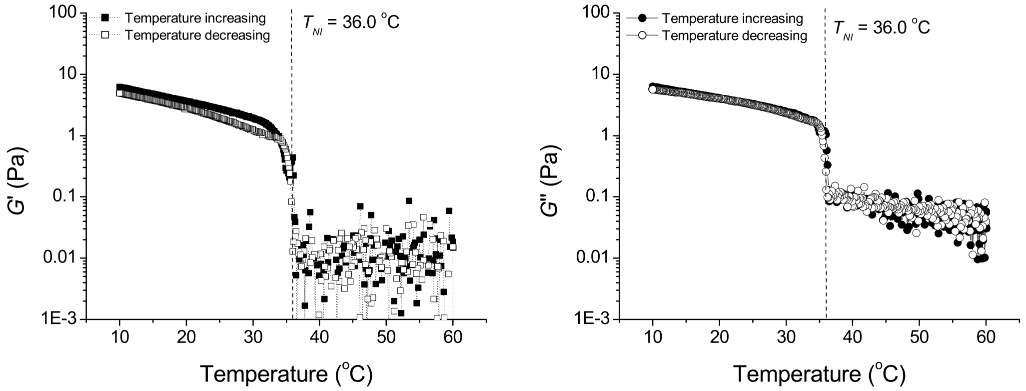

Figure 5.14: Dynamic storage modulus (G') and loss modulus (G'') of 5 wt % 530(60) AB diblock in 5CB while heating (closed symbols) and cooling (open symbols) at 0.5 ^{o}C/min

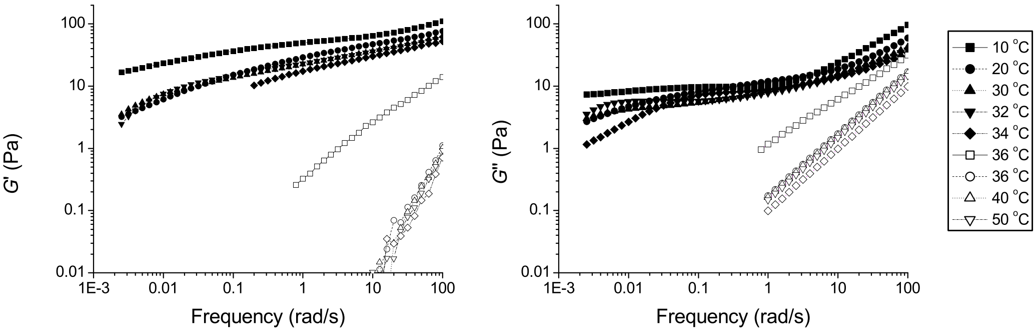

Figure 5.15: Dynamic storage modulus(G') and loss modulus (G'') of 5 wt % 890(70) AB diblock in 5CB. The mixture is single-phase nematic for all $T \leq 35.9$ ^{o}C (closed symbols) and single-phase isotropic for $T > 35.9$ ^{o}C (open symbols).

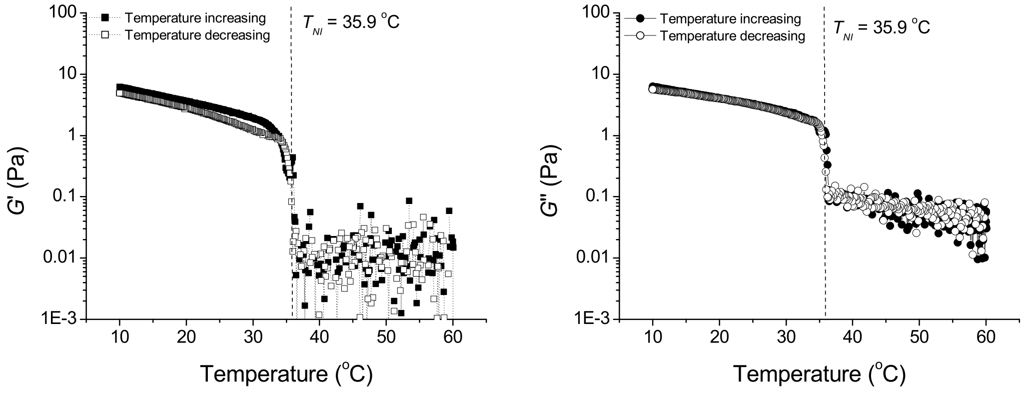

Figure 5.16: Dynamic storage modulus (G') and loss modulus (G'') of 5 wt % 890(70) AB diblock in 5CB while heating (closed symbols) and cooling (open symbols) at 0.5 ^{o}C/min

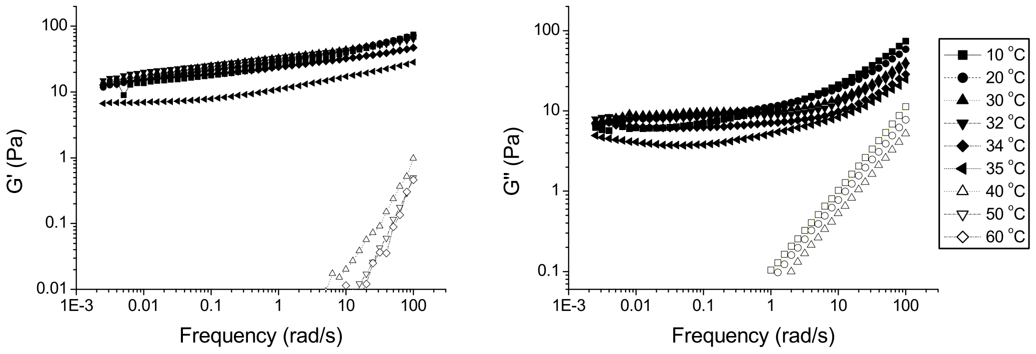

Figure 5.17: Dynamic storage modulus (G') and loss modulus (G'') of 5 wt % 620(80)AB diblock in 5CB. The mixture is single-phase nematic for all $T \leq 35.5$ ^{o}C (closed symbols) and single-phase isotropic for $T \geq 40.0$ ^{o}C (open symbols).

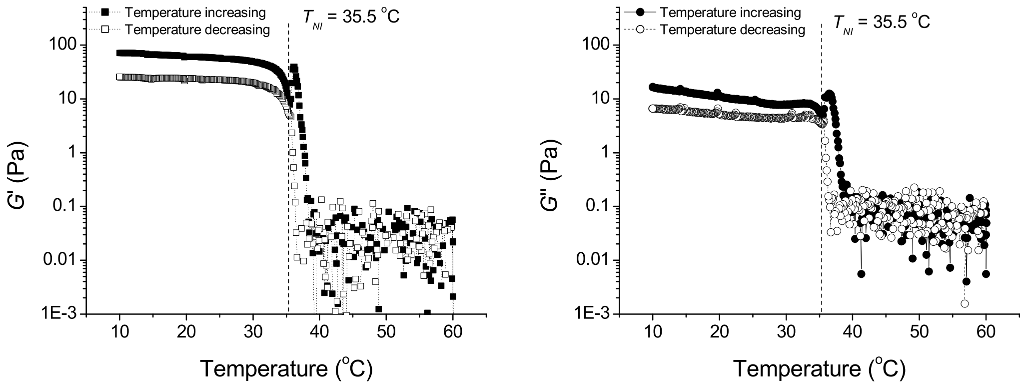

Figure 5.18: Dynamic storage modulus (G') and loss modulus (G'') of 5 wt % 620(80) AB diblock in 5CB while heating (closed symbols) and cooling (open symbols) at 0.5 ^{o}C/min

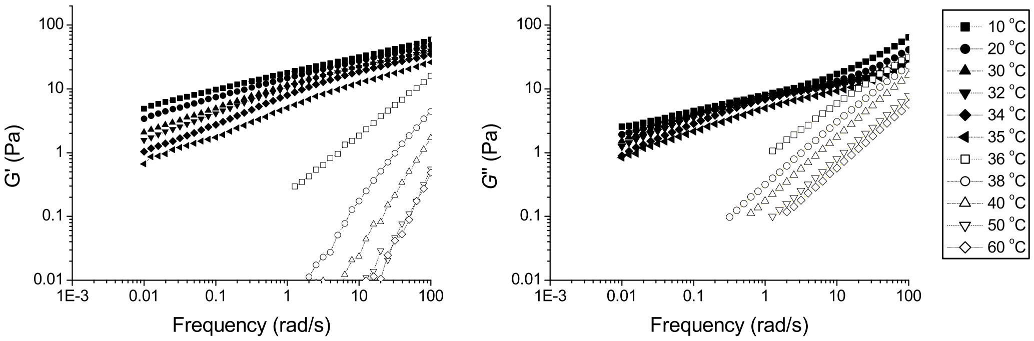

Figure 5.19: Dynamic storage modulus (G') and loss modulus (G'') of 5 wt % 450(120) AB diblock in 5CB. The mixture is single-phase nematic for all $T \leq 35.8\ ^o$C (closed symbols) and single-phase isotropic for $T > 35.8\ ^o$C (open symbols).

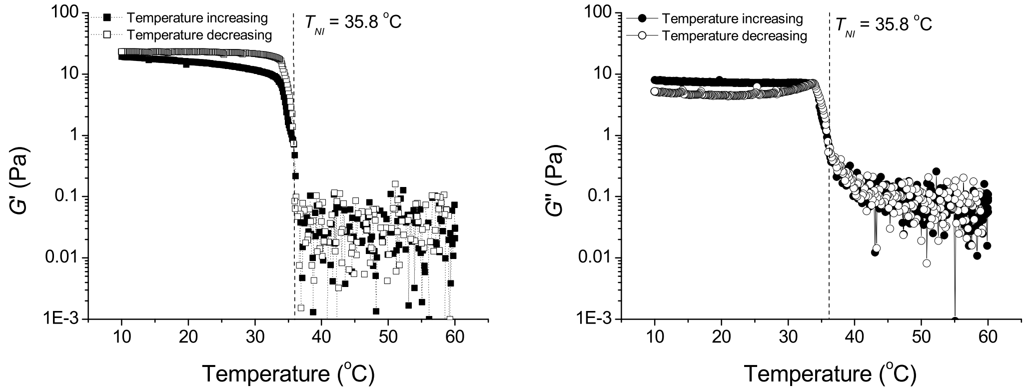

Figure 5.20: Dynamic storage modulus (G') and loss modulus (G'') of 5 wt % 450(120) AB diblock in 5CB while heating (closed symbols) and cooling (open symbols) at 0.5 ^{o}C/min

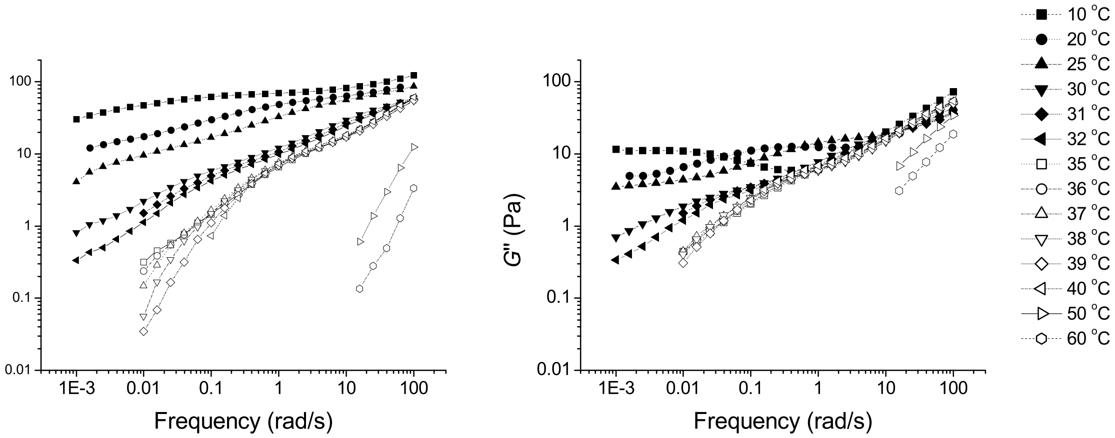

Figure 5.21: Dynamic storage modulus (G') and loss modulus (G'') of 5 wt % 840(190) AB diblock in 5CB. The mixture is single-phase nematic for all $T \leq 32.0$ ^{o}C (closed symbols) and single-phase isotropic for $T \geq 35.0$ ^{o}C (open symbols).

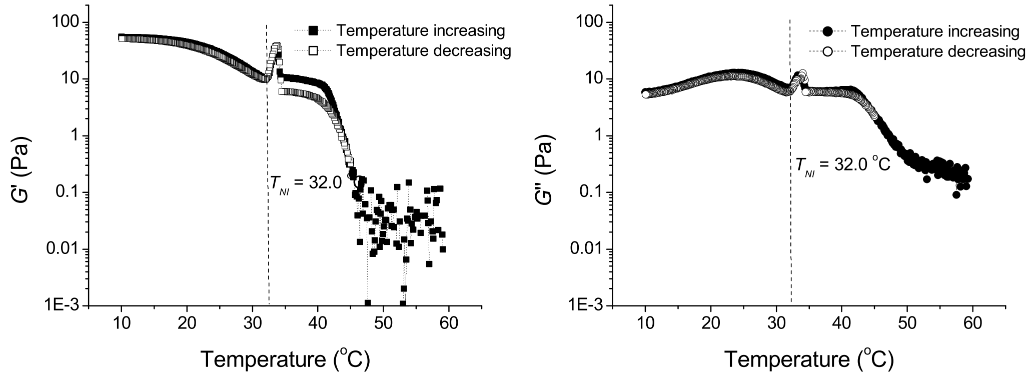

Figure 5.22: Dynamic storage modulus (G') and loss modulus (G'') of 5 wt % 840(190) AB diblock in 5CB while heating (closed symbols) and cooling (open symbols) at 0.5 ^{o}C/min

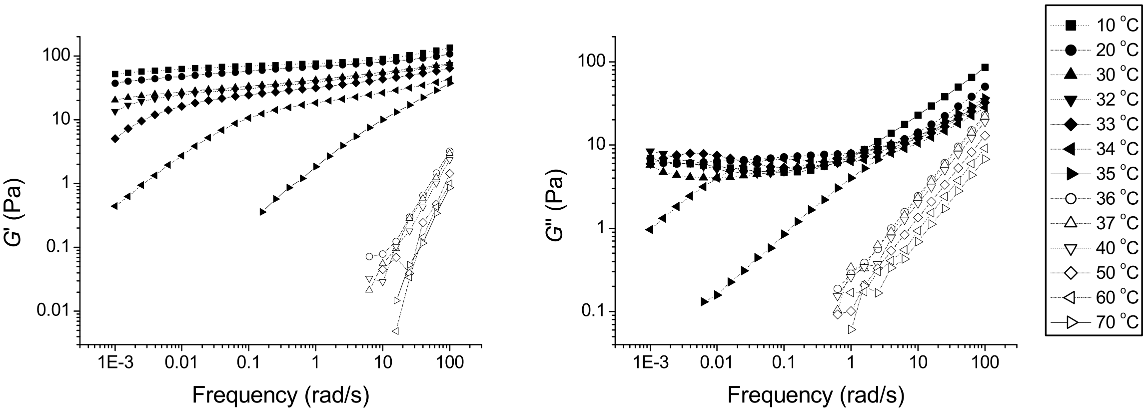

Figure 5.23: Dynamic storage modulus (G') and loss modulus (G'') of 5 wt % 1320(60)ABA in 5CB. The mixture is single-phase nematic for all $T \leq 35.2$ ^{o}C (closed symbols) and single-phase isotropic for $T > 35.2$ ^{o}C (open symbols).

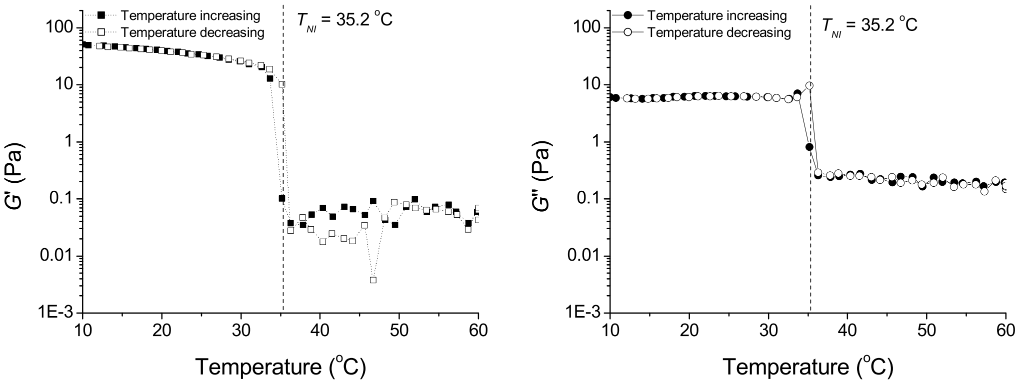

Figure 5.24: Dynamic storage modulus (G') and loss modulus (G'') of 5 wt % 1320(60) ABA triblock in 5CB while heating (closed symbols) and cooling (open symbols) at 5.0 ^{o}C/min

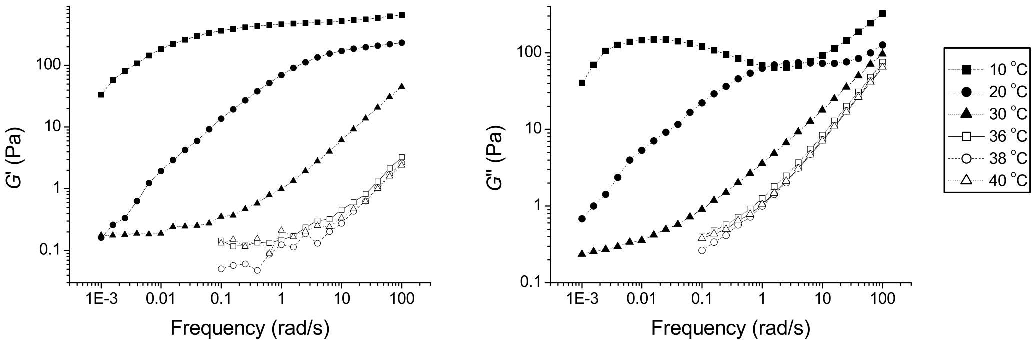

Figure 5.25: Dynamic storage modulus (G') and loss modulus (G'') of 5 wt % 800(20)ABA in 5CB. The mixture is single-phase nematic for all $T \leq 31.7$ ^{o}C (closed symbols) and single-phase isotropic for $T \geq 34.5$ ^{o}C (open symbols).

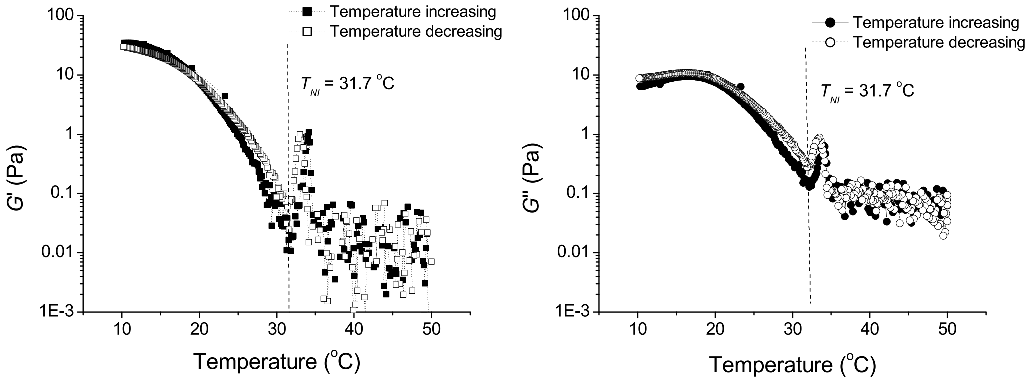

Figure 5.26: Dynamic storage modulus (G') and loss modulus (G'') of 5 wt % 800(20)ABA in 5CB while heating (closed symbols) and cooling (open symbols) at 0.5 ^{o}C/min

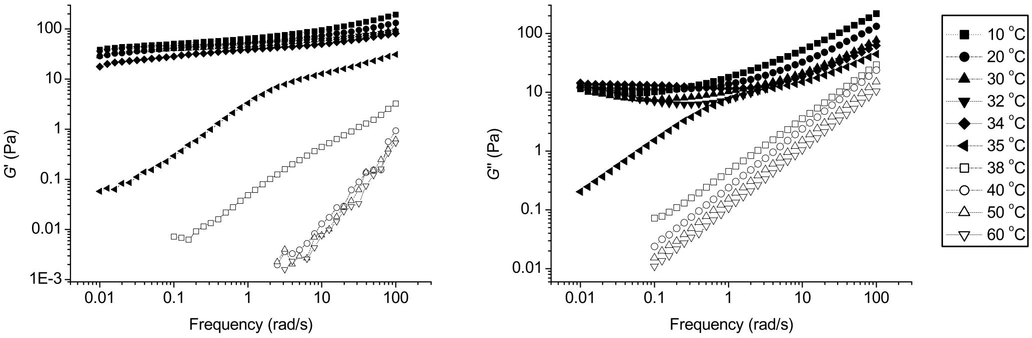

Figure 5.27: Dynamic storage modulus (G') and loss modulus (G'') of 10 wt % 590(40) AB diblock in 5CB. The mixture is single-phase nematic for all $T \leq 35.5$ ^{o}C (closed symbols) and single-phase isotropic for $T \geq 37.5$ ^{o}C (open symbols).

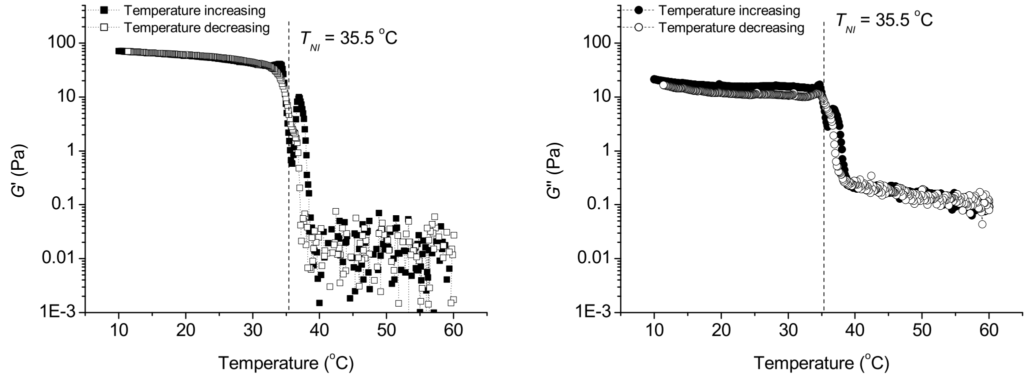

Figure 5.28: Dynamic storage modulus (G') and loss modulus (G'') of 10 wt % 590(40) AB diblock in 5CB while heating (closed symbols) and cooling (open symbols) at 0.5 ^{o}C/min

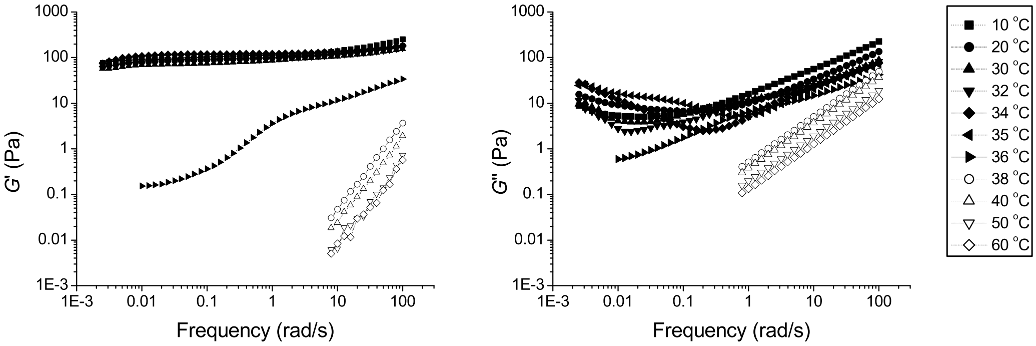

Figure 5.29: Dynamic storage modulus (G') and loss modulus (G'') of 10 wt % 530(60) AB diblock in 5CB. The mixture is single-phase nematic for all $T \leq 36.2$ ^{o}C (closed symbols) and single-phase isotropic for $T > 36.2$ ^{o}C (open symbols).

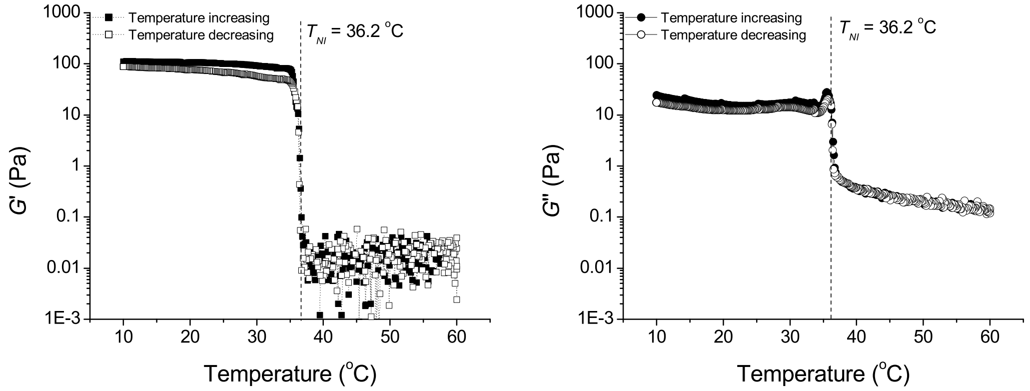

Figure 5.30: Dynamic storage modulus (G') and loss modulus (G'') of 10 wt % 530(60) AB diblock in 5CB while heating (closed symbols) and cooling (open symbols) at 0.5 ^{o}C/min

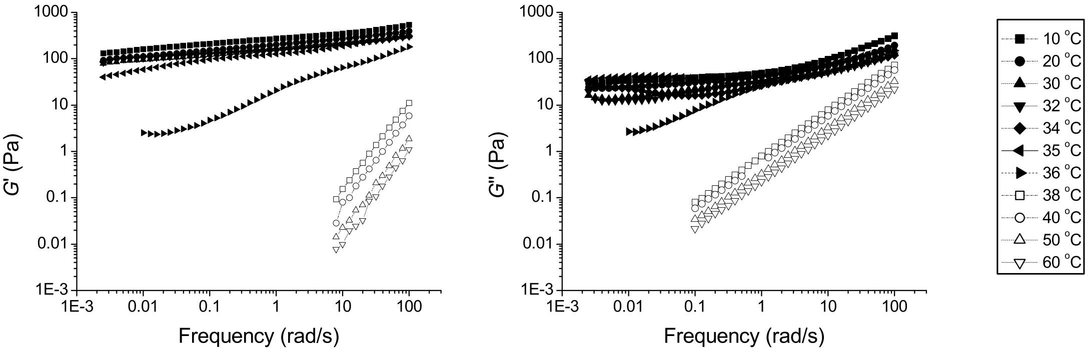

Figure 5.31: Dynamic storage modulus (G') and loss modulus (G'') of 10 wt % 890(70) AB diblock in 5CB. The mixture is single-phase nematic for all $T \leq 36.1$ ^{o}C (closed symbols) and single-phase isotropic for $T > 36.1$ ^{o}C (open symbols).

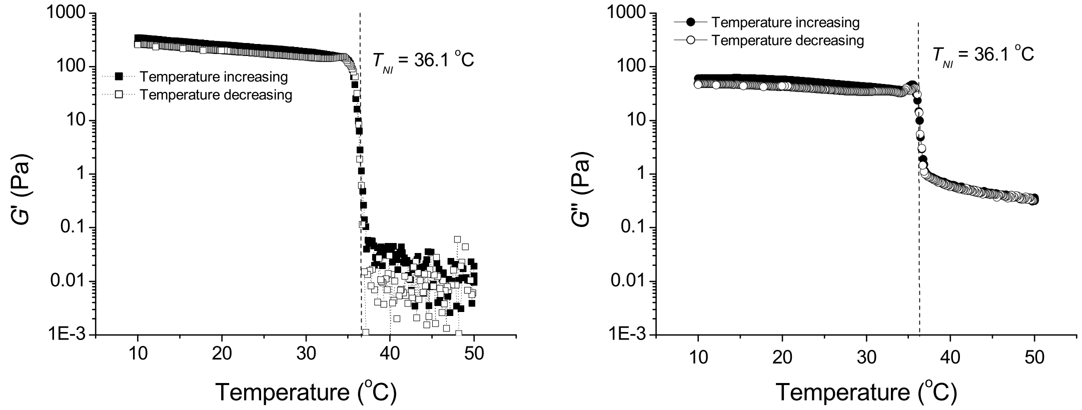

Figure 5.32: Dynamic storage modulus (G') and loss modulus (G'') of 10 wt % 890(70) AB diblock in 5CB while heating (closed symbols) and cooling (open symbols) at 0.5 ^{o}C/min

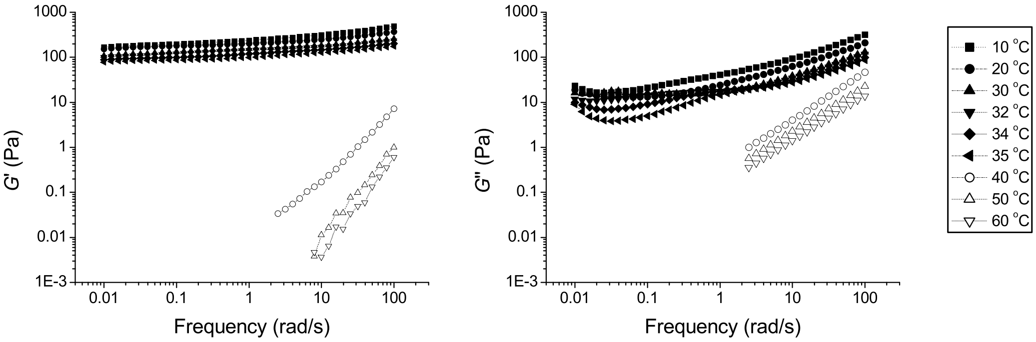

Figure 5.33: Dynamic storage modulus (G') and loss modulus (G'') of 10 wt % 620(80)AB diblock in 5CB. The mixture is single-phase nematic for all $T \leq 35.5$ ^{o}C (closed symbols) and single-phase isotropic for $T \geq 40.0$ ^{o}C (open symbols).

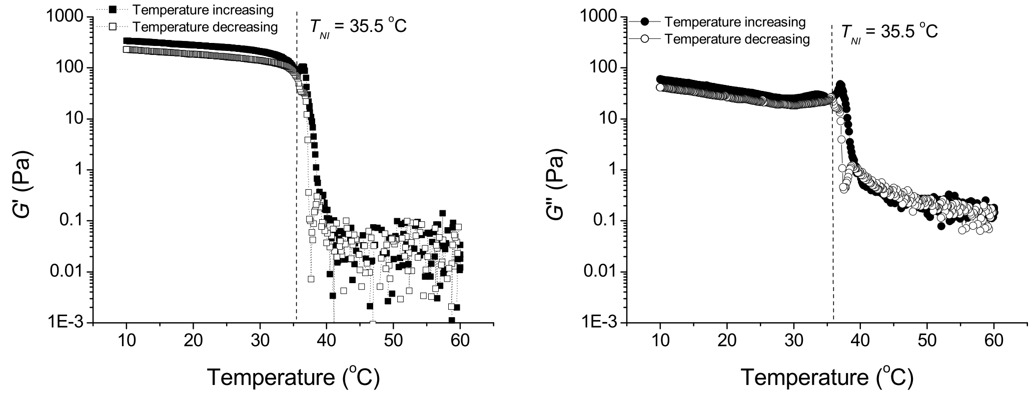

Figure 5.34: Dynamic storage modulus (G') and loss modulus (G'') of 10 wt % 620(80) AB diblock in 5CB while heating (closed symbols) and cooling (open symbols) at 0.5 ^{o}C/min

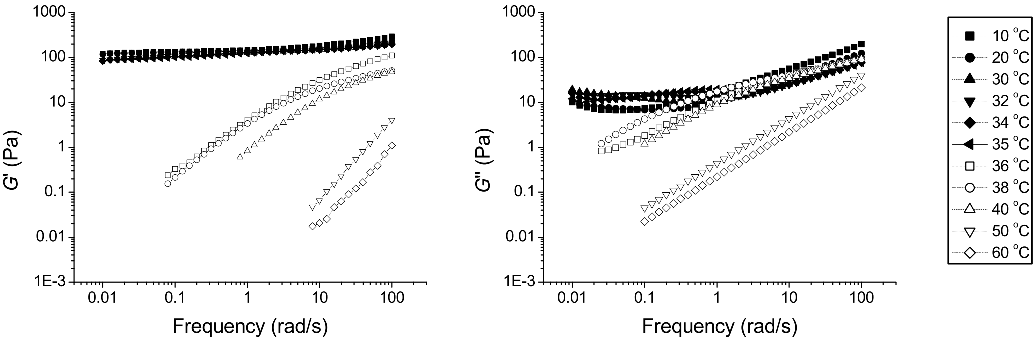

Figure 5.35: Dynamic storage modulus (G') and loss modulus (G'') of 10 wt % 450(120) AB diblock in 5CB. The mixture is single-phase nematic for all $T < 36.0$ ^{o}C (closed symbols) and single-phase isotropic for $T \geq 36.0$ ^{o}C (open symbols).

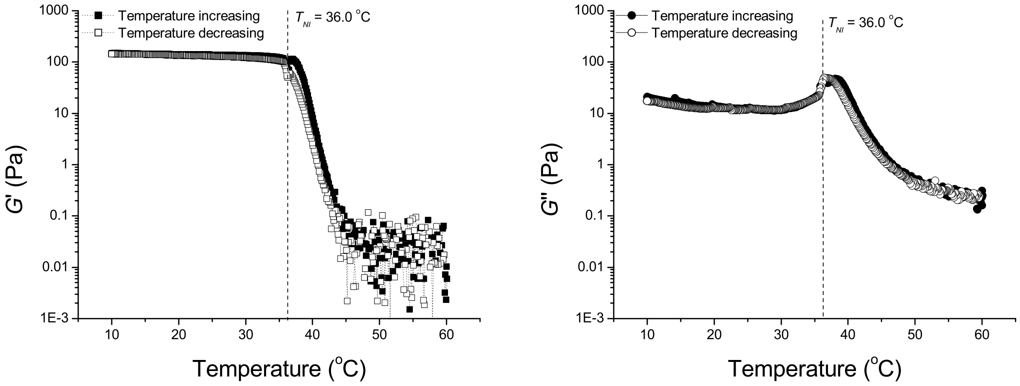

Figure 5.36: Dynamic storage modulus (G') and loss modulus (G'') of 10 wt % 450(120) AB diblock in 5CB while heating (closed symbols) and cooling (open symbols) at 0.5 ^{o}C/min

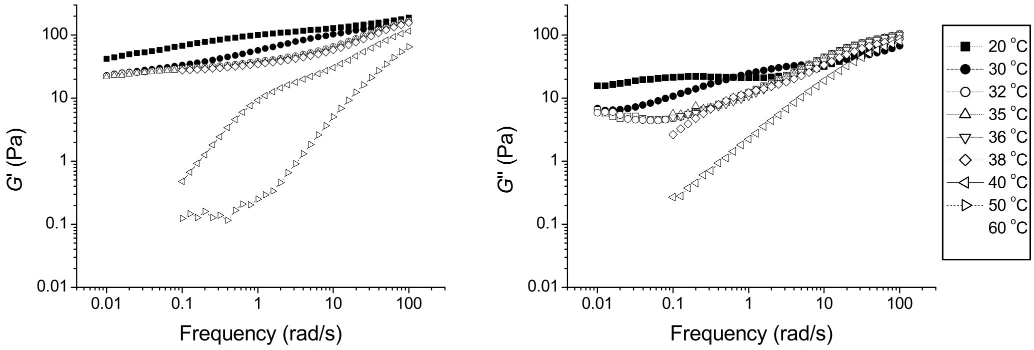

Figure 5.37: Dynamic storage modulus (G') and loss modulus (G'') of 10 wt % 840(190) AB diblock in 5CB. The mixture is single-phase nematic for all $T \leq 31.8$ ^{o}C (closed symbols) and single-phase isotropic for $T \geq 34.0$ ^{o}C (open symbols).

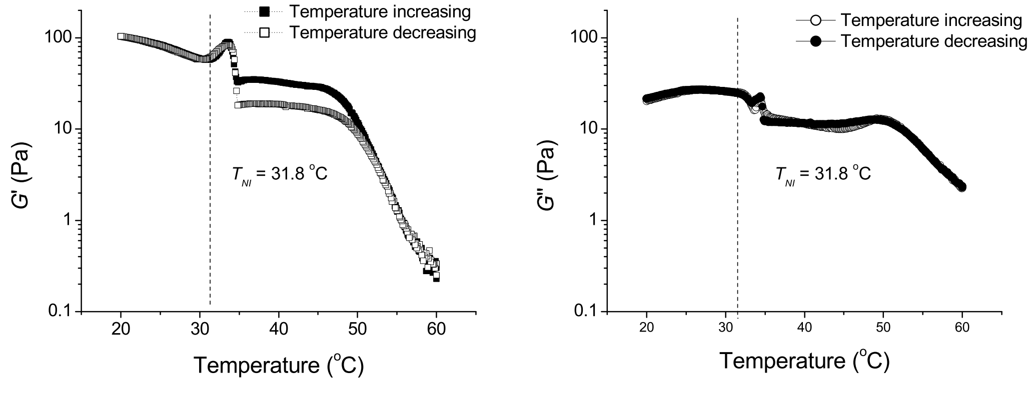

Figure 5.38: Dynamic storage modulus (G') and loss modulus (G'') of 10 wt % 840(190) AB diblock in 5CB while heating (closed symbols) and cooling (open symbols) at 0.5 ^{o}C/min

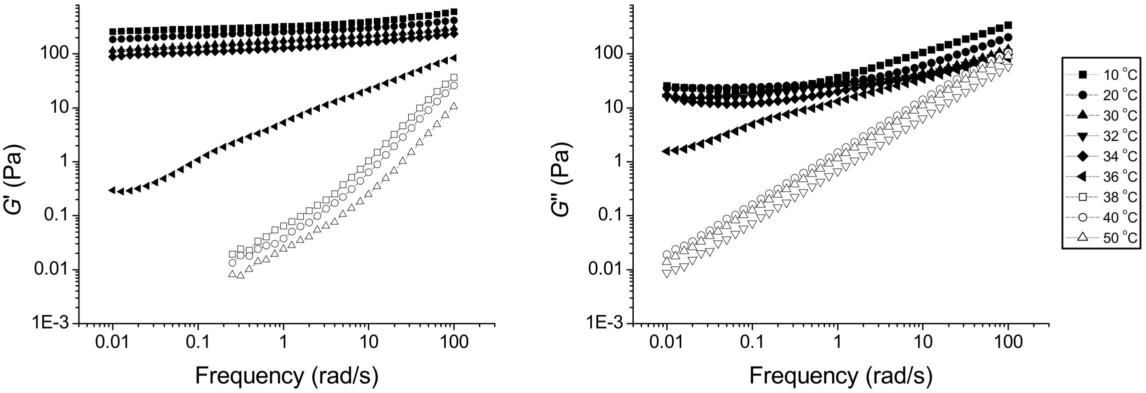

Figure 5.39: Dynamic storage modulus (G') and loss modulus (G'') of 10 wt % 1320(60)ABA triblock in 5CB. The mixture is single-phase nematic for all $T \leq 37.0$ ^{o}C (closed symbols) and single-phase isotropic for $T > 37.0$ ^{o}C (open symbols). The experiments were performed with a parallel-plate fixture with a gap of 500 μm.

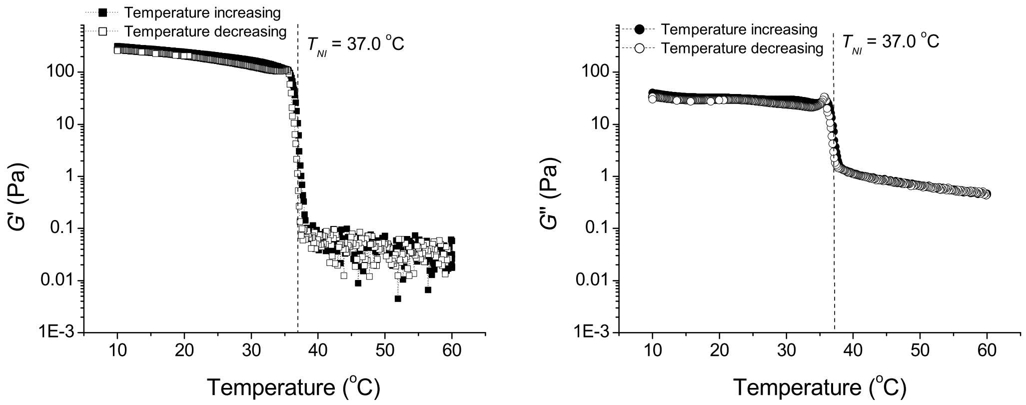

Figure 5.40: Dynamic storage modulus(G') and loss modulus (G'') of 10 wt % 1320(60) ABA triblock in 5CB while heating (closed symbols) and cooling (open symbols) at 0.5 ^{o}C/min. The experiments were performed with a parallel-plate fixture with a gap of 500 μm.

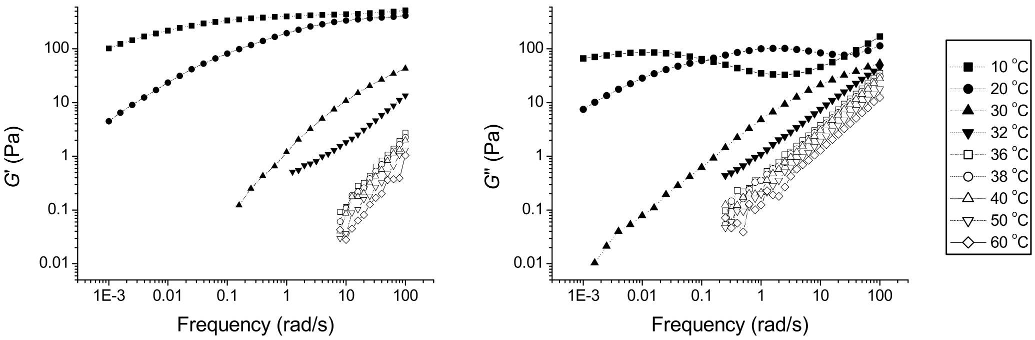

Figure 5.41: Dynamic storage modulus (G') and loss modulus (G'') of 10 wt % 800(20)ABA triblock in 5CB. The mixture is single-phase nematic for all $T \leq 32.0$ ^{o}C (closed symbols) and single-phase isotropic for $T \geq 35.7$ ^{o}C (open symbols).

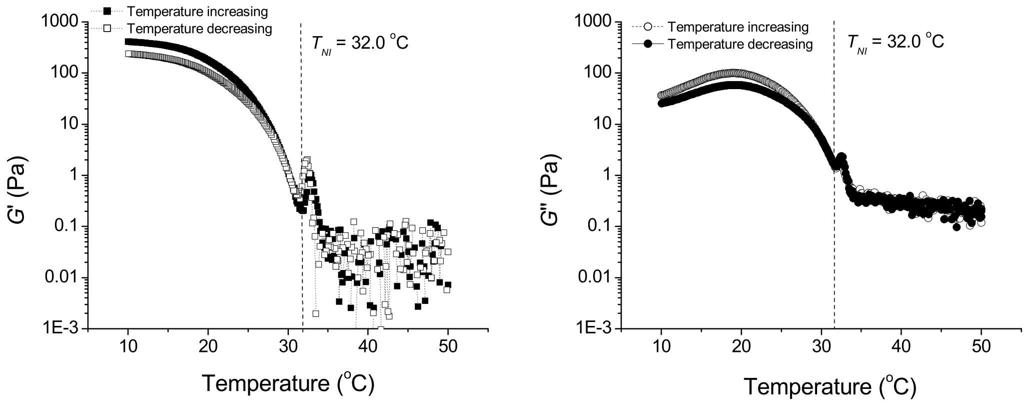

Figure 5.42: Dynamic storage modulus (G') and loss modulus (G'') of 10 wt % 800(20) ABA triblock in 5CB while heating (closed symbols) and cooling (open symbols) at 0.5 ^{o}C/min

Bibliography

[1] Z. Ergundor, C. W. Manke, and E. Gulari. Atomization and elongational viscosity of associating triblock copolymer solutions. *J. Non-Newtonian Fluid Mech.*, 97(2-3):159–167, 2001.

[2] W. Shen, R. G. H. Lammertink, J. K. Sakata, J. A. Kornfield, and D. A. Tirrell. Assembly of an artificial protein hydrogel through leucine zipper aggregation and disulfide bond formation. *Macromolecules*, 38(9):3909–3916, 2005.

[3] H. Hori, O. Urakawa, and K. Adachi. Dielectric relaxation in phase-segregated mixtures of polystyrene and liquid crystal 5cb. *Macromolecules*, 37:1583–1590, 2004.

[4] S. T. Wu, Q. H. Wang, M. D. Kempe, and J. A. Kornfield. Perdeuterated cyanobiphenyl liquid crystals for infrared applications. *J. Appl. Phys.*, 92(12):7146–7148, 2002.

[5] M. D. Kempe, N. R. Scruggs, R. Verduzco, J. Lal, and J. A. Kornfield. Self-assembled liquid-crystalline gels designed from the bottom up. *Nat. Mater.*, 3(3):177–182, 2004.

[6] M. Walther, H. Faulhammer, and H. Finkelmann. On the thread-like morphology of lc/i block copolymers in nematic solvents. *Macromol. Chem. Phys.*, 199:223–237, 1998.

[7] N. Leroux, P. Keller, M. F. Achard, L. Noirez, and F. Hardouin. Small angle neutron scattering experiments on “side-on fixed” liquid crystal polyacrylates. *J. Phys. II France*, 3:1289–1296, 1993.

[8] S. Lecommandoux, M. F. Achard, F. Hardouin, A. Brulet, and J. P. Cotton. Are nematic side-on polymers totally extended? a sans study. *Liq. Cryst.*, 22(5):549–555, 1997.

[9] M. H. Li, A. Brulet, P. Davidson, P. Keller, and J. P. Cotton. Observation of hairpin defects in a nematic main-chain polyester. *Phys. Rev. Lett.*, 70(15):2297–2300, 1993.

[10] G. A. McConnell, A. P. Gast, J. S. Huang, and S. D. Smith. Disorder-order transitions in soft sphere polymer micelles. *Phys. Rev. Lett.*, 71(13):2102–2105, 1993.

[11] I. W. Hamley, J. P. A. Fairclough, A. J. Ryan, C. Y. Ryu, T. P. Lodge, A. J. Gleeson, and J. S. Pedersen. Micellar ordering in concentrated solutions of di- and triblock copolymers in a slightly selective solvent. *Macromolecules*, 31:1188–1196, 1998.

[12] J. S. Higgins, S. Blake, P. E. Tomlins, S. B. Ross-Murphy, E. Staples, J. Penfold, and J. V. Dawkins. Comparison of the structural and rheological consequences of micelle formation in solutions of a model di-block copolymer. *Polymer*, 29:1968–1978, 1988.

[13] I. W. Hamley. Amphiphilic diblock copolymer gels: the relationship between structure and rheology. *Phil. Trans. R. Soc. Lon. A*, 359:1017–1044, 2001.

[14] J. S. Pedersen. Analysis of small-angle scattering data from colloids and polymer solutions: modeling and least-squares fitting. *Adv. Colloid Interface Sci.*, 70:171–210, 1997.

[15] Kell Mortensen. Structural studies of aqueous solutions of peo-ppo-peo triblock copolymers, their micellar aggregates and mesophases; a small-angle neutron scattering study. *J. Phys.: Condens. Matter*, 8:A103–A124, 1996.

[16] T. P. Lodge, Joona Bang, Moon Jeong Park, and Kookheon Char. Origin of the thermoreversible fcc-bcc transition in block copolymer solutions. *Phys. Rev. Lett.*, 92(14):145501, 2004.

[17] T. P. Lodge, X. Xu, C. Y. Ryu, I. W. Hamley, J. P. A. Fairclough, A. J. Ryan, and J. S. Pedersen. Structure and dynamics of concentrated solutions of asymmetric block copolymers in slightly selective solvents. *Macromolecules*, 29:5955–5964, 1996.

[18] F. S. Bates, J. H. Rosedale, and G. H. Frekrickson. Fluctuation effects in a symmetric diblock copolymer near the order-disorder transition. *Macromolecules*, 92(10):6255–6270, 1990.

[19] N. R. Scruggs. PhD thesis, California Institute of Technology, 2007.

[20] G. Holden, E. T. Bishop, and N. R. Legge. Thermoplastic elastomers. *J. Polym. Sci., Part C: Polym. Sym.*, page 37, 1969.

[21] K. Almdal, J. Dyre, S. Hvidt, and O. Kramer. What is a gel? *Makromol. Chem., Macromol. Sym.*, 76:49–51, 1993.

[22] H. Li, G.-E. Yu, C. Price, and C. Booth. Concentrated aqueous micellar solutions of diblock copoly(oxyethylene/oxybutylene) $e_{41}b_8$: A study of phase behavior. *Macromolecules*, 30:1347–1354, 1997.

[23] H. Watanabe, S. Kuwahara, and T. Kotaka. Rheology of styrene-butadiene-styrene triblock copolymer in *n*-tetradecane systems. *J. Rheol.*, 28(4):393–409, 1984.

[24] N. R. Scruggs, J. A. Kornfield, and J. Lal. Using the “switchable” quality of liquid crystal solvents to mediate segregation between coil and liquid crystalline polymers. *Macromolecules*, 39(11):3921–3926, 2006.

[25] A. Halperin, M. Tirrell, and T. P. Lodge. Tethered chains in polymer microstructures. *Adv. Polym. Sci.*, 100:31–71, 1992.

Chapter 6

Covalent Liquid Crystal Networks via "Click" Chemistry

The work in this chapter was done jointly with Yan Xia, under the mentorship of Professor Robert H. Grubbs.

6.1 Introduction

Liquid crystal elastomers are composed of flexible, liquid crystal polymers crosslinked to form a network. The combination of LC order and rubber elasticity results in a polymer network that is responsive to a variety of external influences, including heat, light, and electric and magnetic fields. These materials display remarkable shape-changing and optical properties which make them of interest for technological applications [1].

The first method for preparing an LC elastomer was devised by Finkelmann et al. [2, 3] and involved the functionalization and crosslinking of poly(methyl)hydrosiloxane. Subsequent studies have produced a number of different types of LC elastomers and investigated the significance of various molecular parameters to the macroscopic behavior, including the size, type, and concentration of crosslinker [4, 5, 6]; the use of polyacrylates or polymethacrylates [7, 8]; the incorporation of mesogens into the polymer backbone [9]; and the effect of the side-group [10]. While these materials have shown interesting and useful properties, the preparation methods rely on uncontrolled radical reactions or random crosslinking of polysiloxane, resulting in poorly defined materials. There is a need for materials with better defined molecular properties. More recent endeavors have been aimed at achieving these goals, and recent studies have utilized the self-assembly of block copolymers to produce LC elastomers [11, 12, 13, 14]. These materials show promising new properties that emphasize the need for a well-defined network structure. Here, we report the preparation of a covalent LC network by controlled "click" crosslinking of telechelic LC polymers. Specifically, we used copper(I)-catalyzed azide-alkyne cycloaddition of azide-terminated LC polymers and triacetylene crosslinker. This reaction has gained increasing attention in polymer and material research [15, 16, 17, 18, 19], due to its extraordinary specificity, quantitative yield, and wide functional group tolerance. Recently, it has been utilized to produce well-defined hydrogels [20] and model networks [21] through controlled crosslinking of telechelic polymers. The LC polymers are prepared via ring-opening metathesis polymerization (ROMP), which, in the presence of a chain transfer agent (CTA), allows for the preparation of polyalkenamers with high functionalities [22, 23, 24, 25] and simultaneous facile control of the end group functionality [26, 27, 28].

We produce a covalent LC network with a regular network architecture, including a controlled molecular weight between crosslinks and crosslink functionality. The resulting LC elastomer can be swollen in small molecule LC to produce LC gels. We first present the preparation and characterization of the LC network, and then we present results on the temperature-dependent swelling and electro-optic response of the gel.

6.2 Experimental

All reagents were purchased from Aldrich unless otherwise stated. Refer to Chapter 2 for details on differential scanning calorimetry, polarized optical microscopy, and electro-optical measurements. NMR spectra were recorded on a Varian Mercury 300 MHz spectrometer. All NMR spectra were recorded in $CDCl_3$ or DMSO-d_6. For end group analysis, a Varian Mercury 500 MHz ^{1}H NMR was used.

Gel permeation chromatography (GPC) was carried out in tetrahydrofuran (THF) on two PLgel 5 m mixed-C columns (Polymer Labs) connected in series with a DAWN EOS multiangle laser

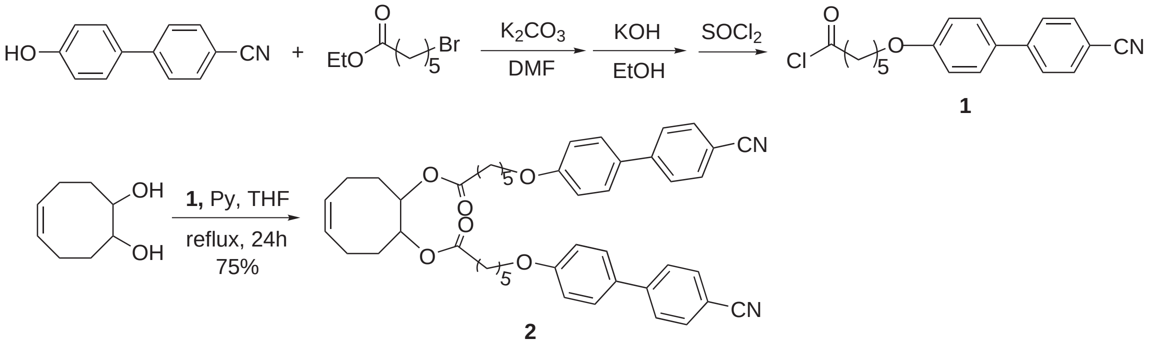

Figure 6.1: Synthesis of substituted octene monomer

light scattering (MALLS) detector and an Optilab DSP differential refractometer (both from Wyatt Technology). No calibration standards were used, and dn/dc values were obtained for each injection by assuming 100% mass elution from the columns.

Fourier transform infrared spectroscopy (FTIR) was performed on a Nicolet Nexus 470 spectrometer with a DTGS detector, a KBr beam splitter, and a 1 mW He-Ne laser (633 nm). The chamber was purged using dry N_2 gas and a background was taken using a blank card (3M type 2 IR cards, poly(tetrafluoroethylene) substrate). The samples were prepared by dissolving the material in a volatile solvent, placing a few drops of the solution on the card, and allowing the solvent to evaporate.

6.2.1 Synthesis of 5,6-disubstituted cyclooctene-based mesogen 2

The ester ethyl 6-bromohexanoate (99% pure) (19.8 mL, 111 mmol) was attached to the mesogen 4-cyano-4′-hydroxybiphenyl (95% pure from TCI) (15.4g, 78.9 mmol) by a Williamson's ether synthesis (Fig. 6.1 in anhydrous N,N-dimethylformamide ($>$ 99.8% pure under nitrogen in Sure/Seal bottles) (100 mL) with anhydrous K_2CO_3 ($>$ 99% pure) (10.8 g, 78.1 mmol) at 90 ^{o}C for 6 h and monitored by TLC. The product was recrystallized in ethanol (95% pure denatured from EMD) for an 89% yield.

The ethyl ester was deprotected by reacting with anhydrous KOH (6 g, 150 mmol) in anhydrous ethanol (95% denatured ethanol from EMD, dried over CaH) (200 mL) at 90 ^{o}C for 6 h. 1 M

HCl (from JT Baker) (50 mL) was added to precipitate the acid product which was collected by filtration, washed with H_2O, and dried in vacuo at 60 ^oC for a 95% yield.

The acid chloride was produced by reacting the acid (13.3 g, 45 mmol) in $SOCl_2$ ($>$ 99% pure) (60 mL, 766 mmol) at 70 ^oC for five hours. Excess $SOCl_2$ was removed under reduced pressure to yield the acid chloride.

5-Cyclooctene-1,2-diol was synthesized according to previously published procedures [29].

To attach the mesogen to the octene diol, the acid chloride (5.3 g, 16.2 mmol) was added dropwise to a solution of octene diol (0.77 g, 5.4 mmol) in anhydrous pyridine ($>$ 99% pure)(5 mL, 63.2 mmol) and anhydrous tetrahydrofuran ($>$ 99% pure) (50 mL). The mixture was refluxed for 24 h and the product was purified by extraction with 1 N HCl (20 mL, repeat 3 times), followed by extraction with a saturated solution of aqueous $NaHCO_3$ (50 mL) and with a saturated aqueous solution of KCl (50 mL). The product was dried over $MgSO_4$ and purified by fractionation on a silica gel column with 30% ethyl acetate in hexanes (75% yield).

6.2.2 Polymerization via ROMP and end-group functionalization

In a typical experiment, 0.725 g (1.0 mmol) of monomer and a stir bar were added to a small vial. Under an argon atmosphere, 1.0 ml of degassed dichloroethane (DCE) was then added via syringe. The vial was then degassed through three freeze-pump-thaw cycles. Next, the desired amount of CTA was injected from its stock solution in degassed DCE. 84 μl of a 10.0 mg/ml catalyst **4** solution in degassed DCE was injected to initiate the polymerization. The reaction vial was stirred at 55 C under argon for 24 h. The reaction mixture was quenched with 0.1 ml of ethyl vinyl ether and then dissolved in 2 ml CH_2Cl_2 and precipitated into 200 ml stirring methanol (MeOH). The light yellow precipitate was washed with fresh MeOH and dried in vacuo overnight to yield 0.7 g polymer.

The substitution of the bromide endgroups was carried out by first dissolving 0.7 g (0.1 mmol -Br) dibromo-terminated polymer and 13 mg (0.2 mmol) NaN_3 in 15 ml DMF. The resulting solution was stirred at 25 ^oC overnight. The solution was then concentrated and precipitated into 200 ml MeOH three times and dried in vacuo overnight to yield 0.65 g white polymer.

6.2.3 Crosslinking of telechelic polymers by "click" chemistry

The desired diazido-terminated polymer and CuBr (3 eq. to alkyne) were added to a small vial. The vial was evacuated and backfilled with argon three times. Degassed DMF (3 ml/g of polymer) and pentamethyl diethylene triamine (PMDETA) were injected, and the vial was stirred for 5 min. The correct amount of crosslinker was then injected from its stock solution. The mixture was stirred at 50 ^{o}C, and within 5 min an insoluble material was evident. The resulting gels were repeatedly washed with DMF and then THF to remove copper catalyst, and were dried in vacuo to yield light yellow elastomers.

6.3 Results

6.3.1 Synthesis of covalent LC network

Cyclooctene based monomer **2** was used to make the telechelic LC polymers. While ROMP has been widely used to synthesize LCP from norbornene-based monomers, ROMP of cyclooctene-based monomers with large, pendant substituents has been rarely reported [30, 31], presumably due to the lower ring strain of cyclooctene compared to norbornene. However, in contrast to norbornene-based monomers, polymerization of a functionalized cyclooctene monomer results in a polymer with a flexible backbone, which is required for the present application. Additionally, control of chain end via a CTA during ROMP is readily achieved for cyclooctene.

The monomer was polymerized by the highly active ruthenium catalyst **4** $(IMesH_2)(PCy_3)RuCl_2(CHPh)$ in dichloroethane at 55 ^{o}C for 24 h in the presence of a CTA, as depicted in Fig. 6.2. Since the ruthenium catalyst is known to be incompatible with azide groups, 1,8-dibromo-4-octene is utilized as the CTA to give the resulting telechelic polymers primary bromide end groups which can then be converted to azide groups in quantitative yield. In general, the polymer yield for ROMP reactions is improved with increasing monomer concentration, especially for substituted cyclooctenes, but at very high polymer concentrations the increased solution viscosity can retard the chain transfer and decrease the functionality of the chain ends. We used a concentration of 1.5 M, which we found to

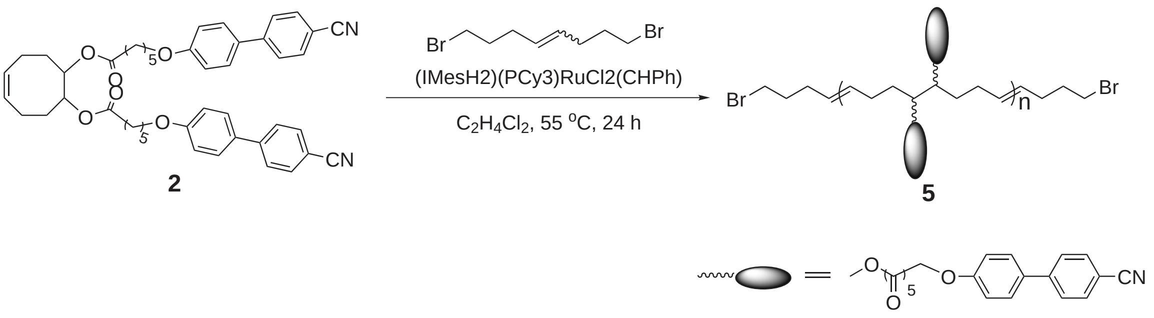

Figure 6.2: Reaction scheme for ROMP of substituted cyclo-octene

be the highest monomer concentration possible without making the solution so viscous as to impede good mixing. A monomer-to-catalyst ratio of 1000 was used. Complete monomer conversion was achieved at this catalyst loading, as indicated by the disappearance of the monomer olefin peaks in ^{1}H-NMR, while a catalyst loading ratio of 2000 resulted in incomplete conversion.

ROMP of **2** reached full monomer conversions under the optimized conditions. The molecular weight determined by GPC was 24.8 kg/mol, and this agrees well with the value determined by ^{1}H-NMR end group analysis of 26.2 kg/mol. Good agreement between the two measurements indicates that the polymer is telechelic. The polydispersity index (PDI) of the polymer was 1.84, as measured by GPC. Polymer **3** was nematic at room temperature, as confirmed by polarized optical microscopy (POM). The polymer had a nematic to isotropic transition temperature (T_{NI}) between 50 and 60 ^{o}C, as measured by differential scanning calorimetry (DSC) and polarized optical microscopy.

Controlled “click” crosslinking of these telechelic polymers was achieved by reacting a tri-acetylene species, tripropargylamine, with the polymer azide end groups in the presence of CuBr as catalyst and PMDETA as a ligand in DMF at 50 ^{o}C (Fig. 6.3). Gelation occured within 5 min of addition of a stochiometric amount of crosslinker.

To remove excess Cu, we washed the gels in DMF and THF several times before drying the LC elastomer in vacuo. IR spectrometry shows complete disappearance of the azide absorbance, indicating that most of the azide end groups had reacted in the crosslinking.

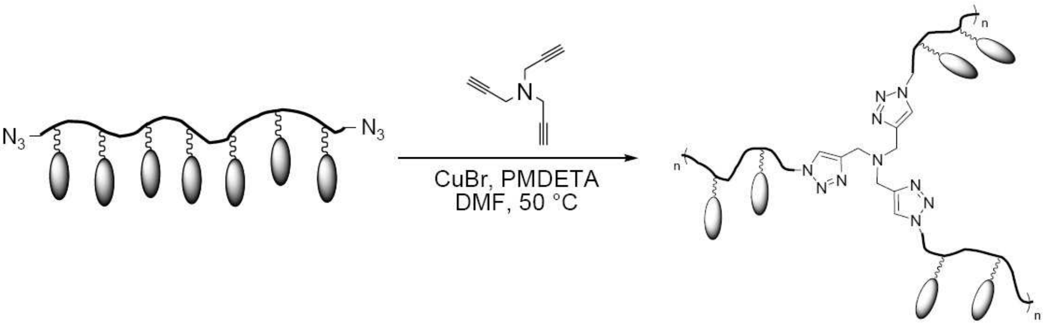

Figure 6.3: Crosslinking of telechelic LC polymers by “click” chemistry

6.3.2 Temperature-dependent swelling of covalent LC networks in liquid crystal

To create an LC gel, the dried elastomer was first swollen in THF and 4-pentyl-4′-cyanobiphenyl (5CB) for one day. The THF was then removed in vacuo, resulting in an LC covalent network swollen with 5CB. The LC gel had a degree of swelling, defined as the ratio of the mass of the gel to the mass of the dried polymer, of 17.5.

At 35.0 ^{o}C, 5CB transitions to the isotropic phase, but the gel remains nematic up to 36.0 ^{o}C. Heating the gel to temperatures above 35 ^{o}C but below 36 ^{o}C causes the gel to deswell (Figs. 6.4 and 6.5). The gel deswells due to the changing order parameter of the LC solvent, which in its pure state is isotropic above 35.0 ^{o}C. Heating the LC gel to temperatures above 36.0 ^{o}C causes the gel to phase transition to the isotropic phase, and it reswells with isotropic 5CB. This swelling and deswelling with temperature has been observed in previous LC gels, and the behavior is captured by a mean field theory that incorporates the free energy of isotropic mixing, the free energy of nematic ordering, and the elastic free energy of the network [32, 33].

6.3.3 Electro-optical properties of LC gels

LC elastomers and gels can respond to electric fields by quickly changing texture and shape. The dynamics of the response depends on the polymer content, with a lower content correlated with a faster response, and therefore LC gels are generally more responsive than elastomers to electric fields

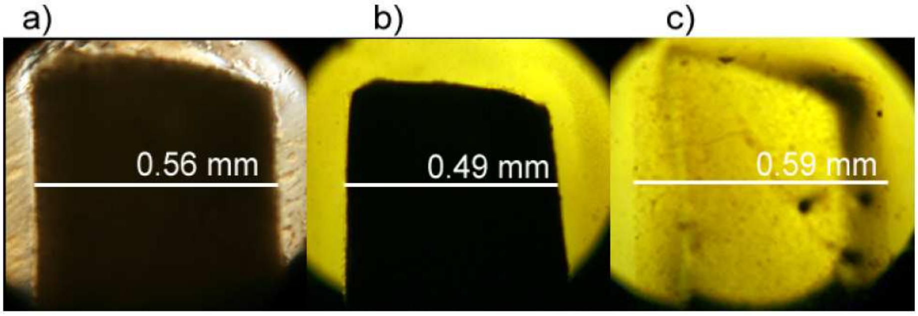

Figure 6.4: LC gels at a) 34.5 ^{o}C, b) 35.5 ^{o}C, and c) 37.0 ^{o}C. Image **a** was taken with crossed polarizers, and images **c** and **d**were taken with uncrossed polarizers. The gel scatters light and appears dark when nematic (**a** and **b**) because it is not uniformly aligned.

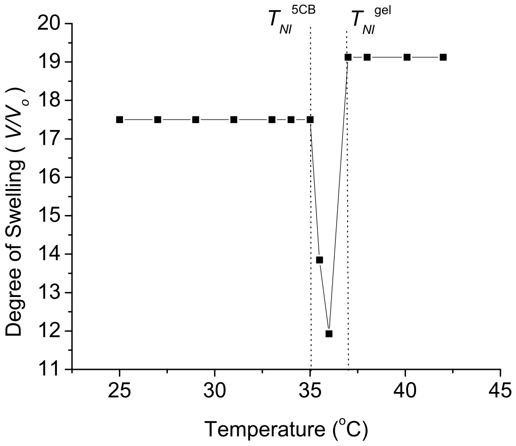

Figure 6.5: Degree of swelling V/V_o of covalent LC network, where V is the volume of the gel, and V_o is the volume of the dry elastomer

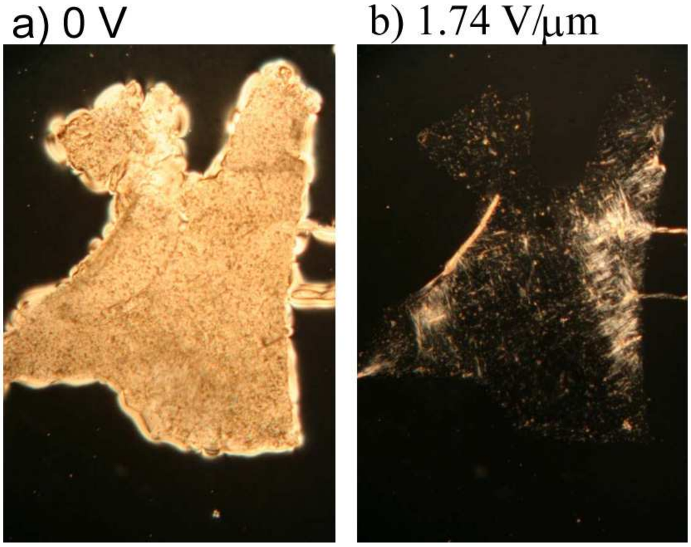

Figure 6.6: Polarized optical micrograph of unconstrained covalent LC gel under an AC field of a) 0 V/μ, and b) 1.74 V/μm. The gap between electrodes is 100 μm, and the gel is approximately 18 μm thick.

[34, 35]. Here, we investigate the electro-optic response of the covalent LC gels. We are interested in the threshold for obtaining a response, the dynamics of the response, and the texture and shape changes associated with the electro-optic response.

Previous experiments on the electro-optic behavior have observed a significant difference in the electro-optic properties for LC gels constrained between cell electrodes and unconstrained LC gels that are freely floating in a solvent between the electrodes [36, 37]. We examine the electro-optical response for both constrained and unconstrained samples. Constrained samples were prepared by pressing a LC gel sample between ITO-coated quartz plates separated by spacers. The initial thickness of the LC gel was larger than the final gap. Unconstrained samples were prepared by carefully cutting away a thin ($\sim$ 7 μm) piece of the LC elastomer and placing it in a 100 μm-thick gap between ITO coated plates filled with 5CB. The sample was allowed to swell for several days; equilibrium swelling was confirmed by measuring the T_{NI}, which matched the previously measured value of the swollen gel described in the previous section.

For the unconstrained gel, the electric-field threshold for a response is approximately 0.5 V/μm, and the gel is uniformly aligned above 1.7 V/μm (Fig. 6.6). In the case of the constrained gel, the

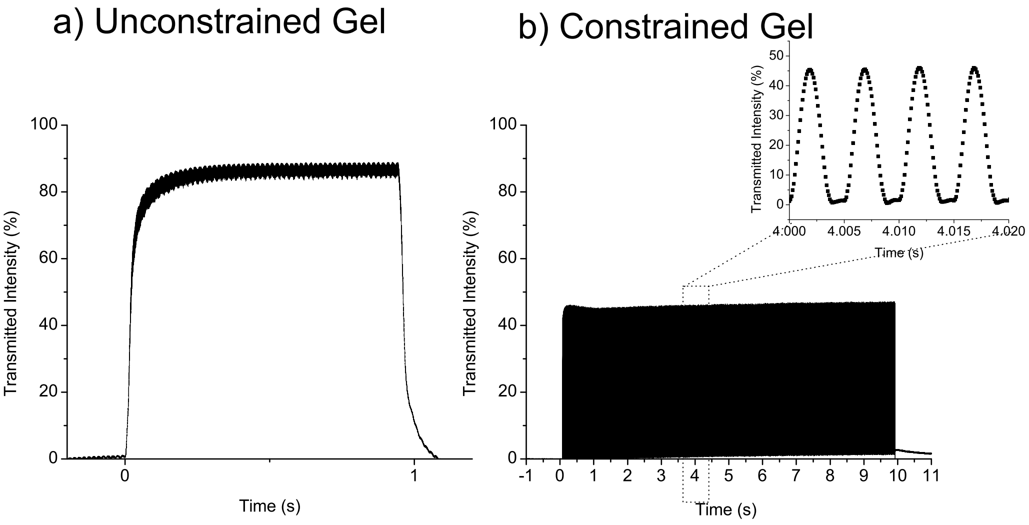

Figure 6.7: Dynamic electro-optic behavior of a) unconstrained gel under a 1.9 V/μm, 1000 Hz AC signal, and b) constrained gel under a 19 V/μm, 100 Hz AC signal. The transmittance is measured at a rate of 10,000 counts/s. A lower frequency is used for the constrained gel in order to accurately measure the time-dependent transmittance, which oscillates rapidly with the applied AC field.

threshold is approximately 10 V/μm, and uniform alignment is not achieved for fields as high as 20 V/μm. No significant shape change is observed for either constrained or unconstrained gels.

The dynamic electro-optic behavior is fast for both constrained and unconstrained gels (Fig. 6.7). In the case of the unconstrained gel, the transmittance reaches 90% of its maximum value in $\sim$ 70 ms after application of the AC field, and the transmittance drops down to 10% of its maximum within 100 ms of removing the field. These response times are much faster than bulk LC elastomer and are comparable to those found in previous studies of elastomers swollen with an LC solvent [38, 36]. Other LC gel systems, on the other hand, such as polymer-stabilized liquid crystals [39], triblock LC gels [11], LC gels formed by small-molecule gelators [40], and polymer-dispersed LCs [41] show a faster response than the present gels.

The unconstrained gel has extremely fast director oscillations that follow the AC signal (Fig. 6.7b). The director oscillates at twice the frequency of the applied field, due to the uniaxial symmetry of the nematic director. These large amplitude oscillations reflect the extremely fast director dynamics in contrained gels. Nevertheless, the large threshold for an electro-optic response precludes the use of constrained gels in electro-optic applications.

6.4 Discussion

The preparation of covalent LC elastomers and gels via “click” crosslinking is a significant achievement. They represent the first examples of LC networks with precise control of network structure, including crosslink density and functionality. The present gels capture the fast and low threshold electro-optic response and swelling/deswelling across the T_{NI} that have been reported in LC gels produced by uncontrolled radical reactions [33, 34]. Therefore, the covalent LC gels can be used to pursue careful studies of the relationship between network structure and material properties. These materials will prove useful in testing existing theories [42, 43], as discussed below, and investigating structure-property relationships of LC networks.

The synthetic method of ROMP combined with the azide-tri-acetylene “click” crosslinking provides the opportunity to vary several network parameters: The molecular weight of the network strands can be tuned by the concentration of CTA during ROMP, the degree of substitution can be halved by starting with a monosubstituted cyclooctene monomer, and the crosslinker functionality can be changed. Modifying the spacer length or the mesogenic side-group can result in a stronger coupling between the backbone conformation and LC order, resulting in gels and elastomers that display large spontaneous shape changes [10] and significant shape changes in response to electric fields [44, 45].

Several questions pertaining to the equilibrium and dynamical properties of LC networks remain unanswered [43, 46, 47]. For example, theoretical work by Oyerokun et al., which accounts for excluded volume interactions in nematic rubbers, predicts that increasing the crosslink density will decrease the spontaneous distortion of LC elastomers when heating through the T_{NI} [43]. The theory furthermore predicts a strain-induced softening of the modulus, especially near the T_{NI}. The system presented here provides a systematic way to vary the crosslink density to test this prediction, which has not been experimentally investigated. Another area of debate pertains to the dynamic mechanical properties of LC elastomers [42, 46, 47], which are predicted to have distinct, widely separated relaxation modes of the network and the nematic director. This has not been observed in previous experimental investigations [47, 48, 46, 49], but it is possible that the disparity between theory and experiment arises from the non-uniform structure of prior materials. The present system with a controlled network structure and proper choice of LC side group is a promising candidate to elucidate the dynamic behavior of LC elastomers.

One of the unresolved challenges of these materials is achieving a uniformity of alignment and control of the specimen size, and this represents the next major hurdle to utilizing the covalent LC networks for careful physical studies. The popular “two-step” crosslinking method [3] for obtaining aligned elastomers is not applicable to the present LC networks. However, a promising idea to accomplish uniform alignment is to perform the crosslinking step in an LC solvent, which can be uniformly aligned with coated cell substrates.

6.5 Conclusions

Covalent LC networks were prepared by “click” chemistry, specifically by the copper(I)-catalyzed cycloaddition of an azides and alkynes. Azide-terminated LC polymers were produced by ROMP and crosslinked with a tri-acetyline species to produce covalent LC networks. The resulting networks provide model systems that capture the fascinating properties of LC gels, specifically swelling/deswelling across the T_{NI} and fast and low-threshold electro-optic behavior. The covalent networks open the door for structure-property studies of LC elastomers and gels. Future work includes developing a method for producing aligned LC elastomers and gels of a controlled size and shape.

Bibliography

[1] M. Warner and E. M. Terentjev. *Liquid Crystal Elastomers.* Oxford University Press, Oxford, 2003.

[2] H. Finkelmann, Hans-J. Kock, and Gunther Rehage. Investigations on liquid crystalline polysiloxanes 3. liquid crystalline elastomers – a new type of liquid crystalline material. *Makromol. Chem., Macromol Chem. Phys.*, 2:317–322, 1981.

[3] J. Küpfer and H. Finkelmann. Nematic liquid single-crystal elastomers. *Makromol. Chem., Macromol Chem. Phys.*, 12(12):717–726, 1991.

[4] Y. G. Jia, B. Y. Zhang, X. Z. He, and J. Z. Ning. Synthesis and phase behavior of nematic liquid-crystalline elastomers derived from smectic crosslinking agent. *J. Appl. Polym. Sci.*, 98(4):1712–1719, 2005.

[5] J. J. Zanna, P. Stein, J. D. Marty, M. Mauzac, and P. Martinoty. Influence of molecular parameters on the elastic and viscoelastic properties of side-chain liquid crystalline elastomers. *Macromolecules*, 35(14):5459–5465, 2002.

[6] D. Lacey, H. N. Beattie, G. R. Mitchell, and J. A. Pople. Orientation effects in monodomain nematic liquid crystalline polysiloxane elastomers. *J. Mater. Chem.*, 8(1):53–60, 1998.

[7] H. Hirschmann, P. M. S. Roberts, F. J. Davis, W. Guo, C. D. Hasson, and G. R. Mitchell. Liquid crystalline elastomers: the relationship between macroscopic behaviour and the level of backbone anisotropy. *Polymer*, 42(16):7063–7071, 2001.

[8] C. H. Legge, F. J. Davis, and G. R. Mitchell. Memory effects in liquid-crystal elastomers. *J. Phys. II*, 1(10):1253–1261, 1991.

[9] David Ribera, Marta Giamberini, Angels Serra, and Ana Mentecn. Lightly crosslinked, mesomorphic networks obtained through the reaction of dimeric, liquid-crystalline epoxy-imine monomers and heptanedioic acid. *J. Polym. Sci., Part A: Polym. Chem.*, 44:6270–6286, 2006.

[10] D. L. Thomsen, P. Keller, J. Naciri, R. Pink, H. Jeon, D. Shenoy, and B. R. Ratna. Liquid crystal elastomers with mechanical properties of a muscle. *Macromolecules*, 34(17):5868–5875, 2001.

[11] M. D. Kempe, N. R. Scruggs, R. Verduzco, J. Lal, and J. A. Kornfield. Self-assembled liquid-crystalline gels designed from the bottom up. *Nat. Mater.*, 3(3):177–182, 2004.

[12] M.-H. Li, P. Keller, J. Yang, and P.-A. Albuoy. An artificial muscle with lamellar structure based on a nematic triblock copolymer. *Adv. Mater.*, 16(21):1922–1925, 2004.

[13] A. J. Gabert, E. Verploegen, P. T. Hammond, and R. R. Schrock. Synthesis and characterization of aba triblock copolymers containing smectic c* liquid crystal side chains via ring-opening metathesis polymerization using a bimetallic molybdenum initiator. *Macromolecules*, 39(12):3993–4000, 2006.

[14] S. V. Ahir, A. R. Tajbakhsh, and E. M. Terentjev. Self-assembled shape-memory fibers of triblock liquid-crystal polymers. *Adv. Funct. Mater.*, 16(4):556–560, 2006.

[15] C. J. Hawker and K. L. Wooley. The convergence of synthetic organic and polymer chemistries. *Science*, 309(5738):1200–1205, 2005.

[16] B. Helms, J. L. Mynar, C. J. Hawker, and J. M. J. Frechet. Dendronized linear polymers via ”click chemistry”. *J. Am. Chem. Soc.*, 126(46):15020–15021, 2004.

[17] M. Malkoch, R. J. Thibault, E. Drockenmuller, M. Messerschmidt, B. Voit, T. P. Russell, and C. J. Hawker. Orthogonal approaches to the simultaneous and cascade functionalization of macromolecules using click chemistry. *J. Am. Chem. Soc.*, 127(42):14942–14949, 2005.

[18] B. Parrish, R. B. Breitenkamp, and T. Emrick. Peg- and peptide-grafted aliphatic polyesters by click chemistry. *J. Am. Chem. Soc.*, 127(20):7404–7410, 2005.

[19] P. Wu, A. K. Feldman, A. K. Nugent, C. J. Hawker, A. Scheel, B. Voit, J. Pyun, J. M. J. Frechet, K. B. Sharpless, and V. V. Fokin. Efficiency and fidelity in a click-chemistry route to triazole dendrimers by the copper(i)-catalyzed ligation of azides and alkynes. *Angew. Chem. Int. Ed.*, 43(30):3928–3932, 2004.

[20] M. Malkoch, R. Vestberg, N. Gupta, L. Mespouille, P. Dubois, A. F. Mason, J. L. Hedrick, Q. Liao, C. W. Frank, K. Kingsbury, and C. J. Hawker. Synthesis of well-defined hydrogel networks using click chemistry. *Chem. Commun.*, (26):2774–2776, 2006.

[21] J. A. Johnson, D. R. Lewis, Dddu Az, M. G. Finn, J. T. Koberstein, and N. J. Turro. Synthesis of degradable model networks via atrp and click chemistry. *J. Am. Chem. Soc.*, 128(20):6564–6565, 2006.

[22] C. W. Bielawski and R. H. Grubbs. Highly efficient ring-opening metathesis polymerization (romp) using new ruthenium catalysts containing n-heterocyclic carbene ligands. *Angew. Chem., Int. Ed.*, 39(16):2903–2906, 2000.

[23] M. A. Hillmyer, W. R. Laredo, and R. H. Grubbs. Ring-opening metathesis polymerization of functionalized cyclooctenes by a ruthenium-based metathesis catalyst. *Macromolecules*, 28(18):6311–6316., 1995.

[24] B. R. Maughon, M. Weck, B. Mohr, and R. H. Grubbs. Influence of backbone rigidity on the thermotropic behavior of side-chain liquid crystalline polymers synthesized by ring-opening metathesis polymerization. *Macromolecules*, 30(2):257–265, 1997.

[25] O. A. Scherman, R. Walker, and R. H. Grubbs. Synthesis and characterization of stereoregular ethylene-vinyl alcohol copolymers made by ring-opening metathesis polymerization. *Macromolecules*, 38(22):9009–9014, 2005.

[26] C. W. Bielawski, T. Morita, and R. H. Grubbs. Synthesis of aba triblock copolymers via a tandem ring-opening metathesis polymerization: Atom transfer radical polymerization approach. *Macromolecules*, 33(3):678–680, 2000.

[27] T. Morita, B. R. Maughon, C. W. Bielawski, and R. H. Grubbs. A ring-opening metathesis polymerization (romp) approach to carboxyl- and amino-terminated telechelic poly(butadiene)s. *Macromolecules*, 33(17):6621–6623, 2000.

[28] O. A. Scherman, G. B. W. L. Ligthart, H. Ohkawa, R. P. Sijbesma, and E. W. Meijer. Olefin metathesis and quadruple hydrogen bonding: A powerful combination in multistep supramolecular synthesis. *Proc Natl Acad Sci USA*, 103(32):11850–11855, 2006.

[29] J. L. Jernow, D. Gray, and W. D. Closson. Neighboring-group participation by oxirane oxygen during oxymercuration of 1,5-diene monoxides. *J. Org. Chem.*, 36(23):3511–3515, 1971.

[30] K. Breitenkamp, J. Simeone, E. Jin, and T. Emrick. Novel amphiphilic graft copolymers prepared by ring-opening metathesis polymerization of poly(ethylene glycol)-substituted cyclooctene macromonomers. *Macromolecules*, 35(25):9249–9252, 2002.

[31] B. Winkler, A. Rehab, M. Ungerank, and F. Stelzer. A novel side-chain liquid crystal polymer of 5-substituted cis-cyclooctene via ring-opening metathesis polymerisation. *Macromol. Chem. Phys.*, 198(5):1417–1425, 1997.

[32] K. Urayama, Y. Okuno, T. Nakao, and S. Kohjiya. Volume transition of nematic gels in nematogenic solvents. *J. Chem. Phys.*, 118(6):2903–2910, 2003.

[33] K. Urayama, Y. Okuno, T. Kawamura, and S. Kohjiya. Volume phase transition of liquid crystalline gels in a nematic solvent. *Macromolecules*, 35:4567–4569, 2002.

[34] Y. Yusuf, J. H. Huh, P. E. Cladis, H. R. Brand, H. Finkelmann, and S. Kai. Low-voltage-driven electromechanical effects of swollen liquid-crystal elastomers. *Phys. Rev. E*, 71(6), 2005.

[35] K. Urayama, S. Honda, and T. Takigawa. Electrooptical effects with anisotropic deformation in nematic gels. *Macromolecules*, 38(9):3574–3576, 2005.

[36] R. Zentel. Shape variation of cross-linked liquid-crystalline polymers by electric-fields. *Liq. Cryst.*, 1(6):589–592, 1986.

[37] K. Urayama, S. Honda, and T. Takigawa. Deformation coupled to director rotation in swollen nematic elastomers under electric fields. *Macromolecules*, 39(5):1943–1949, 2006.

[38] D. U. Cho, Y. Yusuf, S. Hashimoto, P. E. Cladis, H. R. Brand, H. Finkelmann, and S. Kai. Electro-optical effects of swollen polydomain liquid crystal elastomers. *J. Phys. Soc. Jpn.*, 75(8), 2006.

[39] R. A. M. Hikmet and H. M. J. Boots. Domain structure and switching behavior of anisotropic gels. *Phys. Rev. E*, 51(6):5824–5831, 1995.

[40] N. Mizoshita, Y. Suzuki, K. Kishimoto, K. Hanabusa, and T. Kato. Electro-optical properties of liquid-crystalline physical gels: a new oligo(amino acid) gelator for light scattering display materials. *J. Mater. Chem.*, 12:2197–2201, 2002.

[41] I.-C. Khoo and S.-T. Wu. *Optics and Nonlinear Optics of Liquid Crystals.* World Scientific, Singapore, 1993.

[42] O. Stenull and T. C. Lubensky. Dynamics of nematic elastomers. *Phys. Rev. E*, 69:051801, 2004.

[43] F. T. Oyerokun and K. S. Schweizer. Thermodynamics, orientational order and elasticity of strained liquid crystalline melts and elastomers. *J. Phys. Chem. B*, 109(14):6595–6603, 2005.

[44] K. Urayama, H. Kondo, Y. O. Arai, and T. Takigawa. Electrically driven deformations of nematic gels. *Phys. Rev. E*, 71:051713, 2005.

[45] J. H. Huh, J. Xin, Y. Yusuf, and S. Kai. Temperature dependence of electromechanical effects in a swollen polydomain liquid crystalline elastomer. *J. Phys. Soc. Jpn.*, 74(1):242–245, 2005.

[46] E. M. Terentjev and M. Warner. Linear hydrodynamics and viscoelasticity of nematic elastomers. *Eur. Phys. J. E*, 4:343–353, 2001.

[47] P. Martinoty, P. Stein, H. Finkelmann, H. Pleiner, and H. R. Brand. Mechanical properties of monodomain side chain nematic elastomers. *Eur. Phys. J. E*, 14:311–321, 2004.

[48] P. Stein, N. Aßfalg, H. Finkelmann, and P. Martinoty. Shear modulus of polydomain, monodomain and non-mesomorphic side-chain elastomers: Influence of the nematic order. *Eur. Phys. J. E*, 4:255–262, 2001.

[49] O. Stenull and T. C. Lubensky. Commentary on "mechanical properties of monodomain side chain nematic elastomers" by p. martinoty et al. *Eur. Phys. J. E*, 14:333–337, 2004.

Chapter 7

Outlook

The field of liquid crystal elastomers and gels has typically been dominated by polymer and liquid crystal scientists with a physics background. This has led to a deep understanding of the molecular basis for nematic rubber elasticity, but at the same time advanced chemical methods for producing liquid crystal networks have not been fully employed. It is my belief that obtaining a complete physical understanding of liquid crystal-polymer materials can only be achieved with a stronger effort from scientists interested in constructing well-defined elastomers and gels. Fortunately, more recent work, including the work described in this thesis, has taken a closer look at the chemical details in liquid crystal elastomers and gels [1, 2, 3, 4, 5]. Much remains to be explored. For example, compared to nematic elastomers, much less is known about elastomers and gels with higher order phases, such as the chiral smectic C* phase – presumably due to the difficulty in producing, aligning, and characterizing smectic networks. Light-induced changes in liquid crystal elastomers and gels have only recently been explored, and future efforts can focus on producing a faster and more controlled response [5, 4]. Other effects, such as the flexoelectric effect in liquid crystals, have not yet been incorporated into liquid crystal elastomers or gels [6]. Future work will undoubtedly tackle these challenges and, with some luck, produce liquid crystal-polymer materials with technologically viable properties.

Bibliography

[1] M. D. Kempe, N. R. Scruggs, R. Verduzco, J. Lal, and J. A. Kornfield. Self-assembled liquid-crystalline gels designed from the bottom up. *Nat. Mater.*, 3(3):177–182, 2004.

[2] M.-H. Li, P. Keller, J. Yang, and P.-A. Albuoy. An artificial muscle with lamellar structure based on a nematic triblock copolymer. *Adv. Mater.*, 16(21):1922–1925, 2004.

[3] S. V. Ahir, A. R. Tajbakhsh, and E. M. Terentjev. Self-assembled shape-memory fibers of triblock liquid-crystal polymers. *Adv. Funct. Mater.*, 16(4):556–560, 2006.

[4] M. Camacho-Lopez, H. Finkelmann, P. Palffy-Muhoray, and M. Shelley. Fast liquid-crystal elastomer swims into the dark. *Nat. Mater.*, 3:307–310, 2004.

[5] Y. L. Yu, M. Nakano, and T. Ikeda. Directed bending of polymer film by light – miniaturizing a simple photomechanical system could expand its range of applications. *Nature*, 425(6954):145, 2003.

[6] J. Harden, B. Mbanga, N. Eber, K. Fdor-Csorba, S. Sprunt, JT. Gleeson, and A. Jakli. Giant flexoelectricity of bent-core nematic liquid crystals. *Phys. Rev. Lett.*, 97(15):157802, 2006.

Appendix A

Transient Electro-Optic Properties of Liquid Crystal Gels

The dynamics of the electro-optic response has significance for the use of our gels in display devices and also reveals important effects of the polymer network. In order to study this behavior, we recorded the transmitted intensity before, during, and after applying a voltage to the gel. This allowed us to measure the response time for aligning the gel in the presence of a voltage and the relaxation time after the voltage was removed. In the following we analyze the dynamics of 5 wt % and 10 wt % gels confined to a 15 μm gap. These samples reveal the general characteristics of the dynamics of the electro-optic response and its dependence on the applied voltage and the electro-mechanical history.

Cells were prepared with 25 mm x 25 mm x 1.1 mm Delta ITO-coated glass plates. The glass plates are SiO_2 passivated and contain no alignment layers. The plates were fastened together using epoxy, and teflon spacers were placed in between the plates to create a well-defined gap. We measured the gap thickness with a micrometer, and loaded the cell by placing a small amount of gel on the side of the gap, heating it to 40 ^{o}C, and letting the gel flow in by capillary action.

The optical properties and electro-optic responses of the gels were measured using a polarized HeNe laser, a beam splitter, two CCD cameras, and a function generator. A beam splitter between the laser and the sample sent half of the incident laser intensity to the sample and half to a CCD camera which was used to normalize the intensity of laser light incident on the sample. A CCD camera 10 cm behind the sample measured the intensity of transmitted light, and this intensity was

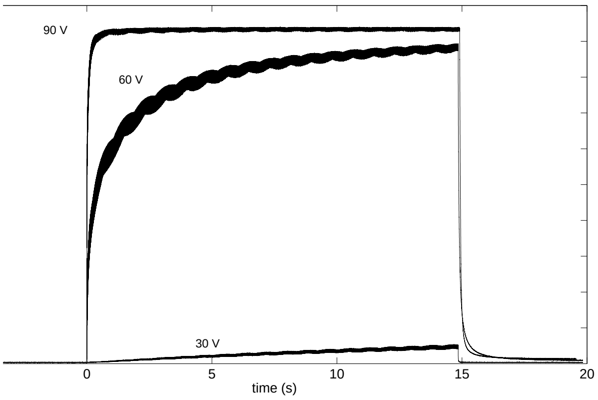

Figure A.1: Response of a 5 wt % gel in a 15μ gap to an external voltage of 30 V, 60 V, and 90 V. The voltage is applied at 0 s and removed at approximately 15 s.

normalized by the intensity transmitted for the sample in the isotropic state. The function generator was used to apply voltages from 0 V to 270 V at 1000 Hz.

For each run, a voltage was applied for only 15 s. After allowing the gel to sit for 2 minutes at 0 V, the process was repeated with the same voltage 4 times, for a total of 5 runs for each experiment. Then, before the start of the next experiment, the gel was heated into the isotropic state and allowed to cool.

The response of the gels depends on the applied voltage (Fig. A.1). At low voltages, near the voltage threshold, the long-time transmission is very low, as would be expected. Voltages at twice and three times the threshold give a much higher long-time transmission. At 30V, the response is very slow but relaxation is fast. At higher voltages, the response time gets faster and the relaxation time slower. We can define a response time and relaxation time for the gel. The time for the gel to reach 90% of its long-time transmission after turning on the signal, τ_{90}, is a characteristic response time for the gel. The time for the transmission to decay back down to 10% of its long-time transmission, τ_{10}, is a characteristic relaxation time. The τ_{90} are 10.0547 s, 3.7630 s, and 0.1070 s for 30 V, 60 V, and 90 V, respectively, and the τ_{10} are 0.0160 s, 0.2508 s, and 0.1342 s for 30 V, 60 V, and 90 V, respectively, for the 5 wt % gel. This indicates that applying a high enough voltage imprints alignment into the polymer network, resulting in a slow response (larger τ_{10}). Also, at high

Table A.1: Results for transient switching experiments of 5 wt % and 10 wt % gels in a 15 μ gap.

Polymer Concentration	Voltage	τ_{90} (s)	τ_{10} (s)
5 wt %	$V_{threshold}(30V)$	10.0547	0.0160
5 wt %	$2\times V_{threshold}(60V)$	3.7630	0.2508
5 wt %	$3\times V_{threshold}(90V)$	0.1070	0.1342
10 wt %	$V_{threshold}(45V)$	8.1635	0.0007
10 wt %	$2\times V_{threshold}(90V)$	4.4864	0.5533
10 wt %	$3\times V_{threshold}(135V)$	0.1395	0.4510

enough voltages the electric field dominates the dynamics and the liquid crystal director rotates very quickly, as indicated by a small τ_{90} for large applied voltages.

We can study the effect of polymer concentration by comparing 5 wt % and 10 wt % gels of the same thickness (Tab. A.1). Both behave the same qualitatively, with a faster switch-on time and slower switch-off time at higher voltages. At low voltages, the 10 wt % gel has a much faster switch-off time than the 5 wt % gel – the τ_{10} is 0.016 s for the 5 wt % gel compared with 0.0007 s for the 10 wt % gel. At twice the threshold voltage, the τ_{90} values are comparable at ~ 4 s, but the τ_{10} is 0.25 s for the 5 wt % gel compared to 0.55 s for the 10 wt % gel. At three times the threshold voltage the disparity in relaxation times is greater, with the 5 wt % gel exhibiting a τ_{10} of 0.13 s compared with 0.45 s for the 10 wt % gel. Therefore, the gels of greater polymer concentration appear to have significantly slower relaxation times, except for voltages near the threshold. Since the polymer network dictates the long-time relaxation behavior, this indicates that the electric field modified the network morphology at voltages significantly higher than the threshold. Interestingly, the relaxation time is seen to decrease slightly with voltage at high voltages. This suggests the presence of competing interactions, which result in an increased relaxation time with voltage near the threshold but a decreased relaxation time at much higher voltages. At very large voltages, when the polymer network is significantly perturbed from equilibrium, it may have a larger restoring force once the applied voltage is removed.

Gels with a voltage previously applied tend to show faster switching and slower relaxation. At

Table A.2: Results for successive transient voltage runs on 5 wt % LC gel in a 15 μm gap. The voltage is at the threshold, 30 V.

Run	τ_{90} (s)	τ_{10} (s)
1	10.0547	0.0160
2	9.7084	0.0185
3	9.8387	0.0183
4	9.6162	0.0195
5	9.4906	0.0205
6	9.5682	0.0198
7	9.1146	0.0210
8	9.4956	0.0217
9	9.4956	0.0218
10	8.9699	0.0217

voltages just above the threshold, there is very little effect on the subsequent electro-optic behavior of the gel (Tab. A.2). At twice the voltage, the τ_{90} values decrease dramatically between the first and second experiments, between which the gel is allowed to relax for two minutes but is not reheated into the isotropic state (Tab. A.3). The response time steadily decreases in the subsequent experiments, but the rate of decrease is much smaller than that observed for the first and second experiments. This decrease in τ_{90} with the application of a large voltage indicates that the modified morphology of the polymer network presents a decreased resistance to reorientation of the liquid crystal director along the electric field, and therefore the polymer network itself is being aligned with application of large voltages. At three times the voltage, both the τ_{90} and the τ_{10} values decrease further (Tab. A.4). The decrease in the τ_{90} is more dramatic, by about an order of magnitude, and suggests that the applied field is dominating the reorientation time. The decrease in τ_{90} may arise from a greater reorientation force when the polymer network is significantly perturbed from the morphology imprinted during crosslinking.

Table A.3: Results for successive transient voltage runs on 5 wt % LC gel in a 15 μm gap. The voltage is at twice the threshold, 60 V.

Run	τ_{90} (s)	τ_{10} (s)
1	3.7630	0.2508
2	0.1645	0.2388
3	0.0560	0.2715
4	0.0457	0.3116
5	0.0315	0.3621
6	0.0300	0.4120
7	0.0245	0.4630
8	0.0207	0.5201
9	0.0185	0.5581
10	0.0232	0.6009

Table A.4: Results for successive transient voltage runs on 5 wt % LC gel in a 15 μm gap. The voltage is at three times the threshold, 90 V.

Run	τ_{90} (s)	τ_{10} (s)
1	0.1070	0.1342
2	0.0020	0.1213
3	0.0015	0.1418
4	0.0015	0.1620
5	0.0013	0.1841
6	0.0012	0.2040
7	0.0015	0.2298
8	0.0015	0.2505
9	0.0010	0.2723
10	0.0007	0.2936